

Instituto Tecnológico y de Estudios Superiores de Monterrey

Campus Monterrey

School of Engineering and Sciences



**In-building measurement-based radio propagation modeling using a
geostatistical interpolation technique**

A dissertation presented by

Melissa Eugenia Diago Mosquera

Submitted to the
School of Engineering and Sciences
in partial fulfillment of the requirements for the degree of

Doctor of Philosophy

In

Engineering Science

Major in Telecommunications

Monterrey Nuevo León, December 1st, 2022

Instituto Tecnológico y de Estudios Superiores de Monterrey

Campus Monterrey

School of Engineering and Sciences

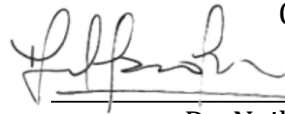
The committee members, hereby, certify that have read the dissertation presented by Melissa Eugenia Diago Mosquera and that it is fully adequate in scope and quality as a partial requirement for the degree of Doctor of Philosophy in Engineering Science, with a major in Telecommunications.



Dr. Alejandro Aragón Zavala
Tecnológico de Monterrey
School of Engineering and Sciences
Principal Advisor



Dra. Leyre Azpilicueta Fernandez de las Heras
Tecnológico de Monterrey
School of Engineering and Sciences
Committee Member



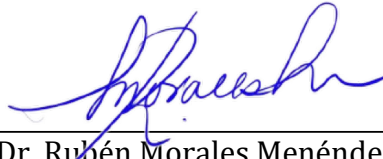
Dr. Neil Guerrero Gonzalez
Universidad Nacional de Colombia
Committee Member



Dr. César Vargas Rosales
Tecnológico de Monterrey
School of Engineering and Sciences
Committee Member



Dr. Alejandro Garcia Juarez
Universidad de Sonora
Committee Member



Dr. Rubén Morales Menéndez
Dean of Graduate Studies
School of Engineering and Sciences

Monterrey Nuevo León, December 1st, 2022

Declaration of Authorship

I, Melissa Eugenia Diago Mosquera, declare that this dissertation titled, In-building measurement-based radio propagation modeling using a geostatistical interpolation technique and the work presented in it are my own. I confirm that:

- this work was done entirely or mainly while in candidature for a research degree at this University;
- where any part of this dissertation has previously been submitted for a degree or any other qualification at this University or any other institution, this has been clearly stated;
- where I have consulted the published work of others, this is always clearly attributed;
- where I have quoted from the work of others, the source is always given. With the exception of such quotations, this dissertation is entirely my own work;
- I have acknowledged all main sources of help;
- where the dissertation is based on work done by myself jointly with others, I have made clear exactly what was done by others and what I have contributed myself.



Melissa Eugenia Diago Mosquera
Monterrey Nuevo León,
December 1st, 2022

@2022 by Melissa Eugenia Diago Mosquera
All rights reserved

*Mommy, Daddy, Nani and my lovely George, finally I can say you that my Doctoral Research have finished with wonderful results in many aspects of my life. Thanks for all your unconditional confidence, support, patience, and encouragement, especially at those times of difficulties. You were my main motivation for pushing through this work.
This is with all my love for you.*

Melissa Eugenia Diago Mosquera

Acknowledgements

I would like to express my deepest gratitude to my supervisor Dr. Alejandro Aragón-Zavala, for his advice and continuous support during my PhD study. I would also like to thank Dra. Leyre Azpilicueta for all her invaluable support during my research, to Dr. Neil Guerrero to trust in me and connect me with all the opportunities that Tecnológico de Monterrey has given me. I would like to thank all the members of my Doctoral Committee. It is their comments that have done solid research. Additionally, I would like to express my gratitude to Dr. Mauricio Rodriguez for his treasured support which was really influential in shaping my doctoral stay results. I also appreciate all the support I received from Dr. Neale Smith and Dra. Esmeralda Uribe with the coordination of the administrative processes. Finally, I wish to acknowledge the support received from the Tecnológico de Monterrey on tuition and the National Council of Science and Technology, CONACYT on living costs, under student scholarship number 746015, without this economical support I would not have been able to do my PhD.

In-building measurement-based radio propagation modeling using a geostatistical interpolation technique

By

Melissa Eugenia Diago Mosquera

Executive Summary

Channel modeling can enhance communication efficiency through an accurate design to deliver higher quality to mobile users inside buildings. Clear processes and methodologies that can provide a high level of confidence in the design of indoor radio propagation systems are thus required. With the deployment of wireless communication and the need to accommodate for the shorter signal range, millimeter-wave (mmWave) enabled networks will have a high density of base stations. In such a dense network, interference is an important factor affecting network performance. In this way, accurate channel modeling combined with more spectrum availability is essential to achieve the ongoing demands faced by wireless carriers. Therefore, it is important to explore suitable in-building mathematical propagation modeling approaches that can accurately make predictions and support the ever-growing consumer data rate demands of modern communication systems. The research here report is aimed at providing solid theoretical and empirical foundations of how radio waves behave in practical wireless channels; validating the improvement in predictions when Kriging is included for path loss modeling not only in indoor scenarios, such as offices, classrooms, long corridors, libraries, and rooms but also in complex scenarios as is a stadium. In order to quantify the accuracy of the proposed methodology, it is compared with several traditional models described in the literature. Extensive path loss measurements were collected at different frequencies and heights providing the empirical basis for the three-dimensional (3D) Kriging-aided model. Through numerous studies during this doctoral research, It was found that this method significantly improves the accuracy as it considers all the singularities and site-associated features that are implicit in measured samples. The findings of this doctoral research lay a good foundation for a greater understanding of mmWave channel propagation, but mainly provide one of the most accurate methods for indoor 3D modeling, using few measurements and low computational complexity, yielding a practical and fast solution.

List of Figures

| | |
|--|----|
| Fig. 1.1 Channel model methodology when shadowing is predicted through Kriging..... | 5 |
| Fig. 1.2 Channel model methodology when the complete path loss is predicted through Kriging..... | 5 |
| Fig. 9.1 Overview of the guidelines for indoor radio propagation predictions..... | 86 |

List of Tables

| | |
|--|----|
| Table 9.1 Principal contributions of the journal papers published..... | 87 |
| Table 9.2 Principal contributions of the doctoral thesis to different areas..... | 88 |

Contents

| | |
|--|------------|
| Executive Summary | i |
| List of Figures | ii |
| List of Tables | iii |
| | |
| Chapter 1 | |
| Introduction | 1 |
| 1.1 Context and Motivation | 1 |
| 1.2 Problem Statement | 2 |
| 1.3 Proposal and Objectives | 3 |
| 1.4 Main Contributions | 3 |
| 1.5 Methodology | 4 |
| 1.6 Thesis Outline | 5 |
| | |
| Chapter 2 | |
| Bringing It Indoors: A Review of Narrowband Radio Propagation Modeling for Enclosed Spaces | 7 |
| 2.1 Summary of the Chapter | 7 |
| 2.2 Full Article | 7 |
| | |
| Chapter 3 | |
| The performance of in-building measurement-based path loss modeling using kriging | 33 |
| 3.1 Summary of the Chapter | 33 |
| 3.2 Full Article | 33 |
| | |
| Chapter 4 | |
| Testing a 5G Communication System: Kriging-Aided O2I Path Loss Modeling Based on 3.5 GHz Measurement Analysis | 47 |
| 4.1 Summary of the Chapter | 47 |
| 4.2 Full Article | 47 |
| | |
| Chapter 5 | |
| Tuning Selection Impact on Kriging-Aided In-Building Path Loss Modeling | 61 |
| 5.1 Summary of the Chapter | 61 |

| | | |
|--|------------------------------|-----------|
| 5.2 | Full Article | 61 |
| Chapter 6 | | |
| A 3D Indoor Analysis of Path Loss Modeling Using Kriging Techniques | | 67 |
| 6.1 | Summary of the Chapter | 67 |
| 6.2 | Full Article | 67 |
| Chapter 7 | | |
| Towards Practical Path Loss Predictions in Indoor Corridors Considering 5G mmWave 3D Measurements | | 73 |
| 7.1 | Summary of the Chapter | 73 |
| 7.2 | Full Article | 73 |
| Chapter 8 | | |
| mmWave Channel Measurements for 3D Path Loss Analysis and Model Design in Stadiums..... | | 79 |
| 8.1 | Summary of the Chapter | 79 |
| 8.2 | Full Article | 79 |
| Chapter 9 | | |
| Conclusions | | 85 |
| 9.1 | Guidelines | 85 |
| 9.2 | Contributions | 87 |
| 9.3 | Publications | 89 |
| 9.4 | Future Work | 90 |
| Appendix A | | |
| Abbreviations and Acronyms | | 91 |
| Appendix B | | |
| Units..... | | 92 |
| Bibliography | | 93 |
| Curriculum Vitae | | 95 |

Chapter 1

Introduction

The concept of using radio propagation models for delivering data or voice communications inside buildings started to become an attractive idea many years ago, since more users demanded better services anytime, anywhere, and especially at locations where they spent most of their time: indoors. For this reason, deep knowledge of how radio waves behave in a practical wireless channel is required for effective planning and deployment of radio access networks in indoor environments for new fifth and sixth generation (5G, 6G) standards. Therefore, there is a promising field of study to fill gaps in the wireless industry to deliver service indoors. This field needs a clear methodology with guidelines that provide a high level of confidence in the design of indoor radio propagation systems, especially for small cells.

1.1 Context and Motivation

The widespread use of mobile communications, since its initial implementation in the early 1980s, has led not only to an increase of personal communication systems but also to large demands of grade of service (GoS) of mobile users, stressing the coverage to handle more consumers with heterogeneous GoS levels. These users, on average, spend approximately 90% of their time indoors, where they are mobile network subscribers of small cells. In this way, an efficient radio access—constructed by accurate channel modeling—combined with more spectrum availability is essential to achieve the ongoing demands faced by wireless carriers [1]. Therefore, it is important to explore suitable in-building mathematical propagation modeling approaches which can accurately make predictions, avoiding undesirable effects—e.g., interference, which may result to a low Signal to Interference plus Noise Ratio (SINR), throughput, and in some cases a total disruption of service [2]—and support ever-growing consumer data rate demands of modern 5G and 6G communication systems.

Engineers need processes and methodologies to provide a high level of confidence in the design of indoor radio propagation systems, considering that the efficiency of those approaches depend on the prediction level of the signal strength behavior according to probabilistic distributions, to obtain realistic values of signal strength, at least above certain thresholds that guarantee enough coverage in a certain area and minimize outage zones. Therefore, the scientific community has inspired to work towards understanding and predicting indoor radio wave propagation performance through path loss models to help radio network engineers to achieve efficient radio coverage estimation, determine the optimal base station (BS) location, select the most suitable antenna, and perform interference feasibility studies; understanding how wireless signals are affected over distance due to penetration losses through walls and floors and multipath propagation. According to [3], the following approaches outline the importance of an accurate channel modeling:

1. The in-building radio propagation phenomena, complex by nature, can be characterized with channel models.
2. The range of a wireless communication system can be calculated assessing the expected coverage—path loss map—inside a building, including the expected range of antennas and their potential locations.
3. Signal strength/path loss can be predicted more accurately everywhere in a building.
4. Channel performance predictions can be made quickly, e.g., signal-to-noise-ratio (SNR), received signal power, among others.
5. Signal strength predictions can be useful for areas where measurements cannot be made.

Indoor radio propagation models for small cells must be explored with a higher degree of accuracy due to the indoor channel differs considerably from the outdoor. Besides, numerous attempts to characterize and estimate received signal in indoor environments have been reported. Particularly reported measurements—in these environments—exhibit fluctuations as a result of radio propagation effects, e.g., fast fading and shadowing.

1.2 Problem Statement

In channel modeling the accuracy and efficacy trade-off of the designed model is essential. Purely empirical models are not accurate enough to be employed in all types of buildings, their accuracy depends not only on the measurement results but also on the similarity of the measured and predicted environment; and purely physical models still need a good amount of computational resources, requiring a large quantity of building details and therefore becoming unviable for practical radio prediction work. In hybrid models, measurement-based methods, rigorous tuning, and validation stages are included, taking advantage from empirical and physical models [4]–[6]. The possibility to collect large amounts of data from measurement campaigns can be very limited for practical designs. Venues often permit data collection campaigns having restrictions on measurement areas, test antenna location placements, available times, and dates to conduct the measurements, etc. Nevertheless, with a careful design of the measurement campaign, valuable information can be extracted and used in channel modeling. Kriging, as a linear interpolation technique, shows its potential to estimate measurements in such situations, by significantly improving the results with few available samples as is reported in numerous studies [7]–[9]. Also, it allows us to extract as much information as possible from existing sources and explore the accuracy and efficacy trade-off of the desired model.

Numerous studies that only consider two-dimensional effects in indoor path loss models have been reviewed [3]. However, these reports do not analyze the effects of parameters that include a third dimension, e.g., the antenna height of transmitter or receiver, where there is a study niche to fill gaps. The path loss consists of three major components: median path loss, shadowing, and fast fading [10]. These components depend on both the relative position of the elements of a wireless system and the obstructions in the channel. The median path loss is predicted by any standard path loss model, such the classical single slope path loss model. Fast fading results from rapid signal variations on the scale of half-wavelength and is often removed by filtering. For indoor channels, shadowing occurs due to the large variability of

obstructions present in the venue, which results in a received power that fluctuates randomly over time. Only median path loss modeling cannot be used to estimate shadowing, but it is empirically known that shadowing has a spatial correlation. Therefore, it can be estimated by applying an appropriate weighted average to the observation dataset in the framework of spatial statistics or by including a method of linear geostatistics that minimizes the variance of estimation errors under the constraint of unbiased estimation [11] instead of the most classical assumption of shadowing as a random variable as is reported in [12]–[14].

Considering the problem description, the following research questions is formulated: How to accurately predict radio coverage inside complex environments such as buildings without excessive computational resources or excessive building information?

1.3 Proposal and Objectives

In order to design an indoor channel model with an outstanding trade-off between accuracy and efficacy, the research proposed in this thesis is inspired by the novel approach of the measurement-based radio propagation modeling method. With the aim of presenting a complete methodology to predict three-dimensional (3D) coverage in indoor environments with Kriging as part of the post-processing stage, clear guidelines are included in this doctoral thesis, reducing the cost of measurement campaigns, time-consuming, and computational complexity, as well as improving the design work with the use of suitable antenna locations and types.

This proposed solution aims to develop 3D in-building measurement-based radio propagation models for narrowband channels in the ultra-high frequency (UHF), super high frequency (SHF) and extremely high frequency (EHF) bands for small cells based on Kriging. This general objective will be achieved through:

- Designing a 3D in-building measurement-based radio propagation model.
- Developing a methodology to validate the model designed, where the post-processing includes Kriging.
- Performing measurement campaigns in UHF, SHF and EHF bands including different types of indoor antennas to enhance predictions.
- Achieving 3D path loss predictions, through the radio propagation model designed for the environments selected.
- Developing guidelines to the design and deployment of indoor small cells.

1.4 Main Contributions

The principal contribution of this doctoral research is to provide one of the most accurate methods for indoor 3D modeling (considering the error reported by the studies when predicting path loss), using few measurements and low computational complexity, which allows the algorithm to be implemented as part of radio propagation software tools for modeling and designing indoor wireless systems, providing a practical and fast validated solution. Helping radio network engineers to achieve efficient radio coverage estimation;

estimating measurements in situations where the possibility to collect large amounts of data from measurement campaigns is very limited; and performing channel design with Kriging as an effective tool to improve modeling accuracy.

This doctoral research presents an opportunity of taking advantage of the combination of both the design of mathematical models and the geostatistical interpolation technique of Kriging, which allows us to predict signal strength inside buildings for environments that are often complicated to model, including three-dimensional scenarios. Presenting a clear methodology with guidelines to perform coverage and path loss predictions in indoor scenarios, thanks to the measurement-based model proposed and the use of suitable antenna locations and types to enhance predictions.

Motivated by the need of people communication and continuous improvements for wireless communication services. This experimental assessment contributes not only to the academic sector but also to the commercial sector, offering the opportunity of analyzing the indoor signal reception quality that allows homologating new mobile equipment or indoor performance technology in small cells. Thus, the research in the telecommunications field leads to the achievement of strategic approaches to science and technology, providing economic and social benefits.

1.5 Methodology

Inspired by the practical approach of the measurement-based method to predict path loss and considering the remarkable benefits of including Kriging to calculate unmeasured values. The methodology proposed to predict path loss in this thesis, first, takes into account the availability of radio measurements to provide the empirical basis of the mathematical model proposed. Then, the path loss is extracted from the received signal-strength measurements according to the link budget of the radio channel, providing a set of samples that will be divided into tuning and testing datasets. Through the tuning dataset, it will be possible to train the Kriging-aided model to estimate unmeasured values and calculate the path loss at specific locations selected as unmeasured samples, i.e., the testing dataset. Finally, the error of the predictions is quantified once the values predicted are compared to the real measured values.

At the beginning of the research, the path loss was modeled according to a classic single slope model, i.e., the median path loss, plus the shadowing. Where the shadowing was considered as the variable to be predicted using Kriging. However, during the doctoral stay, one of the objectives was to analyze if the accuracy improved when using Kriging to predict the complete path loss and not only the shadowing, this approach was assessed in [15]. Where, based on the experimental measurements, when Kriging was included to interpolate and predict unmeasured path loss, the predictions were more accurate, reducing the error by more than 60%. Therefore, it was a milestone in the research and the methodology followed changed. Now, the variable to interpolate according to Kriging was the path loss extracted instead of shadowing. In order to overview the overall methodology employed in the

following chapters, Fig. 1.1 and Fig. 1.2 illustrate the channel model methodology employed in Chapters 3 to 6 and 7 to 8, respectively.

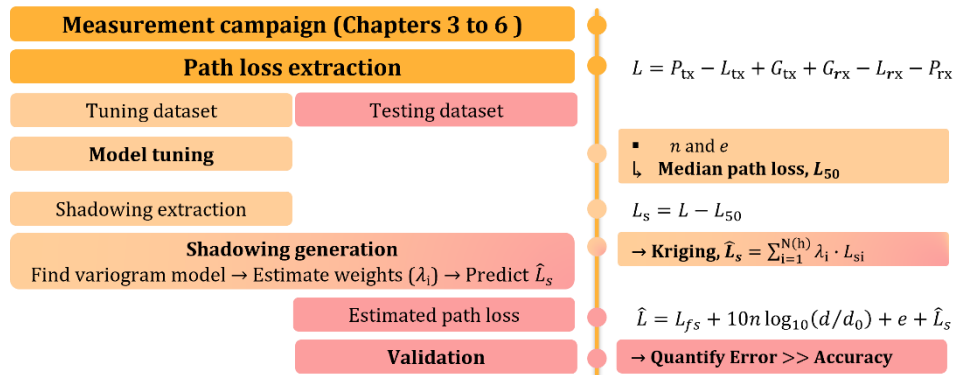


Fig. 1.1 Channel model methodology when shadowing is predicted through Kriging.

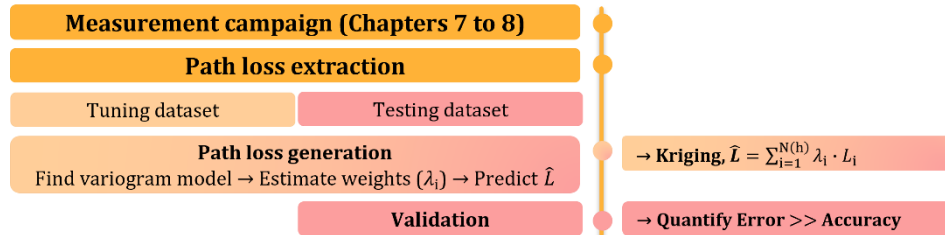


Fig. 1.2 Channel model methodology when the complete path loss is predicted through Kriging.

1.6 Thesis Outline

This thesis provides comprehensive research on how radio waves behave in practical wireless channels, validating the improvement in predictions when Kriging is included for path loss modeling yielding an accurate, practical and fast solution. Chapters 2 to 8 are organized according to the qualified published papers, which summarize the findings in the timeline of the PhD under the objectives and the research question (this format was approved by the doctoral committee and the leader of the Doctoral Program in Engineering Sciences). Chapter 2 surveys the state of the art of indoor path loss models and is dedicated to the publication [3]. Then, the complete indoor mathematical model proposed is presented in Chapter 3, as well as the validation of the accuracy of the model, which is complemented by Chapter 4. Later, Chapter 5 aims to suggest enough quantity of training data to guarantee accurate predictions. In line with the objectives, the methodology and the model proposed are employed for 3D millimeter-wave (mmWave) path loss predictions in Chapters 6 and 7. In addition, Chapter 8 has been included to characterize the path loss of a complex scenario and validate the benefits of employing the proposed model for predictions. Finally, in Chapter 9 the conclusions, contributions and future work are presented. The objectives of Chapters 3 to 8 are summarized as follows:

- Chapter 3 is dedicated to the publication [16], where the selection of the following three approaches are studied: variogram function, tuning dataset method and tuning dataset size. Besides, 57 indoor scenarios are considered to validate if ordinary Kriging is the best linear unbiased predictor. To finally test the accuracy of the mathematical measurement-based model proposed, which predicts the unmeasured shadowing according to the ordinary Kriging technique, against a classic linear interpolation and the traditional assumption of shadowing as a normally distributed variable.
- Chapter 4 presents the research article [17], where the Kriging-aided path loss model is employed for an Outdoor-to-Indoor (O2I) scenario at 3.5 GHz. And the accuracy of the model is validated when it is compared to the results of the following standard models: 3GPP, ITU-R, WINNER+ and COST231.
- Chapter 5 corresponds to the publication [18] where the question of how do you know you select enough tuning dataset from measurements to guarantee model prediction accuracy? is answered through the useful cost function that has been suggested in this study.
- Chapter 6 is dedicated to the article [19], where the first 3D indoor analysis is achieved considering the proposed model and radio measurements at 28 GHz, including two different receiver heights to provide the empirical basis for the 3D path loss model. Furthermore, the spatial structure of shadowing is investigated through the three variography tools in order to understand which one provides the best accuracy.
- Chapter 7 presents the article [20], which validates the improvement in predictions when Kriging is employed at 28 and 60 GHz and provides a better understanding on long indoor corridors when the effect of corners and three different receiver heights are considered.
- Chapter 8 corresponds to the publication [21], where the seating area of a stadium is characterized at mmWave frequencies to validate the effectiveness of the Kriging-aided model proposed.

Chapter 2

Bringing It Indoors: A Review of Narrowband Radio Propagation Modeling for Enclosed Spaces

2.1 Summary of the Chapter

Over the years indoor radio propagation systems have evolved, motivating engineers and researchers to provide continuous improvements for wireless communication services. To overcome all the challenges in channel modeling for in-building scenarios deep knowledge of how wireless signals are affected over distance is needed, as well as the best and most accurate way to characterize them. In this chapter, state-of-the-art in indoor narrowband channel models is presented, considering their disadvantages, and proposing a new taxonomy to analyze them.

The purpose of this part of the research is to introduce the main propagation characteristics for wireless communications in indoor scenarios, review mathematical models proposed for this type of venue over more than 30 years and, finally, suggest remarks for indoor radio propagation modeling.

2.2 Full Article

Received May 20, 2020, accepted May 28, 2020, date of publication June 3, 2020, date of current version June 15, 2020.

Digital Object Identifier 10.1109/ACCESS.2020.2999848

Bringing It Indoors: A Review of Narrowband Radio Propagation Modeling for Enclosed Spaces

MELISSA EUGENIA DIAGO-MOSQUERA¹, ALEJANDRO ARAGÓN-ZAVALA¹,
AND GERARDO CASTAÑÓN²

¹Computing Department, School of Engineering and Science, Tecnológico de Monterrey, Querétaro 76130, Mexico

²Department of Electrical and Computing Engineering, Tecnológico de Monterrey, Monterrey 64849, Mexico

Corresponding author: Melissa Eugenia Diago-Mosquera (a00829220@itesm.mx)

This work was supported in part by the National Council of Science and Technology (CONACyT) under the student scholarship number 746015.

ABSTRACT Small cells are now widely deployed indoors to address hot-spot areas where capacity uplift is needed. This deployment leads to the increase of wireless networks as a challenge to service demands of personal communication systems, which has inspired the scientific community to work towards understanding and predicting in-building radio wave propagation performance. Despite this, only a few reviews have attempted to overview channel modeling for specific indoor environments and even fewer outline remarks that include a methodology for designing and planning indoor radio systems. Consequently, a comprehensive survey of indoor narrowband channel models is presented, spanning more than 30 years of continuous research to overview and contrast significant developments including their disadvantages, and proposing a new taxonomy to analyze them. Finally, remarks on indoor radio propagation modeling with a vision for future research opportunities are presented.

INDEX TERMS Indoor channel models, indoor radio wave propagation, wireless propagation.

I. INTRODUCTION

The widespread use of mobile communications, since its initial implementation in the early 1980s, has led not only to an increasing wealth of this technology but also to a reasonable increase in grade of service (GoS) demands of mobile users, thereby stressing the coverage to handle more users with heterogeneous GoS levels. According to the Cisco Visual Networking Index (VNI) report published in [1], by 2022, global mobile devices will grow from 8.6 billion in 2017 to 12.3 billion by 2022.

Considering the challenges of this explosive growth and the fact that people (mobile network subscribers initially), on average—according to the United States Environmental Protection Agency, EPA—spend approximately 90% of their time indoors [2], in-building wireless performance takes a fundamental place on network operation management for allowing coverage all the time, everywhere. The adaptation of this mobile technology to in-building scenarios is what makes it flexible and robust, responding to the changing needs

of people and businesses to deliver a satisfactory in-building experience to mobile users.

From the early stages of 5G planning to the detailed evolution of 5G requirements, it has been clear that small cells are a key component for making the path to 5G practical and profitable. A small cell is a radio access point with low radio frequency power output, footprint and range. It is operator-controlled and can be deployed indoors or outdoors. Small cells complement the macro network to improve coverage, add targeted capacity, and support new services while improving user experience [3].

In order to deliver higher quality to mobile users inside buildings, small cells have been deployed to address hot-spot areas where an increase in capacity is needed. This has led to a growing interest among wireless engineers for understanding and predicting how radio waves propagate inside buildings and other enclosed spaces. As this rise of mobile communications continues, it is valuable to have processes and methodologies that can provide a high level of confidence in the design of indoor radio propagation systems. Therefore, it is important to explore in-building mathematical propagation models with a high degree of accuracy, understanding how wireless signals are affected over distance due to wall

The associate editor coordinating the review of this manuscript and approving it for publication was Jiayi Zhang.

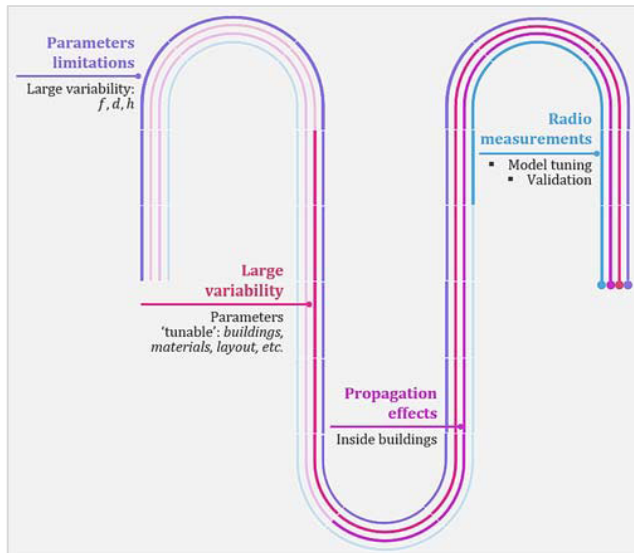


FIGURE 1. Propagation modeling challenges.

and floor penetration losses and multipath effects. Some key points that outline the importance of accurate channel modeling are:

- The in-building radio propagation phenomena, complex by nature, can be characterized with appropriate channel models that include key propagation effects.
- The range of a wireless communication system can be estimated assessing the expected coverage—path loss map—inside a building, including potential antenna locations and their expected coverage range.
- Signal strength/path loss can be predicted more accurately everywhere in a building or enclosed space.
- Channel performance predictions can be made quickly, e.g., signal-to-noise ratio (SNR), received signal power, carrier-to-interference ratio (C/I), etc.
- Signal strength predictions can be useful for areas where measurements cannot be made.

Propagation modeling challenges are shown Fig. 1, according to Aragoïn-Zavala [4, Ch. 5]. For indoor deployments, the following challenges are identified:

- Parameter limitations—approximations that are necessary to describe a system using mathematical concepts within a computational development—due to the large variability that exists in indoor radio propagation.
- Model parameter calibration that depends on specific building characteristics that otherwise could not be modeled.
- High complexity in considering propagation effects inside buildings, having in mind that in many cases it is hard to separate them and characterize those individually.
- Conditions under which radio measurements were performed at different times. Since measurements are used for both model tuning and validation, it is expected to have a scenario under similar conditions.

A. RELATED LITERATURE REVIEWS PUBLISHED

In 2002, Iskander and Yun [5] focused on deterministic prediction models for path loss based on ray-tracing techniques. The authors briefly discussed efforts to characterize walls of complex structures and develop equivalent ray-tracing models for windows and metal-framed structures, considering venues such as office and factory buildings. One year later, Sarkar *et al.* [6] reviewed available information on various propagation models for both indoor and outdoor. They highlighted that the distance/power model is the main propagation modeling approach for path loss, adding wall and floor attenuation factors to the path loss computation.

Later, in 2008, Anusuya *et al.* [7] surveyed different channel models used to characterize indoor wireless systems, and they concluded that the efficiency of a model is measured by computational complexity whereas its accuracy can be measured by estimating its prediction error. In contrast, Neskovic *et al.* [8] mentioned that in order to increase system efficiency, mutual interference should be avoided, thus favoring coexistence as a result of suitable techniques for the prediction of indoor electromagnetic propagation.

By 2009, Neskovic *et al.* [8] and Trincherro and Stefanelli [9] focused their works on analyzing the technical literature to summarize and classify the most important methods for the prediction of electromagnetic propagation inside buildings. Smulders [10] addressed the statistical characterization—one of the classifications made by Neskovic *et al.*—of indoor radio channels operating in the 60 GHz frequency band. Phillips *et al.* [11] reviewed path loss prediction methods, works from 1940 to 2013, although not focusing on indoor environments but subdividing the models into a priori (six categories) and active measurement models (four categories).

Considering that underground mines and tunnels are enclosed spaces, Forooshani *et al.* in 2013 [12] and Hrovat *et al.* in 2014 [13], focused their surveys on these approaches, highlighting the implications of the physical environment (thick concrete walls), antenna placement and radiation characteristics on wireless communication system design.

In the review paper presented by Deb *et al.* in 2017 [14], different path loss models are discussed for indoor femtocells, assuming that the mobile users in that region exclusively access services delivered by femtocells. Additionally, the authors performed a comparative analysis of indoor path loss models at 2 GHz, where they considered the effect of two types of walls: light walls made of glass, plastic, etc. and heavy walls made of concrete and brick. They concluded that the most suitable in-building path loss model could be selected depending on frequency range, building structure, and wall and floor type.

To summarize this section, a survey of model classification and important annotations reported in the literature is given in Table 1.

The related works in Table 1 agree with the idea that at a specific location, the signal path for indoor environments is created by a much larger number of indirect components than

TABLE 1. Propagation model classification.

| Review | Propagation model classification | | Scenario | Contributions |
|--------------------------------------|--|--|---|---|
| Iskander & Yun, 2002 [5] | 1. Deterministic 1.1. Empirical 1.2. Theoretical 1.3. Site-specific | 2. Statistical | Terrestrial wireless communication systems | Schemes to increase computational efficiency and accuracy are discussed. |
| Sarkar <i>et al.</i> , 2003 [6] | 1. Empirical (statistical) | 2. Site-specific (deterministic) | Indoor and outdoor environments | An impulse response characterization for the propagation path is presented. |
| Anusuya <i>et al.</i> , 2008 [7] | 1. Deterministic | 2. Statistical 3. Site-specific | Wireless indoor environment | - |
| Neskovic <i>et al.</i> , 2009 [8] | 1. Statistical (empirical) | 2. Theoretical | Macrocell, microcell and indoor wireless communication channels | Advantages and disadvantages are discussed. |
| Trincherro & Stefanelli, 2009 [9] | 1. Deterministic 1.1. Ray methods 1.2. Integral methods 1.3. Differential equation methods | 2. Heuristic 2.1. Empirical models. 2.2. Statistical models. 3. Hybrid | Indoor environment | - |
| Phillips <i>et al.</i> , 2013 [11] | 1. Apriori 1.1. Theoretical/Foundational Models 1.2. Basic Models 1.3. Terrain Models 1.4. Supplementary Models 1.5. Stochastic Fading Models 1.6. Many-Ray Models | 2. Active measurement 2.1. Explicit mapping 2.2. Partition models 2.3. Iterative Heuristic Refinement 2.4. Active Learning and Geostatistics | Wireless communication systems | <ul style="list-style-type: none"> ▪ Period of more than 60 years was covered. ▪ New taxonomy for path loss models. |
| Forooshani <i>et al.</i> , 2013 [12] | 1. Theoretical | 2. Measurement-based | Underground mines | Period from 1920 to 2012. |
| Hrovat <i>et al.</i> , 2014 [13] | 1. Empirical | 2. Deterministic | Tunnels | - |
| Deb <i>et al.</i> , 2017 [14] | 1. Empirical (statistical) | 2. Semi-Empirical (theoretical) | Indoor environment covered by femtocell | Comparative analysis between: COST 231, MWF, WINNER II NLOS and ITU-R P models. |
| Hemadeh <i>et al.</i> , 2018 [15] | 2. Physical 2.1. Deterministic 2.2. Stochastic | 3. Analytical 3.1. Propagation-based 3.2. Correlation-based | Millimeter wave wireless communication systems | <ul style="list-style-type: none"> ▪ Frequency bands: 28, 38, 60 and 73 GHz. ▪ Measurement campaigns are conducted. |

in the case of an outdoor environment. Therefore, the indoor signal level is more fluctuating than the outdoor one, and thus, more difficult to predict. Multipath results from multiple reflections caused by obstacles and is more severe inside buildings. The received signal arrives as a random and unpredictable set of reflections and/or direct waves, each one with its own degree of attenuation, phase and delay. Consequently, multipath leads to variations in the received signal strength over frequency and antenna location.

Phillips *et al.* [11] believe that measurement-based methods and rigorous—comparative—validation are needed; moreover, that the future of wireless path loss prediction will be active measurement designs that attempt to extract information from measurements and not only from theoretical predictions. In particular, geostatistical approaches that favor robust sampling designs and explicitly model the spatial structure of measurements are mentioned to be promising.

Additionally, Phillips *et al.* [11] state that theoretical models provide valuable physical insights about electromagnetic propagation. However, since most of these models are based on non-realistic assumptions, they need to be evaluated through experiments. Although the cost and effort for

conducting measurements increase in complex environments, the measurement-based approach has proven to be useful and productive.

B. PAPER OUTLINE

This paper provides a comprehensive survey of indoor channel models found in the literature, spanning more than 30 years of continuous research. The objectives of this survey are:

- to introduce the main propagation characteristics for wireless communications in indoor scenarios;
- to survey the available in-building mathematical models in the literature and propose a new taxonomy to analyze them, providing a complete and updated overview; and
- to outline remarks for indoor radio propagation modeling.

The remainder of this paper is organized as follows, noting that the reviewed literature is limited to narrowband systems. In Section II, the main theory to study the indoor propagation phenomena is covered. A thorough explanation and review of in-building radio wave propagation models is presented in Section III, as well as a new classification for indoor path

loss models is introduced. Concluding remarks are presented in Section IV. Finally, in section V, research opportunities and future developments are discussed.

II. INDOOR RADIO WAVE PROPAGATION

In order to understand the nature of the models that will be presented, several definitions need to be highlighted, underlying the theory that introduces the basic concepts of indoor radio propagation.

A. PATH LOSS AND PROPAGATION MECHANISMS

The path loss between a pair of antennas is the ratio of the transmitted power to the received power, usually expressed in decibels. It includes all the possible elements of loss associated with interactions between the propagating wave and any objects between transmitting and receiving antennas. As a result of radio wave propagation over a channel, the radio signal is attenuated due to path loss, as well as fading processes occur [16].

The basic components for performing an analysis of a wireless communication system are illustrated in Fig. 2 (considering the losses and gains in the system). In order to quantify link performance, a link budget of the system is required, taking into account the basic elements shown in Fig. 2.

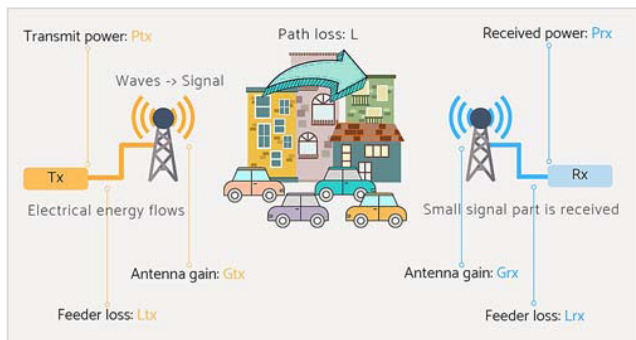


FIGURE 2. Elements of a wireless communication system.

The mechanisms behind electromagnetic wave propagation are diverse but can generally be attributed to: reflection, refraction, diffraction and scattering [17, Ch. 3]. The path between transmitter and receiver inside buildings can be either line-of-sight (LOS) or non-line-of-sight (NLOS). When radio systems do not have a LOS path and the presence of walls and floors causes severe diffraction loss and multiple reflections from various objects, the electromagnetic waves travel along different paths of varying lengths. The interaction between these waves causes multipath fading at a specific location, and field strength decrease as the distance between the transmitter and receiver increases.

1) REFLECTION, REFRACTION AND DIFFRACTION

When a propagating electromagnetic wave impinges upon an object that has very large dimensions compared to the wavelength of the propagating wave, reflection and refraction occur (illustrated in Fig. 3). As a result, two new waves are produced, each with the same frequency as the incident wave.

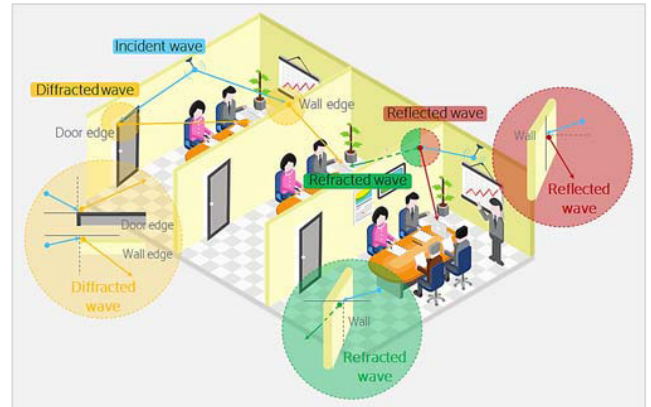


FIGURE 3. Propagation mechanisms: Reflection, refraction and diffraction.

The reflected wave arises from the surface of the floor and roof, from walls, windows and furniture in an enclosed space.

When reflection occurs, the wave may also be partially refracted. Reflection and refraction coefficients are functions of the material properties of the medium and generally depend on wave polarization, angle of incidence and frequency of the propagating wave.

Wall and floor materials have a strong influence on the propagation losses and, thus, in the amount of signal that can be received after going deeper into a building as a result of refraction.

In NLOS propagation, a signal transmitted through a wireless medium reaches the receiver via one or more indirect paths, each having different attenuations and delays. NLOS propagation is responsible for coverage behind walls and other obstructions inside buildings—shadow regions—and this is possible thanks to diffraction that occurs when the radio path between the transmitter and receiver is obstructed by a surface with sharp edges, i.e., a door or a wall edge represented in Fig. 3. The waves produced by the obstructing surface are present throughout space and even behind the obstacle, giving rise to propagation into the shadow region.

2) SCATTERING

Similar to reflection, scattering occurs when the wave is reflected, but in this case, the surface consists of irregularities with dimensions that are smaller compared to the signal wavelength and where the number of obstacles per volume unit is large, such as a rough surface like the one shown in Fig. 4. Therefore, the reflected wave becomes scattered from many positions on the surface, broadening the scattered energy [4, Ch. 4], and it increases the energy radiated in other directions. Scattering can become much more significant as frequency increases, such as in the millimeter-wave band for 5G.

3) WAVEGUIDING

This effect is the result of reflections and refractions given in areas such as corridors or other narrow gaps between walls, which wind up carrying the wave along the waveguide to

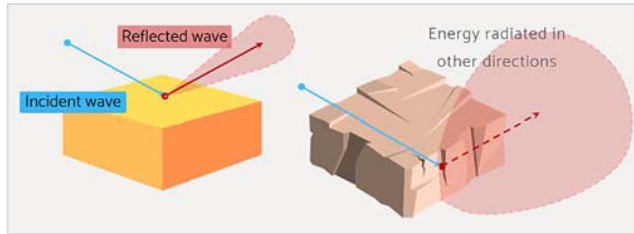


FIGURE 4. Scattering: rough surface.

the receiver. Waveguiding depends on incident angles, material types and distances between walls, and it produces the so-called waveguiding gain [4, Ch. 4], increasing penetration depth along corridors.

In [18], parameters affecting large-scale path loss including waveguiding were analyzed. Under certain conditions, stronger constructive interference can be produced resulting in a better waveguiding effect in the corridor, especially with an increase in transmitter height from 1.6 m to 2.3 m.

B. FAST FADING AND SHADOWING

Multiplicative noise arises from median path loss, shadowing and fast fading processes (Fig. 5) that a wave propagated from the transmitter antenna to the receiver antenna suffers in the propagation link. These processes depend on both the relative position of the elements of a wireless system and the obstructions in the channel. Fast fading results from rapid signal variations on the scale of half-wavelength and is often removed by filtering.

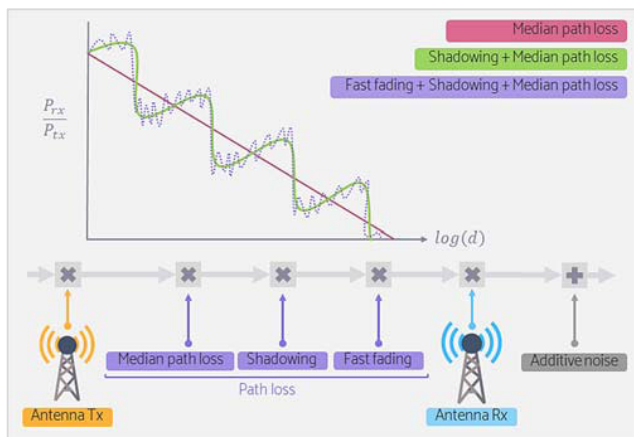


FIGURE 5. Path loss process.

For indoor channels, shadowing occurs due to the large variability of obstructions present in the venue, which results in a received power that fluctuates randomly over time. This behavior is described by a zero-mean log-normally distributed random variable.

Statistical characterization of the received signal variations for both fading and shadowing is useful in the design of transceivers. Thus, knowledge of large-scale variations is

useful in power control techniques and in the evaluation of the coverage service area, as stated in [19].

Common fading models have been characterized in terms of multipath effects related to Nakagami-m, Rayleigh, and Rician distributions [20], [21]. The Fisher-Snedecor F distribution has been recently proposed as a more accurate and mathematically-tractable composite fading model than these traditional established models to describe the combined effects of shadowing and multipath fading in wireless communications [22]–[24]. An example of this is reported in [25], where Yoo *et al.* found that the F distribution can provide a better fit to the experimental data obtained for device-to-device communications within an open office area and an outdoor environment at 5.8 GHz, as compared with the well-established KG model.

C. PARAMETERS AFFECTING RADIO PROPAGATION INSIDE BUILDINGS

According to recommendation ITU-R P.1238-10 [26] propagation impairments in an indoor radio channel are caused mainly by:

- Reflection from, and diffraction around, objects (including walls and floors) within the rooms.
- Transmission loss through walls, floors and other obstacles.
- Channeling of energy, especially in corridors at high frequencies.
- People mobility and objects in the room, including possibly one or both ends of the radio link.
- Temporal and spatial variations of basic transmission loss.
- Multipath effects from reflected and diffracted components of the wave.
- Polarization mismatch due to random alignment of the mobile terminal.

The impact of various parameters affecting radio wave propagation inside buildings is shown in Fig. 6 and is discussed in the next subsections.

1) INDOOR BUILDING GEOMETRY

The extent of coverage inside a building is well-defined by its geometry, and the limits of the building itself affect propagation of signals [26]. The building wall structure frequently has several layers, setting up multipath interference and associated resonances within the structure. These can be analyzed by treating each layer as a section of a transmission line, with a characteristic impedance determined by the wave impedance, the frequency and the angle of incidence [4].

The attenuation introduced by a single layer in the building only slightly reduces the received power. However, the accumulation of such effects has the potential to produce significant radio shadows and may result in other propagation mechanisms affecting in-building radio propagation. Table 2 shows some relevant works that have considered indoor building geometry as a key component to analyze significant effects on propagation.

TABLE 2. Relevant works that consider indoor building geometry.

| Indoor building | Year | Frequency | Contribution |
|--|------|------------------|---|
| Glass door; Composite walls (with studs) [28]. | 2002 | 60 GHz | Depending on measured received locations through glass door and interior walls showed power losses from 8.8 to 35.5 dB through two composite walls and a loss of 2.5 dB through a glass door. The quantity and position of the metallic studs within the composite wall are important factors to determine the penetration loss. |
| Inhomogeneous periodic walls [29] | 2008 | 1.0 GHz | Walls are discretized into finite-size building blocks and a finite-difference time-domain (FDTD) approach is used to compute their electromagnetic response in a periodic arrangement as well as in corner and terminal locations. |
| Glass windows; Drywall; Concrete corners [30]. | 2011 | 1.8GHz | When shelves and books are included against internal walls, reflected paths are attenuated to such an extent that diffraction around the corners of the concrete shaft is observed to dominate propagation into the shadow regions. The inclusion of metal window frames perturbs specular reflection from the glass. |
| Multi-floor [31]. | 2013 | 900MHz 2.4GHz | Six different multi-floor building structures that have a stone block type outer wall and are generally described as university, hospital and office type buildings are considered. |
| Short and long corridors; Wood, glass and mixed doors; Gypsum walls; Textile-wood-glass walls, divisions and metallic cubicles [32]. | 2018 | 915MHz | The attenuation in short corridors is lower than in long corridors, with the variation of around 3 dB and peaks up to 7.96 dB. |

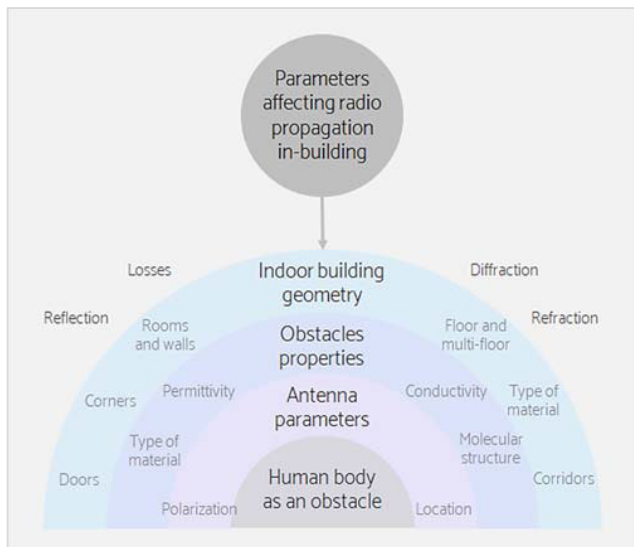


FIGURE 6. Parameters affecting indoor radio propagation.

2) OBSTACLE PROPERTIES

The constitutive parameters of building materials are frequency-dependent, even for relatively uniform walls, due to the specific molecular structure of the materials used. For a lossy medium—highly conductive—or for very high frequencies, the skin surface depth is small, thus most of the current stays on the surface of the material and the penetration depth is small. Therefore, a window with metallization will have a high current on its surface near an antenna but will allow little wave penetration. Conversely, even a highly conductive material that is thinner than its skin depth will still allow energy to pass through.

According to ITU-R recommendations, propagation prediction models may need the information on the complex

permittivity of building materials and of building structures as basic input data (ITU-R P.2040 [27]). Consequently, all possible obstacle properties need to be considered between the transmitter and receiver antenna. In Table 3, some relevant works that take into account these parameters are described in detail.

3) ANTENNA PARAMETERS

A wireless system design aims at delivering optimal signal distribution to all areas inside a building. This power distribution among propagation modes is governed by the position of the transmitter antenna [38]. Over the years, researchers have studied antenna performance and techniques to overcome some restrictions for wireless indoor system design that have been identified, as depicted in Table 4.

For several decades, multiple-input multiple-output (MIMO) antenna technologies have been considered as a promising next-generation technology due to its ability to offer adaptive beamforming gains and spatial multiplexing, substantially increasing capacity for wireless links and especially inside buildings where rich multipath can contribute to higher gains. Therefore, studies that consider this technology have been reported, such as in [39], where the authors survey three new multiple antenna technologies that can play key roles in beyond 5G networks: cell-free massive MIMO, beamspace massive MIMO, and intelligent reflecting surfaces. The advantages of cell-free massive MIMO systems in terms of their energy and cost efficiency are quantified in [40].

4) THE HUMAN BODY AS AN OBSTACLE

The movement of people and objects within a room causes temporal variations of the indoor propagation characteristics. This variation, however, is very slow compared to the

TABLE 3. Relevant works that consider electromagnetic properties.

| Obstacle and property | Year | Frequency | Contribution |
|--|------|-------------------------------|--|
| <ul style="list-style-type: none"> Slab wall and complex wall. Permittivity [33]. | 2004 | 90MHz | The patterns of the local mean power distribution for the complex wall cases are quite different from that of the slab and effective wall cases. The areas covered by power contours with same power levels are also different by as much as 40% to 50%. |
| <ul style="list-style-type: none"> Single floor. Temperature and relative humidity [34]. | 2008 | 2.4 GHz | A direct influence of relative humidity on signal attenuation is identified. |
| <ul style="list-style-type: none"> Metallic. Reflective insulation [35]. | 2011 | 70, 200, and 600 MHz | The effects of reflective (metallic) insulation on indoor digital television (DTV) signal reception in rural houses were investigated. Simulation results indicated that under NLOS conditions, the presence of reflective insulation may significantly degrade indoor signal reception and causes a large variation of signal level inside a house. |
| <ul style="list-style-type: none"> Solid concrete block wall; Cavity concrete block wall; Red brick wall; Plasterboard wall; Tile roof; Slate roof; Modern windows. Conductivity; Thickness [36]. | 2018 | Range from 400 MHz to 2.7 GHz | <p>A maximum attenuation of around 50 dB is observed for windows.</p> <p>Difference in the polarization responses for the windows can be observed. Reasons for the diversity in the results are different composition and structure of the glasses, different metal coating material (conductivity and thickness), and a difference in the number of coated glasses.</p> <p>Due to the largest total thickness, the highest delay is found for cavity concrete block, while the small thickness of slates and plasterboard results in low delay.</p> |
| <ul style="list-style-type: none"> Plaster slabs(wall); Aluminum plates (wall). Permittivity [37]. | 2019 | Range from 26 to 40 GHz | The deduced incident angle highly depends on the material permittivity. |

TABLE 4. Relevant works that consider antenna parameters.

| Parameter | Year | Frequency | Contribution |
|---|------|-------------------------------|---|
| Polarization [41]. | 2007 | 10.5GHz | Horizontal polarization mitigates the effects of rays reflected from the human body. |
| Mean effective gain (MEG) [42]. | 2008 | 2.1975 GHz | <p>A method is investigated for evaluating the MEG of mobile antennas in LOS street microcells with low base station antennas.</p> <p>The proposed statistical distribution model is valid and effective in both estimating the MEG values of mobile antennas and designing the LOS street microcell systems with low base station antennas.</p> |
| Location [43]. | 2008 | 1800 MHz | Critical regions are identified, where a new transmitter should be placed to provide a better signal for indoor coverage. |
| Radiation pattern [44]. | 2013 | Range from 2 GHz to 6 GHz | <p>Signal attenuation can be reduced by using antennas with suitable radiation patterns at appropriate locations.</p> <p>While omnidirectional antennas offer better signal coverage in NLOS tunnel regions, directional antennas perform better in LOS regions.</p> |
| Elevation; Azimuth [45] | 2017 | 2.52 – 2.54 GHz band | The authors provide the elevation and azimuth angular spreads for the measurements done in an urban macro-cellular and urban micro-cellular in an outdoor-to-indoor (O2I) environment and study their dependence on the user equipment (UE) height. |
| Location; Azimuth angle [18]. | 2018 | 14 GHz 22 GHz | Azimuth angle is considered at the receive side, where the directional horn antenna was rotated over azimuth angles in 10° azimuth steps. |
| Polarization: vertical-vertical (V-V) and horizontal-horizontal (H-H) [36]. | 2018 | Range from 400 MHz to 2.7 GHz | <p>The attenuation introduced by brick (5.24 dB for V-V and 5.54 dB for H-H) and solid block wall (4.32 dB for V-V and 4.36 dB for H-H) is not very significant and there is no advantageous polarization for any of these materials.</p> <p>Plasterboard introduces negligible attenuation with no polarization dependence.</p> <p>Strong polarization dependence of the attenuation is observed with significant transmission losses.</p> |
| Radiation pattern; MIMO [46]. | 2020 | 3 to 4 GHz band | An analysis of the effect that the radiation pattern of the antenna element that makes up the base station array has on the structure of multi-user MIMO channels is presented. |

data rate likely to be used and can, therefore, be treated as virtually a time-invariant random variable [26]. Apart from people in the vicinity of the antennas or in the direct path,

the people mobility in offices and other locations in and around the building has a negligible effect on propagation characteristics.

TABLE 5. Relevant works that consider human body effects.

| Human body effect | Year | Frequency | Accuracy | Considerations |
|--|------|------------------------------|---|---|
| Excess loss due to scattering, blockage and fades due to motion [51] | 2006 | 2.45 GHz | Fading values: 8 dB - 10 dB | Human body shadowing was studied when a person periodically crosses the link about 0.7 m from the receiving antenna for the radio links. |
| Reflections from body parts [52] | 2010 | 3 - 10 GHz | Standard deviation σ (path loss): 8 dB (PICA) and 6.7 dB (TSA) | The receiver was moved along the front part of the body. Thirty-three different positions were measured on the chest, legs and arms. Two different pairs of planar antennas were used, namely, CPW-fed planar inverted cone antennas (PICA) and miniaturized CPW-fed tapered slot antennas (TSA). |
| Human body influence depending on specific locations [53] | 2010 | 3.5 GHz | Power level decreases from 2 to 5 dB. | The spectrum analyzer used for measurements supports signaling mode, in which it can be set to record or stop automatically by signals captured, which can be used to reduce the influence of the human body. Despite this, the signaling mode is disabled so the influence of the human body can be investigated. |
| Body shadowing [54] | 2014 | 900, 1800, 2100 and 2400 MHz | Mean error (path loss): 900 MHz – 0.8 dB, 1800MHz – 1.96 dB, 2100 MHz – 1.49 dB and 2400 MHz -0.56 dB | The body shadowing parameter was computed as the value of mean number of persons per m ² . |
| Multiple human body shadowing of multipath [55] | 2019 | 4.7 GHz and 66.5 GHz | The RMS error of the propagation loss estimation model (with human body effects) and the measured value improved by about 1 dB on average | Measurements were performed around a wicket gate of Kamioka Station, where about 140,000 people passed through it a day. Many human bodies move in the measuring environment, and since there is nothing constructed between the transmitting and receiving sounds, only the human body obstructs the distance between the transmitting and receiving sounds. |

Many researchers have quantified the human body effect as an obstacle in radio propagation for indoor. Seesai *et al.* [47], observed that body shadowing leads to lower signal strength and more delay time, directly impacting high data rate applications for signal transmission. When the direct path is shadowed by a person, the attenuation generally increases by more than 20 dB [48]. In the project COST action 231, the authors proposed a stochastic model which reproduces a succession of realistic typical human movements performed in a random manner [49].

Other results confirm that human bodies are significant obstacles (and reflectors) for millimeter-wave propagation (60GHz). The movements within the channel cause a problematic “shadowing effect,” especially when the direct path is obstructed. For 2.45, 5.7 and 62 GHz, the propagation channel is at risk from temporal fades caused by people’s movement [50], where density and mobility are essential parameters to be considered.

Efforts have been made to develop models that account for human body effects. Ghaddar *et al.* [41] demonstrated that the presence of the human body might be approximated by a conducting circular cylinder at microwave frequencies. To validate the model, vertically- and horizontally-polarized continuous wave measurements were performed at 10.5 GHz between two fixed terminals inside a room along with the presence of an obstacle—person or metallic cylinder—moving along predetermined parallel and perpendicular crossing paths with respect to the LOS direction. Results indicate that there is a strong correlation between the effects of the human body and those of a conducting circular cylinder. Table 5 summarizes characteristics and outcomes

reported in the literature about the indoor path loss models that consider human body effects.

III. INDOOR RADIO WAVE PROPAGATION MODELS

Interference management is at the heart of a suitable wireless propagation prediction, and it is essential for maintaining a desirable throughput while minimizing the impact of interference. The goal of channel modeling is to provide accurate mathematical representations of radio propagation to be used in radio link and system simulations for the system deployment modeling.

In order to meet indoor design demands in an efficient way, many models have been proposed for ensuring system performance, since predictions will be closely related to real values. As a result of this review process, Fig. 7 shows a new classification for indoor channel models, grouping them into two major categories and six subcategories that provide a complete and updated overview. Various types of indoor environments represent hotspot areas to provide radio coverage on public or private buildings, e.g., residential venues, airports, schools, libraries, universities, shopping centers, restaurants, offices, hotels, factories, tunnels, etc. Most of these buildings are considered in the surveyed models and they are reported as target areas in the relevant works stated for empirical, physical, hybrid and outdoor-to-indoor models.

A. GENERAL CASES

1) EMPIRICAL MODELS

These models are based on measurements and observations that are made under different conditions to obtain valuable and building-specific information. Their accuracy depends

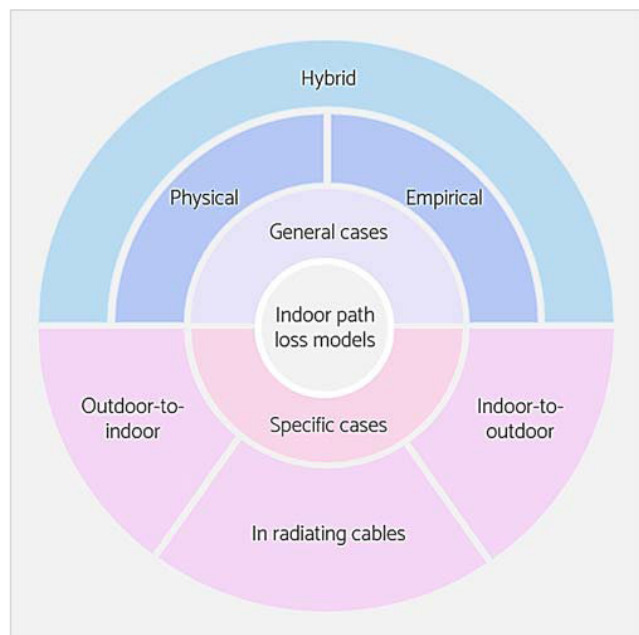


FIGURE 7. Indoor path loss models classification.

not only on the results of measurements but also on the similarity of the environment (measured vs. predicted). Model parameters are tuned with measurements to account for building or site details that otherwise could not be obtained.

Empirical models characterize wave propagation in terms of the distance between transmitter and receiver antenna, operating frequency, antenna heights and angles, number of walls and floors, etc. These models mainly focus on finding path losses from measured data only.

Numerous empirical modeling approaches consider reference models to provide an initial mathematical base, e.g., both the distance power-law model and distance-dependent path loss models are classical references, as the Okumura-Hata is for outdoor. In the case of the distance-dependent path loss model not only the distance between the antennas is taken into account—such as the power-law model [17, Ch. 3]—but also a reference distance (located in the far-field of the radiating antenna [56, Ch. 3]) is considered. Table 6 shows a summary of empirical models published in the literature. Including a specific reference model on each case. Additionally, the standard deviation of the prediction error, σ , is presented as a metric for comparison between measured and modeled data.

According to [32], theoretical models have a high prediction error percentile (average error is the difference between calculated and measured attenuation in [32]), mainly the one-slope model with values between 12% and 27%. Log-distance and ITU models have a better performance for indoor, with different obstacles and corridors considered. An exception for this high error behavior is the empirical model proposed by Morocho-Yaguana *et al.* where the attenuation error is decreased by approximately 10 dB, meaning that the analyzed models have been optimized.

2) PHYSICAL MODELS

Physical models are based on Maxwell's equations to describe the behavior of the electromagnetic field, considering the propagation mechanisms involved. The results provided by physical models are therefore deterministic, i.e., if simulation characteristics remain unchanged the predictions yield the same or very similar results. Although physical models have higher accuracy than empirical, they have the disadvantage of a heavy computational load. Moreover, this high accuracy strongly depends on the accuracy and availability of building databases of the simulated scenarios.

Table 7 summarizes some of the most popular physical models published in the literature, where their principal characteristics are highlighted.

3) HYBRID MODELS

Hybrid models take advantage of the accuracy of physical models and the carefully calibrated radio measurements carried out in empirical models, thus combining the best of both approaches. On this basis, propagation models that combine measurements to adjust parameters that depend on specific building characteristics and consider physical principles for modeling radio wave propagation are known as hybrid models.

According to [26], detailed information of the building structure is necessary for the calculation of indoor field strength, such as in models for indoor prediction based on the uniform geometrical theory of diffraction (UTD) and ray-tracing techniques. These hybrid models combine empirical elements with the theoretical electromagnetic approach of UTD. The hybrid method contemplates direct, single-diffracted and single-reflected rays, and can be extended to multiple diffractions or multiple reflections as well as combinations of diffracted and reflected rays. By including reflected and diffracted rays, the basic transmission loss prediction accuracy is significantly improved.

Table 8 summarizes relevant hybrid indoor models found in the literature.

B. SPECIFIC CASES

1) OUTDOOR-TO-INDOOR (O2I) MODELS

Since 1998, Durgin *et al.* had in mind that measurements and models may aid the development of O2I residential communication wireless systems [84]. The high penetration loss of signals arriving from outdoors limits the range of the covered area inside a building and emphasizes the need for Heterogeneous Networks (HetNet) [85] in providing coverage for obstructed environments.

In accordance with the Small Cell Forum [86], HetNets are defined as “multi-x environment – multi-technology, multi-domain, multi-spectrum, multi-operator and multi-vendor. A HetNet must be able to automate the reconfiguration of its operation to deliver assured service quality across the entire network, and be flexible enough to accommodate changing user needs, business goals and subscriber behaviours”. Small

TABLE 6. Relevant works with empirical indoor models.

| Model Name | Frequency | Target area | Attenuation | Ref model | Antennas | σ | Considerations |
|--|-------------------|-----------------------------------|---|------------------------------------|---|---|--|
| Ericsson Multiple Breakpoint Model (1988) [57] | 900 MHz | Business office | Added isolation between the floors of 10dB | Only propagation measurements | - | - | Four breakpoints are included and both an upper and a lower bound on the path loss are considered. |
| Keenan-Motley Model (1990) [58], [59] | 900 - 1700 MHz | Multi storey office construction | 6dB per floor | Distance power law model | Rx - Dipole | - | Focuses on the physical properties of walls and floors located between transmitting and receiving antennas. |
| | | | | | | | |
| Attenuation Factor Model (1992) [60] | 914 MHz | Office building | 12.9 dB - 16.2dB per floor | Distance-dependent path loss model | Tx - Omnidirectional quarter-wave monopole Rx - Omni discone | 5.8 dB | The effect of building type as well as the variations caused by obstacles are considered. |
| | | | | | | | |
| ITU-R Indoor Model (1997) [61] | 900 MHz - 100 GHz | Residential; office; commercial | 1.8 - 2GHz: residential $4n^*$ dB; office $15+4(n+1)$ dB; commercial $6+3(n+1)$ dB; 900MHz: office: 9dB 1 floor; 19dB 2 floors; 24dB 3 floors; | Distance power law model | - | - | Only floor loss is accounted for explicitly and the loss between points on the same floor is included implicitly by changing the path loss exponent. * n : number of floors |
| | | | | | | | |
| Tuan Empirical Indoor Model (2003) [62] | 900 MHz - 5.7 GHz | University campus | - | - | Horn directional antennas | 6.08 dB at 2.45GHz | Key propagation mechanisms are considered through measurements and key parameters can be tuned using measurements. |
| | | | | | | | |
| Barbosa Indoor Model (2005) [63]; | - | 5 floors building of a university | - | Distance-dependent path loss model | Rx - monopole | 6.05dB | An empirical function (based on Padé approximant) is used, as well as a factor that describes the sign randomness. In [64], the authors employed this model at 2.6 and 3.5 GHz. |
| | | | | | | | |
| Empirical RMS delay spread model (2017) [65] | 2.5 - 2.69 GHz | Indoor stair; corridor; office | - | Distance-dependent path loss model | Tx and Rx - omnidirectional monopole antennas | - | The RMS delay spread is described as a linear function of the path loss, and a normal stochastic variable is introduced. |
| | | | | | | | |
| Morochu-Yaguana Empirical Model (2018) [32] | 915 MHz | University campus | 3 dB - 7.96 dB for short (<22m) and long corridors (>22m) | Distance-dependent path loss model | Tx and Rx - Yagi | Average measured attenuation data error of 2.5% | Loss coefficients for structures, shapes, materials and obstacles typical of a campus environment are provided. |
| | | | | | | | |

TABLE 7. Relevant works with physical indoor models.

| Model Name | Frequency | Target area | Complexity | Ref model | Antennas | σ | Considerations |
|---|------------------|-------------------------------|---|--|---|-------------------------------|---|
| Honcharenko-Bertoni Model (1992) [66] | 852 MHz | Hotel and office building | 40 min | Ray optic methods | Validation with measurements using dipole antennas | 4.4 dB ($d < 30m$) | Two principal mechanisms: attenuation due to walls and diffraction from obstacles near the floor and in the plenum, with additional diffraction around the corners, are considered. |
| | | | | | | | $E_T = \sum_i E_i e^{-jk\Psi_i}$ <p>E_T: total field at a receiving site, E_i: field magnitude, Ψ_i: phase of the i^{th} ray.</p> |
| Ray-Tracing Site-Specific Model (1994) [67] | 4 and 1.3 GHz | University campus | Parallel computing to allow multiple workstations | Ray-tracing | Tx and Rx - Omnidirectional biconical antennas | <5 dB | Deterministic model that is based on the theory of electromagnetic wave propagation. This algorithm predicts multipath impulse responses based on building blueprints. |
| | | | | | | | $E_i = E_o f_{ti} f_{ri} L_i(d) \prod_j \Gamma(\theta_{ji}) \prod_k T(\theta_{ki}) e^{-jkd}$ <p>E_i: complex field amplitude of the i^{th} ray at the receiver, E_o: reference field strength, f_{ti}: field amplitude radiation pattern of the transmitter antenna, f_{ri}: field amplitude radiation pattern of the receiver antenna, $L_i(d)$: path loss distance dependence for the i^{th} multipath component, $\Gamma(\theta_{ji})$: reflection coefficient, $T(\theta_{ki})$: transmission coefficient, e^{-jkd}: propagation phase factor due to path length ($k = 2\pi/\lambda$).</p> |
| Multichannel Coupling Prediction (2000) [68] | 1890 MHz | Office buildings | 20 min | Multi-channel Coupling (MCC) | Commercial base station for wireless telephones | - | The MCC method transforms the propagation problem into a linear system of coupled channels. The coupling coefficients that build the interaction matrix of the channels depend only on the geometry of the environment. Once these coupling coefficients are calculated the unknown power in the channels is easily calculated for different transmitter configurations. |
| | | | | | | | $P_\beta = c_{\alpha\beta} P_\alpha$ <p>P_β: power leaving the channel β at element A_k, P_α: power leaving at element A_j the channel α, $c_{\alpha\beta}$: energy coming from element A_j reaches element A_k by transmission, reflection or scattering at element A_j.</p> |
| AZB Algorithm for Efficient Ray Tracing (2000) [69] | 950 MHz | Third floor of a building | From 3 h to 10 min by using AZB algorithm | Ray-tracing | - | 6.79 dB – 8.33 dB | The Angular Z-Buffer (AZB) model is based on geometrical optics (GO) and the uniform theory of diffraction (UTD). |
| | | | | | | | $\vec{E}_r(O) = \{T_1(\theta_i) E_o(\theta, \phi) \hat{\theta} + T_1(\theta_i) E_o(\theta, \phi) \hat{\phi}\} \frac{\exp(-jk_o r)}{r}$ <p>\vec{E}_r: transmitted field, r: distance between the transmitter antenna and the observation point, $E_o(\theta, \phi)$ and $E_o(\theta, \phi)$: parallel and perpendicular components of the normalized radiation pattern of the transmitter antenna, θ and ϕ: spherical coordinates of the observation point referred to the coordinate system associated with the antenna, T_1 and T_1: parallel and perpendicular transmission coefficients.</p> |
| Lee Ray-Tracing Model (2001) [70] | 5.2 GHz | University campus | - | Ray launching techniques | Tx - Omnidirectional | - | Propagation effects such as reflection, transmission and diffraction are considered via UTD principles. |
| | | | | | | | $E_i = E_o f_{ti} f_{ri} L_{FS}(d) \left\{ \prod_j \bar{R}_j \prod_k \bar{T}_k \prod_l \bar{D}_l A_l(s_l, s_l') \right\} e^{-j\beta d}$ <p>L_{FS}: free space path loss, \bar{R}_j: reflection coefficient for the j^{th} reflection, \bar{T}_k: transmission coefficient for the k^{th} transmission, $\bar{D}_l A_l$: the diffraction coefficient and the spreading attenuation for the l^{th} diffraction, $e^{-j\beta d}$: propagation phase factor ($\beta = 2\pi/\lambda$ and d represents the unfolded path length).</p> |
| Ray-tracing model (2019) [71] | 5, 31 and 90 GHz | Corridors (University campus) | - | Ray-tracing, close-in free space reference distance (CI) path loss model and the floating-intercept (FI) path loss model | 30 and 90 GHz: Directional antennas 5 GHz: Omni-directional antennas | < 2 dB (LOS) < 5 dB (NLOS) | The ray-tracing model X3D in simulation software WI was applied, and the resulting data was post processed and compared with measurement results. Agreement between simulation and measurement results was generally good for average path loss, using both CI and FI models. |
| | | | | | | | $PL_{CI}(f, d) = FSPL(f, d_o) + 10n \log_{10} \left(\frac{d}{d_o} \right) + X_\sigma^{CI}$ $PL_{FI}(d) = \alpha + 10\beta \log_{10}(d) + X_\sigma^{FI}$ <p>$FSPL$: free-space path loss at 1 m, X_σ^{CI}: zero mean random variable with standard deviation σ. α: floating-intercept, β: slope of the line on the log scale, X_σ^{FI}: zero mean random variable.</p> |
| PGMM model [72] | 28 GHz | Indoor conference scenario | - | Normalized power weighted gaussian | *For validation Tx - Omnidirectional | - | A normalized power weighted GMM (PGMM) was introduced to model the channel multipath |

TABLE 7. (Continued.) Relevant works with physical indoor models.

| | | | | | | | |
|--|--|--|--|----------------------|-----------------|--|--|
| | | | | mixture model (PGMM) | Rx Horn antenna | | components (MPCs). With MPC power as a weighted factor, the PGMM can fit the MPCs in accordance with the cluster-based channel models. |
| $H_{n_r, n_t, l}^{3d} = \sum_{m=1}^{M_t} F_{Rx}^{3d}(\theta_{Rx, l}, \phi_{Rx, l}) A_{l, m}^{3d} F_{Tx}^{3d}(\theta_{Tx, l}, \phi_{Tx, l}) e^{j2\pi f_{d, l, m}}$ | | | | | | | |
| <p>$l \in \{1, 2, \dots, L\}$, L: number of the clusters, t: time, M_t: number of MPCs in the l^{th} cluster, Tx and Rx: the transmitting and receiving ends, F_{Rx}^{3d} and F_{Tx}^{3d}: transmitting and the receiving antenna responses, $A_{l, m}^{3d}$: polarization matrix, $f_{d, l, m}$: Doppler frequency, n_t and n_r: transmitting and receiving antenna index, $H_{n_r, n_t, l}^{3d}$: sum of the M_t channel MPCs in the l^{th} cluster.</p> | | | | | | | |

cells—in most cases, for indoor environments—have moved from being a relatively niche technology to fill gaps in coverage and capacity to the central enabler of the emerging HetNet and of 5G. This is the context for the publication of Small Cell Forum’s Release 7 [87], which provides a detailed technique for deploying the HetNet and self-optimizing network (SON) and for laying the groundwork for 5G.

SON network functions are widely recognized as key enablers of small cells. Therefore, in the Small Cell Forum’s Release 9 [88], the main focus described is SON functionality and performance with special attention to interoperability between small cells and macrocells.

O2I models characterize signal propagation inside buildings coming from an external base station, as illustrated in Fig. 8. O2I modeling becomes very relevant especially in situations where indoor coverage is desired at a reduced cost and capacity demands do not justify the deployment of an indoor cell. A summary of the most important O2I models are stated in Table 9.



FIGURE 8. O2I specific case.

Lee *et al.* [89] investigated the multipath dispersion characteristics of O2I propagation in the angular and delay domains. This study is based on field measurement data conducted at 32 GHz in two different office building sites: traditional building and thermally-efficient building.



FIGURE 9. I2O specific case.

2) INDOOR-TO-OUTDOOR (I2O) MODELS

Due to the fact that the deployment of femtocells over macrocells—Fig. 9—is currently considered as an attractive solution for extending the coverage area for indoor users, the interference to macrocell subscribers is a key parameter to consider for deploying these systems. To estimate this interference and to consequently ensure optimum network design and operation, studies in propagation I2O models are needed.

In an effort to evaluate the effects of architectural layouts on I2O channels Hamid *et al.* [96] developed a model that can be utilized to characterize this type of channel for femtocell deployments in large buildings—e.g. corporate offices—as well as residential houses. The channel model for the former was performed using exhaustive measurements at an academic facility with a large number of rooms. For the latter, ray-tracing was employed due to the challenges of performing extensive measurements at a statistically large number of different residential houses. By using complementary approaches in [97], Allen *et al.* did not focus their work on characterizing the channel but on facilitating femtocell network deployment through two empirical I2O path loss models derived from continuous-wave (CW) power measurements.

TABLE 8. Relevant works with hybrid indoor models.

| Model Name | Frequency | Target area | Ref model | Antennas | σ | Considerations |
|--|--|--|--|---|---|--|
| Reduced-Complexity UTD Model (1998) [73] | 900 MHz | University campus | Distance-dependent path loss model; angle-dependent of attenuation factor; UTD | Tx and Rx – omnidirectional antennas | From 20.8 dB (conventional model) to 6.7dB (proposed model) | Additional phenomena suggested by physical models is incorporated in the model, but still the straightforwardness of the empirical approach is retained. The model does not take account of reflected rays. |
| | $PL_D(d, \phi) = -10 \log \left[\sum_{m=1}^M (PL_{\perp}(d_m) PL_{\perp}(d'_m) \times D(d_m, \phi_m, d'_m, \phi'_m) ^2) + PL_{\perp}(d) \right]$ <p>M: number of corners in the building database, $D(d_m, \phi_m, d'_m, \phi'_m)$: diffracted fields, (d_m, ϕ_m): coordinates of the corner relative to the transmitter, (d'_m, ϕ'_m) coordinates of the receiver relative to the corner.</p> | | | | | |
| Measurement-Based Prediction MbP (2006) [74] | 1800 MHz | Old house and modern office building | Distance-dependent path loss model; Keenan–Motley (K&M) model | Tx and Rx – dual-band GSM directional indoor antennas | From 8.43 dB (K&M) to 1.96 dB (MbP) | Path loss is predicted in areas where other indoor models fail to do so. MbP tunes variations with the measurements that are used as part of the modeling process. |
| | $L_{50} = k_1 + 10n \log r + k_2 r$ $L_{50} = L_1 + 20 \log r + n_w a_w + n_f a_f$ <p>L_{50}: median path loss, k_1 and k_2: parameter to tune using the signal strength measurements, n_w and n_f: number of trespassed walls and floors, a_w and a_f: wall and floor factors to tune.</p> | | | | | |
| Hybrid Parabolic Equation-Integral Equation Indoor Model (2007) [75] | 2.45 GHz | Indoor scenario (rooms) | Parabolic wave equation (PE) | - | - | No validations |
| | $\bar{E}_i = \bar{E}_i^0 + \sum_{j=1}^N G_{i,j}^B k_0^2 \Delta \epsilon_j \bar{E}_j S_j$ <p>\bar{E}_i^0: incident electric field, $\Delta \epsilon_j$: Dielectric constant, $G_{i,j}^B$: Green function, S_j: total surface.</p> | | | | | |
| Novel large-scale path loss mode (2015) [76] | 28 and 73 GHz | Corridor, open-plan, and closed-plan (research center) | Close-in free space reference distance (CI); floating-intercept (FI) path loss model; alpha-beta-gamma (ABG) model | Tx and Rx – horn antennas | LOS: 10.4 dB (CI) 9.9 dB (CIF) 9.5 dB (ABG) NLOS: 12.5 dB (CI) 11.9 dB (CIF) 11.6 dB (ABG) | The results show that novel large-scale path loss models provided are simpler and more physically-based compared to previous 3GPP and ITU indoor propagation models that require more model parameters and offer very little additional accuracy and lack a physical basis. |
| | $PL_{CI}(f, d) = FSPL(f, d_o) + 10n \log_{10} \left(\frac{d}{d_o} \right) + X_{\sigma}^{CI}$ $PL_{CIF}(f, d) = FSPL(f, d_o) + 10n \left(1 + b \left(\frac{f - f_o}{f_o} \right) \right) \log_{10} \left(\frac{d}{d_o} \right) + X_{\sigma}^{CIF}$ $PL_{ABG}(f, d) = 10\alpha \log_{10} \left(\frac{d}{d_o} \right) + \beta + 10\gamma \log_{10} \left(\frac{f}{1 \text{ GHz}} \right) + X_{\sigma}^{ABG}$ <p>b: intuitive model-fitting parameter that represents the slope of linear frequency dependency of path loss, f_o: fixed reference frequency that serves as the balancing point or center of the linear frequency dependency of the path loss exponent (n). α and γ: coefficients that describe the distance and frequency dependence on path loss. β: optimized offset parameter that is devoid of physical meaning, X_{σ}^{ABG}: shadowing or large-scale signal fluctuation.</p> | | | | | |
| Time-Variant Fading Statistics Model (2015) [77] | 3.8 GHz | University campus (office building) | Hidden Markov Model; geometry-based second-order statistics; distance-dependent path loss model | Tx and Rx – custom-made dipole antennas | - | The transitions between the fading states by means of a hidden Markov model parameterized from measurements are characterized. The investigated environment was located on the first floor of an office building and consisted of typical offices along a corridor separated by brick or plasterboard walls. |
| | $L = \Lambda_0 + \eta \log_{10} \left(\frac{d}{d_o} \right) + \bar{S}$ <p>Λ_0: deterministic path-loss at the reference distance $d_o = 1$ m, \bar{S}: mean shadowing, η: path loss exponent.</p> | | | | | |

TABLE 8. (Continued.) Relevant works with hybrid indoor models.

| | | | | | | |
|---|---|--|---|--|--|---|
| Measurement-based spatio-temporal statistical channel model (2015) [78] | 60 GHz 70 GHz | Large office rooms, shopping mall, and station scenarios | Power decay and shadow fading model | Tx – Horn antenna Rx – Bicone antenna | ≈ 1 dB (empty office) ≈ 2 dB (station scenarios) | The proposed framework covered not only specular but also diffuse signals to provide a complete description of the channel. The validity of the model was demonstrated by means of pathloss and delay spread. |
| | $\hat{\alpha}_l = P_0 \exp(-\tau_l / \beta_0) \xi$ <p>P_0: initial pathloss, β_0: power decay factor, ξ: normal random variable, τ_l: delay time.</p> | | | | | |
| Optimized Ray Tracing Path Loss Model (2017) [79] | 2.4 GHz | Wide corridor | Ray-tracing deterministic N ray model; path loss model (link budget) | Tx - Router Cisco Rx - Tablet | From 11.47 dB (N ray model) to 10.96 dB (modified ray-tracing model) | The accuracy of ray-tracing for estimating the path loss for indoor NLOS propagation is improved using this approach. The ray-tracing model is modified to have a better agreement with measured data. |
| | $PL_{(nray+Diff+s)} = 10 \log_{10} \left(\frac{P_t}{P_{r-nray}} \right) + L_{epstein}(N) + PL_s$ <p>P_t: transmitted power, P_{r-nray}: received power for an N ray model, $L_{epstein}(N)$: three glass partitions (Epstein Peterson method), PL_s: path loss due to scattering.</p> | | | | | |
| Ray-tracing-based simulation (2017) [80] | 26 GHz | Center hall (university) | Third dimension (3D) ray-tracing | Tx and Rx – Customized biconical antennas (3 types of virtual antenna array topology MIMO) | Mean error of 3.5 dB | The 3D ray-tracing simulator is calibrated based on the provided indoor measurement results and it is observed that the measurement and the ray-tracing-based simulation results have reached a good agreement. |
| | $PL = -10 \log_{10} \left(\frac{1}{N_f} \sum_{i=1}^{N_f} H(f_i) ^2 \right)$ <p>$H(f_i)$: channel transfer function, N_f: number of the measured frequency points.</p> | | | | | |
| Extended S-V model (2017) [81] | 60 GHz | Office environment | Extended Saleh-Valenzuela (S-V) model | Tx and Rx – horn antennas | - | The measured channel has been modeled based on an angular extended S-V model. The authors found that azimuth departure angles are highly related to antenna position and the measurement environment, while the elevation departure angles are more related to antenna height difference. |
| | $h(t, \phi_{tx}, \theta_{tx}) = \sum_i A^{(i)} C^{(i)}(t - T^{(i)}, \phi_{tx} - \Phi_{tx}^{(i)}, \theta_{tx} - \Theta_{tx}^{(i)})$ <p>$h(t, \phi_{tx}, \theta_{tx})$: Channel impulse response for the channel model in multiple-input single-output, ϕ_{tx} and θ_{tx}: azimuth and elevation angles at the Tx, $A^{(i)}$ and $C^{(i)}$: channel coefficient and channel gain for the i^{th} cluster, $T^{(i)}, \Phi_{tx}^{(i)}$ and $\Theta_{tx}^{(i)}$: time-angular coordinates of the i^{th} cluster.</p> | | | | | |
| Wireless sensor network model (2018) [82] | 2.4 GHz and 900 MHz | University campus (laboratory) | Two-ray ground reflection model; distance-dependent path loss model | Tx and Rx – dipole antennas | RMSE: 3.76 (50cm from Tx at 2.4 GHz); 5.05 (50cm from Tx at 900 MHz) | Frequency and three-dimensional link trajectory are considered as key parameters in evaluating path loss. The authors highlighted the effect of height on path loss exponent by means of various measurements taken indoors. |
| | $PL = 48.64 + 10n \log(f) + 10n \log(d) - n \log(h_t) - n \log(h_r) + X_\sigma$ <p>h_t and h_r: heights of the transmitter and receiver, X_σ: is determined by studying the theoretical values and the path loss measurements.</p> | | | | | |
| mmWave path loss model (2019) [83] | 73 GHz | University and airport environments | Close-in reference distance model (CIM); floating-intercept model (FIM) | Tx and Rx – directional horn antenna | - | Results show that the path loss exponent estimated from the CIM is very close to that of the free-space path loss model, while the FIM provides a better fit to the measurement data. |
| | $PL_{CIM}(d) = PL(d_o) + 10n \log_{10} \left(\frac{d}{d_o} \right) + X_0$ $PL_{FIM} = \alpha + 10\beta \log_{10}(d) + X_0$ <p>$PL(d_o)$: close-in free space path loss, d_o: close-in free space reference distance, X_0: normal random variable with mean 0 dB and standard deviation σ. α: floating intercept, β: linear slope.</p> | | | | | |

TABLE 9. Relevant works with O2I models.

| Model Name | Frequency | Target area | Ref model | Antennas | Penetration loss | Considerations |
|--|--------------------------------|---|--|---|---|---|
| Taga-Miura Model (2002) [90] | 8.45 GHz. | Department store | Penetration loss model; loss attenuation model; propagation loss model | Tx - Omnidirectional (d to building <=150m) and directional (d = 300 m) | 17.2 dB | The direct path as well as those radio waves propagating through the structural openings along the walls are considered. Measured propagation loss is about 20 dB larger than predicted at positions beyond 120 m. |
| | | | | | | |
| Broadband Wireless Access (BWA) Penetration Model (2004) [91] | 2.53 and 2.48 GHz | Residential houses; modern apartment complex | COST 231 model; distance-dependent path loss model | - | 3 - 3.5 dB (wooden and stucco walls); 1.2 dB (window wall) | The BWA penetration model is based on measurements for various buildings in USA, considering the impact of wall material, angle of incidence and receiver antenna height. |
| | | | | | | |
| Ichitsubo-Okamoto Outdoor-to-Indoor Model (2009) [92] | 810 MHz, 2.2, 4.7 and 8.45 GHz | Urban area | COST 231 model | Tx and Rx – Dipoles (sleeve antennas) | 10 dB *there is no frequency dependence of the penetration loss in the band evaluated | A penetration loss prediction formula is proposed, which is derived from measurements. It is based on measurements of the propagation loss on 71 floors in 17 buildings. RMSE: 7.7 dB |
| | | | | | | |
| Hybrid TDPE/FDTD of Site-Specific Model (2018) [93] | 300 MHz | Island environment *Only simulation – no measurements | Time-domain parabolic equation/finite-difference time-domain (FDTD) method | - | - | Through a hybrid time-domain parabolic equation/FDTD method for site-specific venues, radio wave propagation was modeled in a geo-based O2I scenario. Far lower computational cost than with a pure FDTD solution is obtained. |
| | | | | | | |
| Statistical O2I Model (2019) [94] | 27.85 GHz | University campus | Fourier resolution techniques, measurements | Tx and Rx - phased array antennas. Rx – omni and directional antennas | 10.6 – 25.2 dB* strongly depends on the angle of incidence | Statistical models for path loss, delay spread, and angular spread are provided. |
| Cluster-based model for azimuth/elevation power spectrum APS/EPS (2019) [95] | 3.5 GHz | Modern business district | Spatial-temporal channel impulse response (CIR) model | Tx and Rx - array antennas | - | The transmitter was placed on the rooftop of a building to emulate a base station and the receiver was moved in the corridors on different floors in another building to emulate user equipment. Based on measurement results, the lifted-superposed Laplace distribution (LS-Laplace) function and lifted-superposed normal distribution (LS-Normal) function to model the APS and EPS are proposed, respectively. |
| | | | | | | |

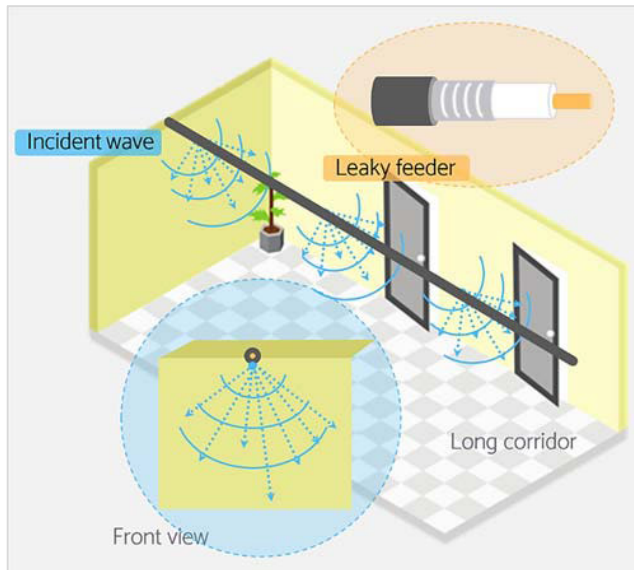


FIGURE 10. Radiating cable used in a building.

When field prediction for indoor base stations or access points is needed both inside and around the building, e.g., for interference assessment and for fingerprinting localization purposes, the model proposed by Degli-Esposti *et al.* in [98] can deliver predictions with good accuracy, based on a combination of a two-parameters propagation formula and a multi-wall model. The model is validated versus both ray-tracing and measurements in different environments, which exhibits good performance in all cases at a small fraction of the ray-tracing computation time.

3) MODELS FOR PROPAGATION IN RADIATING CABLES

Radiating cables or leaky feeders are an alternative solution to provide coverage in challenging enclosed spaces such as tunnels, large corridors or underground mines, as shown in Fig. 10. The cable is leaky, it has gaps or slots in its outer conductor to allow the radio signal to leak into or out of the cable along its entire length, functioning as an extended antenna, making it well adapted to long narrow indoor environments such as corridors, elevators or tunnels [99].

Models for propagating cables have many contributions in wireless systems, some of which are as follows:

- Provide coverage in a small indoor environment: measurements carried out along a corridor in frequencies from 262 MHz to 1226 MHz showed that the leaky feeder is appropriate for coverage in thin indoor environments, which can contribute to the strengthening of the received signal [100].
- Contain signal strength in a better way than a distributed antenna system: in [101], Stamopoulos *et al.* made a comparison of the use of both systems—radiating cable and distributed antenna system (DAS)—to provide coverage in a building and it is clear from their analysis that the radiating cable contains signal strength in a better way than a distributed antenna system. This is due to the characteristics of the radiating cable to provide more

uniformly distributed coverage, avoiding leakage peaks arising from particular antennas in DAS.

- Enable real time localization: in [102] Moschevikin *et al.* and in [103] Serezhina *et al.* studied the possibilities to use leaky feeders also for Time-of-Flight (ToF) based real time localization in such linear topologies, like tunnels, but possibly also for two dimensions (2D) localization. As a general result, leaky feeders might be useful for ToF-based localization using Chirp Spread Spectrum Technologies. However, in [102] they realized that additional signal processing and filtering is required to eliminate the additional variations from the different propagation speeds in the cable and in the air, and the different available propagation paths.

Table 10 summarizes considerations of radiating cable models reported in the literature.

C. INDOOR RADIO PROPAGATION RESEARCH PROJECTS

A general description of COST 231, WINNER II and 3GPP projects are presented below in order to mention the principal projects that were conducted to obtain results about indoor radio propagation modeling.

1) COST 231 [49]

Based on empirical and physical propagation models, the COST 231 project presented adjusted models that were based on propagation measurements, including:

- Empirical models: one-slope model (ISM), multi-wall model (MWM) and linear attenuation model (LAM).
- Physical models: ray launching model (RLM) and image approach method (IAM).
- Frequency: 850, 1800 and 1900 MHz.
- Target areas: office buildings, shopping centers and factories.
- Antennas: Omnidirectional.
- Considerations: the indoor environments were divided into four categories (dense, open, large and corridor) and internal walls are made of thin wood panel.

This model has been suggested in cases where a LOS path exists between a building facade and the external antenna, i.e., single floor propagation. For NLOS, the model relates the loss inside a room to the loss measured outside of it, on the side nearest to the wall of interest, i.e., multi-floor propagation.

Fig. 11 and Fig. 12 summarize the results (standard deviation of prediction error) for the adjusted models taking measurements conducted by Alcatel, TUW and VTT in [49]. The advantage of the MWM and the physical models—IAM and RLM—was most clearly seen in the case when the transmitter and receiver were on different floors. The performance of the ISM and LAM is poor because they only consider the distance and not the number of penetrated floors.

2) WINNER II [107]

The generic WINNER II channel model follows a geometry-based stochastic channel modeling approach, which allows

TABLE 10. Relevant works with models for propagation in radiating cables.

| Model Name | Frequency | Reference model | Penetration loss | σ | Considerations |
|---|----------------|--|---------------------|------------------------------------|--|
| Zhang Model (2001) [104] | 2.0 GHz | Distance power law model; propagation loss (link budget) | 9.9 dB (brick wall) | 1.88 dB (corridor); 1.98 dB (room) | Coupling and longitudinal losses of the cable are considered. Propagation around the cable termination is not clearly specified. |
| | | | | | |
| Carter Model (2006) [105] | 850 MHz | Friis transmission formula; Keenan-Motley model | 5 dB (complex wall) | 1.65 dB - 2.14 dB | The radiating cable is modeled as a line source and waves are spread in a cylindrical surface. A radiating cable straight section is considered. |
| | | | | | |
| Seseña-Aragón-Castañón Model (2013) [106] | 900 - 2500 MHz | Paths from the rays that are perpendicular to cable axis; distance power law model | - | 2.2 dB - 4.6 dB | The modeling of some key propagation mechanisms—reflections, refraction losses, radiating cable paths and cable termination—that are present in a practical indoor environment has been incorporated. This model considers situations where there are cable bends and accounts for propagation around the cable termination. |
| | | | | | |

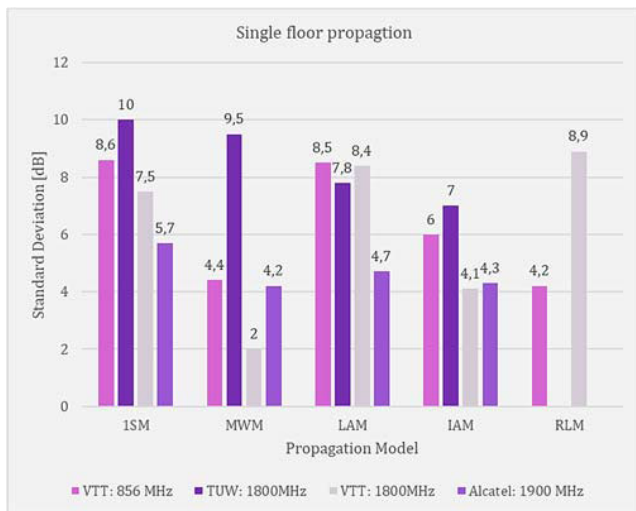


FIGURE 11. Standard deviation of prediction errors for single floor propagation.

the creation of an arbitrary double directional radio channel model. The channel models are antenna-independent, i.e., different antenna configurations and different element patterns can be inserted. The channel parameters are determined stochastically, based on statistical distributions extracted from channel measurements.

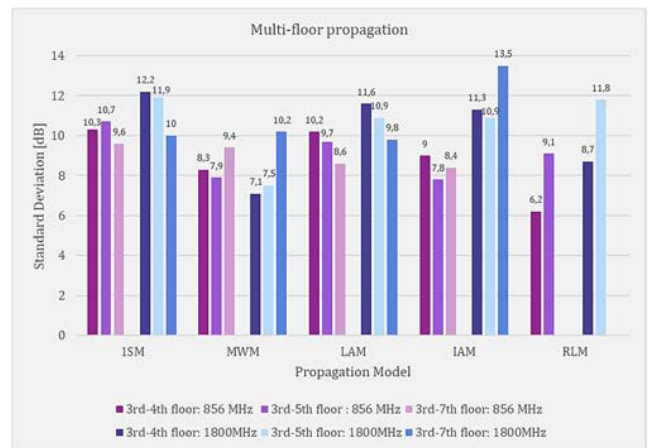


FIGURE 12. Standard deviation of prediction error for multi-floor propagation reported by VTT.

Due to several measurement campaigns carried out in the WINNER II project, the background for the parameterization of the propagation scenarios for LOS and NLOS conditions is provided. The developed models are based on both literature and extensive measurement campaigns. Clustered delay line (CDL) models with fixed large-scale and small-scale parameters were created for calibration and comparison of different simulations. The WINNER II project considered the following characteristics:

- Frequency: 2 – 5 GHz.
- Reference models: 3GPP/3GPP2 spatial channel models and IEEE 802.11n.
- Target areas: indoor office, large indoor hall, indoor-to-outdoor and outdoor-to-indoor scenarios.
- Antennas: different array of antennas.

The path loss models proposed in [107] include four fitting parameters:

- A includes the path-loss exponent.
- B is the path-loss intercept.
- C describes the path loss frequency dependence.
- X is an optional, environment-specific term, e.g., wall attenuation in indoor NLOS scenario).

3) 3GPP

The last technical report about the study on channel model for frequencies from 0.5 to 100 GHz reported by the 3GPP project in [108] considered:

- Reference projects: METIS (Mobile and wireless communications Enablers for the Twenty-twenty Information Society), MiWEBA (Millimetre-Wave Evolution for Backhaul and Access), ITU-R M, COST2100, IEEE 802.11, NYU WIRELESS, Fraunhofer HHI, 5G mmWave Channel Model Alliance, mmMAGIC (Millimetre-Wave Based Mobile Radio Access Network for Fifth Generation Integrated Communications) and IMT-2020 5G promotion association.
- Target areas: office environments, shopping malls and indoor industrial scenarios.

Due to several measurement campaigns carried out in the 3GPP project, the background for the propagation scenarios for LOS and NLOS conditions is provided. The models proposed are based on measurement campaigns.

Besides, in this report, the path loss incorporating O2I building penetration loss was modeled, taking into account material penetration losses with standard deviations of 4.4 dB for low loss model and 6.5dB for high loss model. The composition of low and high loss is a simulation parameter that should be determined by the user of the channel models and is dependent on the use of metal-coated glass in buildings and the deployment scenarios. Such use is expected to differ in different markets and regions of the world and also may increase over the years due to new regulations and energy-saving initiatives. Furthermore, the use of such high-loss glass currently appears to be more predominant in commercial buildings than in residential buildings in some regions of the world.

The study on channel models reported in [108] took into consideration not only O2I building penetration losses but also O2I car penetration losses, applicable for the frequency range 0.6 - 60 GHz. On the other hand, in [109] the studies have found some extensibility of the existing 3GPP models (e.g. 3GPP TR36.873) to the higher frequency bands up to 100 GHz. Conducted measurements indicated that the smaller wavelengths introduce an increased sensitivity of the propagation models to the scale of the environment and show some

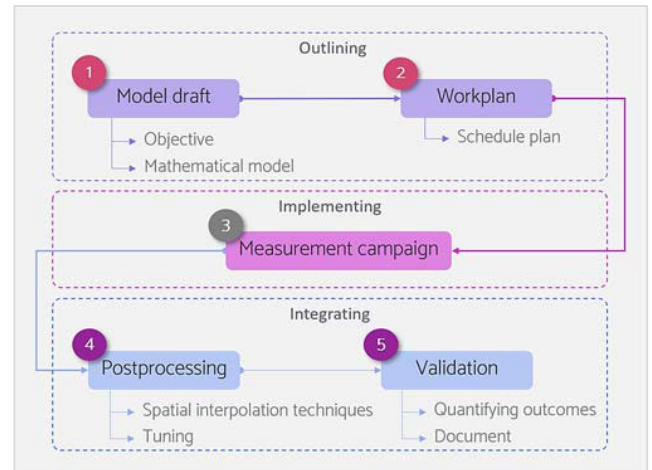


FIGURE 13. Methodology for indoor radio propagation modeling.

frequency dependence of the path loss as well as increased occurrence of blockage. Furthermore, the penetration loss was highly dependent on the material and tended to increase with frequency.

Comparisons of COST-231, WINNER II and 3GPP projects are shown in Table 11. Some important considerations that have been reported in the literature are indicated. In addition to this, standardization organizations and research institutions have also defined several indoor channel models and recommendations, as summarized in Table 12.

IV. INDOOR CHANNEL MODELING REMARKS

Considering all the features of radio wave propagation models reviewed earlier, accurate path loss predictions as well as available radio measurements are very useful tools for any radio system designer. This section focuses on providing remarks for hybrid models due to the inclusion of theoretical and empirical approaches.

Several issues should be considered as key factors when modeling radio wave propagation indoors. These factors are illustrated in Fig. 13 as a methodology and explained hereafter.

The surveyed studies agree on the way results are presented, i.e., a similar method, which reveals three stages: outlining, implementing and integrating. *Outlining* gives a valuable summary of the model draft and workplan to address the radio wave propagation model approach; *implementing* consists on conducting measurement campaigns to collect all necessary data to complement and to adjust the model; and *integrating* uses previous activities to postprocess and to validate the data obtained from the designed model.

A. OUTLINING

1) MODEL DRAFT

As a first step, the aim of the propagation model should be defined, according to specific requirements. For example, in [43], the authors search for optimal transmitter locations in an indoor wireless system and therefore need a model to achieve this. In [120] the model estimates the optimal

TABLE 11. Comparisons of COST-231, WINNER II and 3GPP projects.

| Project | Frequency | Target areas | Considerations |
|-----------|------------------------|--|---|
| COST-231 | 850, 1800 and 1900 MHz | Office buildings, shopping centers and factory environments. | <ul style="list-style-type: none"> Under consideration of a typical O2I model, COST-231 model was the best fit compared to the ray-tracing result at 900, 1800 and 2100 MHz [110]. In [111] the 3D ray-tracing resulted in an estimation similar to the multi-wall (COST-231) model without requiring a 3D model of the structure or demanding computational power. The 3D ray-tracing generated the best results. however, this advantage is almost negligible over multiwall model which offers a greater simplicity. COST-231 model can be used as a reasonable lower bound for received power [112]. |
| WINNER II | 2 – 5 GHz | Indoor office, large indoor hall, I2O and O2I scenarios. | <ul style="list-style-type: none"> At 3.5 GHz with an indoor LOS case only WINNER model remains accurate [112]. In [113], Latinovic et al. demonstrate that WINNER II and similar channel models designed for communications are not suitable, due to: the lack of specular components in los channel, the lack of NLOS bias in NLOS channel and constant delay spread over distance is assumed. |
| 3GPP | 0.5 – 100 GHz | Office environments, shopping malls and indoor industrial scenarios. | <ul style="list-style-type: none"> Delay spread models for O2I scenarios are identical to 3GPP model in both above 6 GHz and below 6 GHz [114]. The 3GPP models i.e., floating intercept (FI) and alpha-beta-gamma (ABG) models provided reliable performance for path loss for both single and multi-frequency models in LOS scenario at 3.5 GHz and 28 GHz [115]. |

TABLE 12. Standardization activities about the indoor channel modeling.

| Project | Frequency | Target areas | Considerations |
|----------------------|-------------------------------|---|--|
| ITU-R P.1238-10 [26] | 300 MHz to 450 GHz | Residential, office, commercial, factory, corridor, data center, TV studio, computer cluster, classroom, conference room, railway station, airport terminal | <ul style="list-style-type: none"> Recommendation that provides guidance on indoor propagation mainly general site-independent models and qualitative advice on propagation impairments encountered in the indoor radio environment. |
| ITU-R M.2135-1 [116] | 2 to 6 GHz | Indoor hotspot, O2I | <ul style="list-style-type: none"> Report that provides guidelines for both the procedure and the criteria (technical, spectrum and service) to be used in evaluating the proposed IMT-Advanced radio interface technologies (RITs) or Sets of RITs (SRITs) for a number of test environments and deployment scenarios for evaluation. The indoor test environment focuses on isolated cells at offices and/or in hotspot based on stationary and pedestrian users. The key characteristics of this test environment are high user throughput or user density in indoor coverage. In the O2I case the users are located indoors and base stations outdoors. |
| IEEE 802.15.4 [117] | 100 to 900 MHZ 2 to 10 GHz | Indoor residential, indoor office | <ul style="list-style-type: none"> Standard that provides models for the UWB channels; it covers indoor residential, indoor office, industrial, outdoor, and open outdoor environments (usually with a distinction between LOS and NLOS properties). For the frequency range from 100 to 900 MHz, it gives a model for indoor office-type environments. |
| IEEE 802.15.2 [118] | 2.4 GHz | Indoor | <ul style="list-style-type: none"> Addresses the issue of coexistence of wireless local area networks and wireless personal area networks Recommends two models for indoor environments where distance is between 0.5 m and 8 m, and greater than 8m. |
| IEEE 802.11n [119] | 2 and 5 GHz | Residential, small office, typical office, large space | <ul style="list-style-type: none"> Standard that is defined through several specifications of WLANs. It defines an over-the-air interface between a wireless client and a base station or between two wireless clients. Provides general two-piece distance partitioned model for received signal strength (RSS) behavior for indoor areas. The RSS is modeled as two piecewise linear segments separated by a break point (including LOS and NLOS conditions). |

position of fingerprints on an indoor map. Therefore, once the model aim is clear, relevant parameters need to be specified. A decision should be made related to whether the model will be selected from previous research or it will be fully designed, taking into account relevant propagation mechanisms that will be included in the model and thus defining the

corresponding material parameters for a particular building or propagation scenario.

2) WORKPLAN

Planning increases design efficiency and facilitates proper coordination during measurement campaigns, helping to

achieve the objectives of the research. At this stage, radio designers should:

- decide which type of measurements need to be taken; indoor locations to be considered; building features (materials, number of walls and floors, etc.); frequency bands and equipment required;
- carry out a preliminary site visit to contemplate potential test antenna locations and to consider specific building and propagation details;
- evaluate if the campaign requires permission to be granted;
- review technical requirements, i.e., equipment calibration, validation, etc.;
- select proper antenna parameters that will be varied, such as locations, heights, elevation angles, etc.;
- plan the walk test routes to be followed to obtain as much information as possible from the propagation mechanisms and path loss; e.g. Aguirre *et al.*, in [121] reported zig-zag moving pattern through the measurement area to obtain NLOS results;
- estimate the timing to complete the measurement campaign according to time restrictions and granted building permissions;
- choose a suitable navigation to be used indoors, considering that GPS is not available inside buildings; and
- achieve a schedule plan—campaign guide—that includes all previous activities with times and resource descriptions.

According to [122, Sec. 19.8], the most common approach to navigation indoors is called *way-point navigation* and consists of having a digital representation of parts of the building, which may be split by floors or regions. The user interacts with the data collection software where it selects their position at a given point in time on the floor. The software begins recording signal strength samples at regular time intervals from the RF receiver hardware, and data collection continues as the user walks until the end-point on the floor layout is indicated by the user. The collection software then uniformly assigns a position to each discrete sample collected over the period between the start time and end time of the walk segment.

Other indoor navigation systems have been employed and suggested using low-cost stationary sensor nodes. This equipment can be casually placed in the facilities by untrained personnel without location measurement. To acquire knowledge of the physical environment without a map, the system collects radio and compass signatures to continually record paths traversed by users. Using this information, paths are automatically aggregated into path clusters, and a navigable Virtual Roadmap (VRM) of the indoor environment is built by the system [123].

B. IMPLEMENTING

Measurement campaigns are a crucial source of information for in-building radio propagation modeling. On this basis, it is essential to conduct such measurements suitably. Tuning and

validation stages should use different measurement samples from the complete campaign for accurate model design and verification [124], [125]. This involves a dynamic and efficient planning stage—executed in the workplan for efficient implementation.

Once the planning is complete, the measurement campaign is conducted, following the schedule plan for effective radio measurements.

C. INTEGRATING

1) POSTPROCESSING

Postprocessing is employed when signal processing is required to be performed on the raw measured data. Averaging and filtering are common operations performed during post-processing. Postprocessing can be performed in the measured data but also after preliminary predictions have been made, for example, to obtain the local mean of the signal. In this context, it is also used to obtain precise positions of unknown points by relating them to known points. It must be noted that the known points are the result of a previous filter stage, where only useful data is considered (samples that are under the noise floor of the receiver are discarded). After an exhaustive review of indoor modeling, there are two complementary techniques that are contemplated: spatial interpolation and tuning.

When a large amount of useful data is available, model accuracy is greatly improved. However, a small amount of measurements is often available in campaigns due to specific permissions for the selected locations, time restrictions and unreachable places where these measurements cannot be performed. Spatial interpolation techniques show how robust estimates can also be made in such situations, significantly improving the results. The most frequently used techniques, according to [126], are inverse distance weighting (IDW), ordinary kriging (OK) and ordinary co-kriging (OCK).

Kriging is an interpolation technique based on the methods of geostatistics where a subject is concerned with spatial data. Geostatistics assumes that there is an implied connection between the measured data value at a point and where the point is in space. Therefore, it is possible to estimate unknown values from the best set of available sample points.

Thanks to kriging, in [127], Konak created an accurate and complete network coverage map of a target service area from a limited number of test point measurements. Thereby, the cost of time-consuming site surveys can be reduced. Kriging has certain advantages over other interpolation techniques. It is an optimal interpolation method because it produces an unbiased estimate with minimum variance. On the other hand, in [128], several spatial interpolation techniques based on IDW are analyzed and compared in terms of reliability bounds of the interpolation errors for an indoor environment, where performance evaluation shows that the spatial interpolation techniques can provide a robust and reliable estimation data.

TABLE 13. Summary of research opportunities for indoor channel modeling.

| Figure of merit | Empirical models | Physical models | Hybrid models |
|--------------------------|--------------------------------|-----------------|--------------------------------|
| Computational complexity | Low | High | Depends on models selected |
| Cost | Medium (measurement campaigns) | Low | Medium (measurement campaigns) |
| Time consumption | Medium | High | Medium – High |
| Technical resources | Many | Few | Many |

When valuable parameters of the mathematical model are tuned from the data obtained in the measurement campaign, the model will be suitable for the actual indoor propagation environment. As reported by Aragón-Zavala [122, Sec. 7.7], the result of model tuning is an optimal trade-off between the benefits and costs of both approaches, saving time and money in the design and implementation.

2) VALIDATION

This process verifies signal strength and coverage predictions made using the model against a set of measurements—only for testing—of the complete campaign. Different estimators for the quantifying validation stage are used. In [18], Oyie and Afullo compared the standard deviation of the signal fluctuation around the mean of the path loss to validate accuracy in predicting path loss. In contrast, in [32] Morocho-Yaguana *et al.* presented a comparative analysis based on the average error, which is the difference between calculated and measured attenuation. The root mean square error (RMSE) is a common estimator for validating the accuracy of a model, as stated in [129]; and the computational complexity is employed for verifying its efficiency.

Finally, it is a good practice to document the survey details, parameters, characteristics, etc. to record the level of accuracy achieved with the indoor radio propagation model. This information may be valuable for future model accuracy comparisons and measurement campaigns.

V. RESEARCH OPPORTUNITIES

The results presented in the works revealed that there are some other sources—techniques—available that could be used to make better in-building predictions, reducing campaign costs and time. Spatial interpolation techniques used for data post-processing can be employed to estimate path loss at unreachable places where measurements cannot be obtained from a limited number of test point measurements conducted at nearby locations, combined with a well-known modeling approach. Future work in this area will take advantage of measurement campaigns, focusing on refining sampling and learning strategies, as well as extracting as much information as possible from existing sources and exploring the trade-off between accuracy and efficacy of the designed model.

The majority of the reviewed work here was predominantly focused in signal strength measurements and propagation

properties in two dimensions (2D). However, indoor models that include a third dimension (3D) are scarce, opening research opportunities in the near future.

Model validation at mm-wave frequencies is also required, where more measurements are needed at different venues. Interoperability of various networks and devices with the deployment of 5G networks at various vertical sectors (health, entertainment, transport, intelligent manufacturing, etc.) and the Internet of Things (IoT) will also require novel approaches to model path loss and system performance in more challenging enclosed environments—e.g. factories—to guarantee the required strict grade-of-service levels that this new technology will demand.

Table 13 presents the most relevant research opportunities from the authors' perspective, classified by figure of merit and indoor channel model type.

VI. CONCLUSIONS

The main indoor radio wave propagation characteristics that affect and characterize model performance have been investigated, including path loss, propagation mechanisms, fast fading and shadowing. Additionally, a new taxonomy of indoor channel models has been proposed and analyzed, including an updated overview of indoor channel models. Finally, relevant indoor modeling remarks were established as part of a radio design methodology that includes three stages: outlining, implementing and integrating.

Once the available scientific literature on indoor radio propagation modeling was reviewed, the importance of appropriate modeling become more evident. Small cells are a mainstream element of operators of mobile network deployments for addressing hot-spot areas, in which capacity uplift is needed, such as indoor scenarios, where people spend most of the time. The novel taxonomy proposed herein considers developments which evaluate the effect of indoor small cells over macrocells (I2O models) and the opposite case (O2I models). These models are important specific cases for a HetNet deployment. Besides, general cases are explained as empirical, physical and hybrid models.

The difference between the environment for which the propagation model was developed and the environment for which the model will be used must be carefully evaluated, considering a trade-off between accuracy and efficacy approaches. In physical models, many ray methods are

promising, their accuracy is higher than empirical models but is tied to enough detail of the building geometry and materials. These models are very time consuming, requiring a large computational complexity even for few predictions. In hybrid models, measurement-based methods, rigorous tuning and validation stages are included, taking advantage from empirical and physical models. For these reasons, the choice of the most suitable propagation model approach to be used is mainly driven by specific project requirements, environment, available measurement data, etc. Empirical models can be employed for fast predictions at specific buildings but are strongly dependent on measurement accuracy and can hardly be extrapolated to other buildings, even if they have similar characteristics. Physical models can provide more accurate predictions but until detailed digital building databases and powerful computing resources are readily available, they are still considered inappropriate for most practical designs. It seems that the most promising approach is still the hybrid method, as long as a solid reference model is employed based on physical principles and complemented with accurate measurements to tune relevant parameters.

For the time being, the interested reader which either is new to the field or would like to seek for strong references in narrowband propagation modeling inside buildings can take this paper as a useful guideline.

REFERENCES

- [1] Cisco Visual Networking Index: Forecast and Trends, Cisco, San Jose, CA, USA, 2019.
- [2] Report to Congress on Indoor Air Quality, vol. 2. Washington, DC, USA: EPA, 1989.
- [3] Small Cell Forum. (2019). *Small Cell Definition*. [Online]. Available: <https://www.smallcellforum.org/what-is-a-small-cell/>
- [4] A. Aragón-Zavala, *Indoor Wireless Communications?: From Theory to Implementation*, 1st ed. Hoboken, NJ, USA: Wiley, 2017.
- [5] M. F. Iskander and Z. Yun, "Propagation prediction models for wireless communication systems," *IEEE Trans. Microw. Theory Techn.*, vol. 50, no. 3, pp. 662–673, Mar. 2002.
- [6] T. K. Sarkar, Z. Ji, K. Kim, A. Medouri, and M. Salazar-Palma, "A survey of various propagation models for mobile communication," *IEEE Antennas Propag. Mag.*, vol. 45, no. 3, pp. 51–82, Jun. 2003.
- [7] K. Anusuya, S. Bharadhwaj, and S. Rani, "Wireless channel models for indoor environments," *Defence Sci. J.*, vol. 58, no. 6, pp. 771–777, Nov. 2008.
- [8] A. Neskovic, N. Neskovic, and G. Paunovic, "Modern approaches in modeling of mobile radio systems propagation environment," *IEEE Commun. Surveys Tuts.*, vol. 3, no. 3, pp. 2–12, 3rd Quart., 2000.
- [9] D. Trincherio and R. Stefanelli, "Review analysis of electromagnetic modeling methods in confined environments. Part 2: Indoor communications," in *Proc. Int. Conf. Electromagn. Adv. Appl. (ICEAA)*, Sep. 2009, pp. 1070–1073.
- [10] P. Smulders, "Statistical characterization of 60-GHz indoor radio channels," *IEEE Trans. Antennas Propag.*, vol. 57, no. 10, pp. 2820–2829, Oct. 2009.
- [11] C. Phillips, D. Sicker, and D. Grunwald, "A survey of wireless path loss prediction and coverage mapping methods," *IEEE Commun. Surveys Tuts.*, vol. 15, no. 1, pp. 255–270, 1st Quart., 2013.
- [12] A. E. Forooshani, S. Bashir, D. G. Michelson, and S. Noghianian, "A survey of wireless communications and propagation modeling in underground mines," *IEEE Commun. Surveys Tuts.*, vol. 15, no. 4, pp. 1524–1545, 4th Quart., 2013.
- [13] A. Hrovat, G. Kandus, and T. Javornik, "A survey of radio propagation modeling for tunnels," *IEEE Commun. Surveys Tuts.*, vol. 16, no. 2, pp. 658–669, 2nd Quart., 2014.
- [14] P. Deb, A. Mukherjee, and D. De, "Study of indoor path loss computational models for femtocell based mobile network," *Wireless Pers. Commun.*, vol. 95, no. 3, pp. 3031–3056, Aug. 2017.
- [15] I. A. Hemadeh, K. Satyanarayana, M. El-Hajjar, and L. Hanzo, "Millimeter-wave communications: Physical channel models, design considerations, antenna constructions, and link-budget," *IEEE Commun. Surveys Tuts.*, vol. 20, no. 2, pp. 870–913, 2nd Quart., 2018.
- [16] S. Ahmadi, "Definition of the performance metrics," in *LTE-Advanced: A Practical Systems Approach to Understanding 3GPP LTE Releases 10 and 11 Radio Access Technologies*. Amsterdam, The Netherlands: Elsevier, 2014, pp. 875–882.
- [17] T. S. Rappaport, *Wireless Communications-Principles And Practice*. Upper Saddle River, NJ, USA: Prentice-Hall, 2002.
- [18] N. O. Oye and T. J. O. Afullo, "Measurements and analysis of large-scale path loss model at 14 and 22 GHz in indoor corridor," *IEEE Access*, vol. 6, pp. 17205–17214, 2018.
- [19] J. Reig and L. Rubio, "Estimation of the composite fast fading and shadowing distribution using the log-moments in wireless communications," *IEEE Trans. Wireless Commun.*, vol. 12, no. 8, pp. 3672–3681, Aug. 2013.
- [20] S. Bhattacharyya, A. Misra, and K. K. Sarma, "A BCH code assisted modified NCO based LSPF-DPLL topology for nakagami-m, Rayleigh and Rician fading channels," *Digit. Commun. Netw.*, vol. 5, no. 2, pp. 102–110, May 2019.
- [21] E. Tanghe, W. Joseph, L. Verloock, L. Martens, H. Capoen, K. Herwegen, and W. Vantomme, "The industrial indoor channel: Large-scale and temporal fading at 900, 2400, and 5200 MHz," *IEEE Trans. Wireless Commun.*, vol. 7, no. 7, pp. 2740–2751, Jul. 2008.
- [22] H. Du, J. Zhang, J. Cheng, and B. Ai, "Sum of Fisher-Snedecor \mathcal{F} random variables and its applications," *IEEE Open J. Commun. Soc.*, vol. 1, pp. 342–356, Mar. 2020.
- [23] P. Zhang, J. Zhang, K. P. Peppas, D. W. K. Ng, and B. Ai, "Dual-hop relaying communications over Fisher-Snedecor \mathcal{F} -Fading channels," *IEEE Trans. Commun.*, vol. 68, no. 5, pp. 2695–2710, May 2020.
- [24] H. Du, J. Zhang, K. P. Peppas, H. Zhao, B. Ai, and X. Zhang, "On the distribution of the ratio of products of Fisher-Snedecor \mathcal{F} random variables and its applications," *IEEE Trans. Veh. Technol.*, vol. 69, no. 2, pp. 1855–1866, Feb. 2020.
- [25] S. K. Yoo, S. L. Cotton, P. C. Sofotasios, M. Matthaiou, M. Valkama, and G. K. Karagiannidis, "The Fisher-Snedecor \mathcal{F} distribution: A simple and accurate composite fading model," *IEEE Commun. Lett.*, vol. 21, no. 7, pp. 1661–1664, Jul. 2017.
- [26] *Propagation Data and Prediction Methods for the Planning of Indoor Radiocommunication Systems and Radio Local Area Networks in the Frequency Range 300 MHz to 450 GHz*, document P.1238-10, International Telecommunication Union, ITU-R, 2019.
- [27] *Effects of Building Materials and Structures on Radiowave Propagation Above About 100 MHz*, document P.2040-1, International Telecommunication Union, ITU-R, 2015.
- [28] H. Xu, V. Kukshya, and T. S. Rappaport, "Spatial and temporal characteristics of 60-GHz indoor channels," *IEEE J. Sel. Areas Commun.*, vol. 20, no. 3, pp. 620–630, Apr. 2002.
- [29] M. Thiel and K. Sarabandi, "A hybrid method for indoor wave propagation modeling," *IEEE Trans. Antennas Propag.*, vol. 56, no. 8, pp. 2703–2709, Aug. 2008.
- [30] A. C. M. Austin, M. J. Neve, and G. B. Rowe, "Modeling propagation in multifloor buildings using the FDTD method," *IEEE Trans. Antennas Propag.*, vol. 59, no. 11, pp. 4239–4246, Nov. 2011.
- [31] O. W. Ata, A. M. Shahateet, M. I. Jawadeh, and A. I. Amro, "An indoor propagation model based on a novel multi wall attenuation loss formula at frequencies 900 MHz and 2.4 GHz," *Wireless Pers. Commun.*, vol. 69, no. 1, pp. 23–36, Mar. 2013.
- [32] M. Morocho-Yaguana, P. Ludeña-González, F. Sandoval, B. Poma-Vélez, and A. Erreyes-Dota, "An optimized propagation model based on measurement data for indoor environments," *J. Telecommun. Inf. Technol.*, vol. 2, pp. 69–75, Jul. 2018.
- [33] Z. Yun, M. F. Iskander, and Z. Zhang, "Complex-wall effect on propagation characteristics and MIMO capacities for an indoor wireless communication environment," *IEEE Trans. Antennas Propag.*, vol. 52, no. 4, pp. 914–922, Apr. 2004.
- [34] R. S. De Souza and R. D. Lins, "A new propagation model for 2.4 GHz wireless LAN," in *Proc. 14th Asia-Pacific Conf. Commun. (APCC)*, 2008, pp. 1–5.

- [35] J.-B. Yan and J. T. Bernhard, "Investigation of the influence of reflective insulation on indoor reception in rural houses," *IEEE Antennas Wireless Propag. Lett.*, vol. 10, pp. 423–426, 2011.
- [36] S. S. Zhekov, Z. Nazneen, O. Franek, and G. F. Pedersen, "Measurement of attenuation by building structures in cellular network bands," *IEEE Antennas Wireless Propag. Lett.*, vol. 17, no. 12, pp. 2260–2263, Dec. 2018.
- [37] D. Shi, C. Wang, and Y. Gao, "A new permittivity measurement method for walls in indoor scenes," *IEEE Trans. Antennas Propag.*, vol. 67, no. 4, pp. 2118–2129, Apr. 2019.
- [38] Z. Sun and I. Akyildiz, "Channel modeling and analysis for wireless networks in underground mines and road tunnels," *IEEE Trans. Commun.*, vol. 58, no. 6, pp. 1758–1768, Jun. 2010.
- [39] J. Zhang, E. Björnson, M. Matthaiou, D. W. K. Ng, H. Yang, and D. J. Love, "Prospective multiple antenna technologies for beyond 5G," *IEEE J. Sel. Areas Commun.*, pp. 1–23, Mar. 2020. [Online]. Available: <https://pure.qub.ac.uk/en/publications/prospective-multiple-antenna-technologies-for-beyond-5g>
- [40] J. Zhang, S. Chen, Y. Lin, J. Zheng, B. Ai, and L. Hanzo, "Cell-free massive MIMO: A new next-generation paradigm," *IEEE Access*, vol. 7, pp. 99878–99888, 2019.
- [41] M. Ghaddar, L. Talbi, T. A. Denidni, and A. Sebak, "A conducting cylinder for modeling human body presence in indoor propagation channel," *IEEE Trans. Antennas Propag.*, vol. 55, no. 11, pp. 3099–3103, Nov. 2007.
- [42] A. Ando, T. Taga, A. Kondo, K. Kagoshima, and S. Kubota, "Mean effective gain of mobile antennas in Line-of-Sight street microcells with low base station antennas," *IEEE Trans. Antennas Propag.*, vol. 56, no. 11, pp. 3552–3565, Nov. 2008.
- [43] A. Dalla-Rosa, A. Raizer, and L. Pichon, "Optimal indoor transmitters location using TLM and Kriging methods," *IEEE Trans. Magn.*, vol. 44, no. 6, pp. 1354–1357, Jun. 2008.
- [44] Y. Coulibaly, D. Gilles, H. Nadir, and A. Dodji, "Experimental characterization of the UWB channel for an underground mining vehicle," in *Proc. 7th Eur. Conf. Antennas Propag. (EuCAP)*, 2013, pp. 2331–2334.
- [45] V. Kristem, S. Sangodoyin, C. U. Bas, M. Kaska, J. Lee, C. Schneider, G. Sommerkorn, C. J. Zhang, R. S. Thoma, and A. F. Molisch, "3D MIMO outdoor-to-indoor propagation channel measurement," *IEEE Trans. Wireless Commun.*, vol. 16, no. 7, pp. 4600–4613, Jul. 2017.
- [46] J. R. Perez and R. P. Torres, "On the impact of the radiation pattern of the antenna element on MU-MIMO indoor channels," *IEEE Access*, vol. 8, pp. 25459–25467, 2020.
- [47] W. Seesai, M. Chamchoy, and S. Promwong, "A body-shadowing model for indoor UWB communication environments," in *Proc. 5th Int. Conf. Electr. Eng./Electron., Comput., Telecommun. Inf. Technol. (ECTI-CON)*, vol. 1, May 2008, pp. 261–264.
- [48] S. Collonge, G. Zaharia, and G. ElZein, "Influence of the human activity on wide-band characteristics of the 60 GHz indoor radio channel," *IEEE Trans. Wireless Commun.*, vol. 3, no. 6, pp. 2396–2406, Nov. 2004.
- [49] *COST Action 231: Digital Mobile Radio Towards Future Generation Systems*, Eur. Commission, Brussels, Belgium, 1999.
- [50] F. Villanese, N. E. Evans, and W. G. Scanlon, "Pedestrian-induced fading for indoor channels at 2.45, 5.7 and 62 GHz," in *Proc. IEEE Veh. Technol. Conf.*, 2000, vol. 1, no. 52, pp. 43–48.
- [51] A. Kara and H. L. Bertoni, "Effect of people moving near short-range indoor propagation links at 2.45 GHz," *J. Commun. Netw.*, vol. 8, no. 3, pp. 286–289, Sep. 2006.
- [52] A. Sani, A. Alomainy, G. Palikaras, Y. Nechayev, Y. Hao, C. Parini, and P. S. Hall, "Experimental characterization of UWB on-body radio channel in indoor environment considering different antennas," *IEEE Trans. Antennas Propag.*, vol. 58, no. 1, pp. 238–241, Jan. 2010.
- [53] Z. Lai, N. Bessis, G. de la Roche, P. Kuonen, J. Zhang, and G. Clapworthy, "The characterisation of human body influence on indoor 3.5 GHz path loss measurement," in *Proc. IEEE Wireless Commun. Netw. Conf. Workshops WCNCW*, Apr. 2010, pp. 1–6.
- [54] M. Ayadi and A. B. Zineb, "Body shadowing and furniture effects for accuracy improvement of indoor wave propagation models," *IEEE Trans. Wireless Commun.*, vol. 13, no. 11, pp. 5999–6006, Nov. 2014.
- [55] M. Nakamura, M. Sasaki, W. Yamada, and Y. Takatori, "Path loss model in crowded indoor environments considering multiple human body shadowing of multipath at 4.7 GHz and 66.5 GHz," in *Proc. 13th Eur. Conf. Antennas Propag. (EuCAP)*, 2019, pp. 1–5.
- [56] M. Rahnema, *UMTS Network Planning, Optimization, and Inter-Operation with GSM*. Hoboken, NJ, USA: Wiley, 2008.
- [57] D. Akerberg, "Properties of a TDMA pico cellular office communication system," in *Proc. IEEE 39th Veh. Technol. Conf.*, May 1988, pp. 1343–1349.
- [58] A. J. Motley and J. M. P. Keenan, "Personal communication radio coverage in buildings at 900 MHz and 1700 MHz," *Electron. Lett.*, vol. 24, no. 12, pp. 763–764, 1988.
- [59] J. M. Keenan and A. J. Motley, "Radio coverage in buildings," *Bell Syst. Tech. J.*, vol. 8, pp. 19–24, Jan. 1990.
- [60] S. Y. Seidel and T. S. Rappaport, "914 MHz path loss prediction models for indoor wireless communications in multifloored buildings," *IEEE Trans. Antennas Propag.*, vol. 40, no. 2, pp. 207–217, Feb. 1992.
- [61] *Propagation Data and Prediction Models for the Planning of Indoor Radiocommunication Systems and Radio Local Area Networks in the Frequency Range 900 MHz to 100 GHz*, document P.1238, International Telecommunication Union, ITU-R, 1997.
- [62] S.-C. Tuan, J.-C. Chen, H.-T. Chou, and H.-H. Chou, "Optimization of propagation models for the radio performance evaluation of wireless local area network," in *Proc. IEEE Antennas Propag. Soc. Int. Symp. Held Conjoint, USNC/CNC/URSI North Amer. Radio Sci. Meeting*, vol. 2, Jun. 2003, pp. 146–152.
- [63] R. N. S. Barbosa, J. do C. Rodrigues, R. N. S. Barbosa, H. S. Gomes, and G. P. S. Cavalcante, "An empirical model for propagation loss prediction in indoor mobile communications using Padé approximant," in *IEEE MTT-S Int. Microw. Symp. Dig.*, 2005, pp. 625–628.
- [64] A. S. Braga, R. L. F. Lopes, S. G. C. Fraiha, J. P. L. Araujo, H. S. Gomes, J. C. Rodrigues, H. R. O. Ferreira, and G. P. S. Cavalcante, "Coverage area simulation for indoor 4G networks in 2.6 GHz and 3.5 GHz," in *Proc. 8th Eur. Conf. Antennas Propag. (EuCAP)*, Apr. 2014, pp. 2125–2129.
- [65] Y. Yu, Y. Liu, W.-J. Lu, and H.-B. Zhu, "Measurement and empirical modelling of root mean square delay spread in indoor femtocells scenarios," *IET Commun.*, vol. 11, no. 13, pp. 2125–2131, Sep. 2017.
- [66] W. Honcharenko, H. L. Bertoni, J. L. Dailing, J. Qian, and H. D. Yee, "Mechanisms governing UHF propagation on single floors in modern office buildings," *IEEE Trans. Veh. Technol.*, vol. 41, no. 4, pp. 496–504, Nov. 1992.
- [67] S. Y. Seidel and T. S. Rappaport, "Site-specific propagation prediction for wireless in-building personal communication system design," *IEEE Trans. Veh. Technol.*, vol. 43, no. 4, pp. 879–891, Nov. 1994.
- [68] M. Liebendorfer, M. Zehnder, and U. Dersch, "Multi channel coupling: Interactive prediction of 3D indoor propagation," in *Proc. Int. Zurich Seminar Broadband Commun. Accessing, Transmiss., Netw.*, 2000, pp. 215–221.
- [69] F. Saez de Adana, O. G. Blanco, I. Gonzalez Diego, J. P. Arriaga, and M. F. Catedra, "Propagation model based on ray tracing for the design of personal communication systems in indoor environments," *IEEE Trans. Veh. Technol.*, vol. 49, no. 6, pp. 2105–2112, Nov. 2000.
- [70] B. S. Lee, "Indoor space-time propagation modelling using a ray launching technique," in *Proc. 11th Int. Conf. Antennas Propag. (ICAP)*, 2001, pp. 279–283.
- [71] J. Liu, D. W. Matolak, M. Mohsen, and J. Chen, "Path loss modeling and ray-tracing verification for 5/31/90 GHz indoor channels," in *Proc. IEEE 90th Veh. Technol. Conf. (VTC-Fall)*, Sep. 2019, pp. 1–6.
- [72] Y. Li, J. Zhang, P. Tang, and L. Tian, "Clustering in the wireless channel with a power weighted statistical mixture model in indoor scenario," *China Commun.*, vol. 16, no. 7, pp. 83–95, Jul. 2019.
- [73] K.-W. Cheung, J. H.-M. Sau, and R. D. Murch, "A new empirical model for indoor propagation prediction," *IEEE Trans. Veh. Technol.*, vol. 47, no. 3, pp. 996–1001, Aug. 1998.
- [74] A. Aragon-Zavala, B. Belloul, V. Nikolopoulos, and S. R. Saunders, "Accuracy evaluation analysis for indoor measurement-based radio-wave-propagation predictions," *IEE Microw., Antennas Propag.*, vol. 153, no. 1, pp. 67–74, Feb. 2006.
- [75] G. K. Theofilogiannakos, T. V. Yioultis, and T. D. Xenos, "An efficient hybrid parabolic equation–integral equation method for the analysis of wave propagation in highly complex indoor communication environments," *Wireless Pers. Commun.*, vol. 43, no. 2, pp. 495–510, Oct. 2007.
- [76] G. R. Maccartney, T. S. Rappaport, S. Sun, and S. Deng, "Indoor office wideband millimeter-wave propagation measurements and channel models at 28 and 73 GHz for ultra-dense 5G wireless networks," *IEEE Access*, vol. 3, pp. 2388–2424, 2015.

- [77] E. Vinogradov, W. Joseph, and C. Oestges, "Measurement-based modeling of time-variant fading statistics in indoor peer-to-peer scenarios," *IEEE Trans. Antennas Propag.*, vol. 63, no. 5, pp. 2252–2263, May 2015.
- [78] K. Haneda, J. Järveläinen, A. Karttunen, M. Kyro, and J. Putkonen, "A statistical spatio-temporal radio channel model for large indoor environments at 60 and 70 GHz," *IEEE Trans. Antennas Propag.*, vol. 63, no. 6, pp. 2694–2704, Jun. 2015.
- [79] A. Bhuvaneshwari, R. Hemalatha, and T. S. Savithri, "Development of an optimized ray tracing path loss model in the indoor environment," *Wireless Pers. Commun.*, vol. 96, no. 1, pp. 1039–1064, Sep. 2017.
- [80] B. Ai, K. Guan, R. He, J. Li, G. Li, D. He, Z. Zhong, and K. M. S. Huq, "On indoor millimeter wave massive MIMO channels: Measurement and simulation," *IEEE J. Sel. Areas Commun.*, vol. 35, no. 7, pp. 1678–1690, Jul. 2017.
- [81] X. Wu, C.-X. Wang, J. Sun, J. Huang, R. Feng, Y. Yang, and X. Ge, "60-GHz millimeter-wave channel measurements and modeling for indoor office environments," *IEEE Trans. Antennas Propag.*, vol. 65, no. 4, pp. 1912–1924, Apr. 2017.
- [82] M. Abdel-Rahim, M. H. Habaebi, J. Chebil, A. H. A. Hashim, M. M. Ahmed, M. R. Islam, and A. Zyoud, "An indoor path loss model for wireless sensor networks," *Int. J. Ultra Wideband Commun. Syst.*, vol. 3, no. 4, pp. 192–200, 2018.
- [83] M. Khatun, C. Guo, L. Moro, D. Matolak, and H. Mehrpouyan, "Millimeter-wave path loss at 73 GHz in indoor and outdoor airport environments," in *Proc. IEEE 90th Veh. Technol. Conf. (VTC-Fall)*, Sep. 2019, pp. 1–5.
- [84] G. Durgin, T. S. Rappaport, and H. Xu, "Measurements and models for radio path loss and penetration loss in and around homes and trees at 5.85 GHz," *IEEE Trans. Commun.*, vol. 46, no. 11, pp. 1484–1496, Nov. 1998.
- [85] A. Damnjanovic, J. Montojo, Y. Wei, T. Ji, T. Luo, M. Vajapeyam, T. Yoo, O. Song, and D. Malladi, "A survey on 3GPP heterogeneous networks," *IEEE Wireless Commun.*, vol. 18, no. 3, pp. 10–21, Jun. 2011.
- [86] *Small Cell Forum*, Small Cell Forum, London, U.K., 2019. [Online]. Available: <https://www.smallcellforum.org/>
- [87] *Small Cell Forum Release 7.0 HetNet and SON Overview*, Small Cell Forum, London, U.K., 2016.
- [88] *Small Cell Forum Release 9.0 LTE Small Cell SON Test Cases: Functionality and Interworking*, Small Cell Forum, London, U.K., 2017.
- [89] J. Lee, K.-W. Kim, M.-D. Kim, J.-J. Park, Y. K. Yoon, and Y. J. Chong, "Measurement-based millimeter-wave angular and delay dispersion characteristics of Outdoor-to-Indoor propagation for 5G millimeter-wave systems," *IEEE Access*, vol. 7, pp. 150492–150504, 2019.
- [90] Y. Miura, Y. Oda, and T. Taga, "Outdoor-to-indoor propagation modelling with the identification of path passing through wall openings," in *Proc. 13th IEEE Int. Symp. Pers., Indoor Mobile Radio Commun. (PIMRC)*, vol. 1, Sep. 2002, pp. 130–134.
- [91] C. Oestges and A. J. Paulraj, "Propagation into buildings for broad-band wireless access," *IEEE Trans. Veh. Technol.*, vol. 53, no. 2, pp. 521–526, Mar. 2004.
- [92] H. Okamoto, K. Kitao, and S. Ichitsubo, "Outdoor-to-indoor propagation loss prediction in 800-MHz to 8-GHz band for an urban area," *IEEE Trans. Veh. Technol.*, vol. 58, no. 3, pp. 1059–1067, Mar. 2009.
- [93] J. Feng, L. Zhou, X. Xu, and C. Liao, "A hybrid TDPE/FDTD method for site-specific modeling of O2I radio wave propagation," *IEEE Antennas Wireless Propag. Lett.*, vol. 17, no. 9, pp. 1652–1655, Sep. 2018.
- [94] C. Umit Bas, R. Wang, S. Sangodoyin, T. Choi, S. Hur, K. Whang, J. Park, C. J. Zhang, and A. F. Molisch, "Outdoor to indoor propagation channel measurements at 28 GHz," *IEEE Trans. Wireless Commun.*, vol. 18, no. 3, pp. 1477–1489, Mar. 2019.
- [95] R. Zhang, H. Xu, X. Du, D. Zhou, and M. Guizani, "Dual-polarized spatial-temporal propagation measurement and modeling in UMa O2I scenario at 3.5 GHz," *IEEE Access*, vol. 7, pp. 122988–123001, 2019.
- [96] S. Hamid, A. J. Al-Dweik, M. Mirahmadi, K. Mubarak, and A. Shami, "Inside-out propagation: Developing a unified model for the interference in 5G networks," *IEEE Veh. Technol. Mag.*, vol. 10, no. 2, pp. 47–54, Jun. 2015.
- [97] B. Allen, S. Mahato, Y. Gao, and S. Salous, "Indoor-to-outdoor empirical path loss modelling for femtocell networks at 0.9, 2, 2.5 and 3.5 GHz using singular value decomposition," *IET Microw., Antennas Propag.*, vol. 11, no. 9, pp. 1203–1211, Jul. 2017.
- [98] V. Degli-Esposti, E. M. Vitucci, and R. Martin, "A simple and versatile field prediction model for indoor and indoor-to-outdoor propagation," *IEEE Access*, vol. 5, pp. 13270–13276, 2017.
- [99] G. De la Roche and J. Zhang, "Indoor coverage techniques," in *Femto-cells: Technologies and Deployment*. Hoboken, NJ, USA: Wiley, 2010, p. 328.
- [100] V. P. A. Santos, F. J. B. da Fonseca, L. J. de Matos, W. D. T. Meza, G. L. Siqueira, and L. A. R. Ramirez, "Indoor signal coverage of a leaky feeder cable," in *IEEE MTT-S Int. Microw. Symp. Dig.*, Aug. 2013, pp. 1–5.
- [101] I. Stamopoulos, A. Aragon, and S. R. Saunders, "Performance comparison of distributed antenna and radiating cable systems for cellular indoor environments in the DCS band," in *Proc. 12th Int. Conf. Antennas Propag. (ICAP)*, 2004, pp. 771–774.
- [102] A. Moschevikin, M. Serezhina, and A. Sikora, "On the possibility to use leaky feeders for positioning in chirp spread spectrum technologies," in *Proc. 2nd Int. Symp. Wireless Syst. Conf. Intell. Data Acquisition Adv. Comput. Syst.*, Sep. 2014, pp. 56–65.
- [103] M. Serezhina, A. Moschevikin, R. Evmenchikov, and A. Sikora, "Using radiating cable for time-of-flight CSS measurements indoors and outdoors," in *Proc. IEEE 8th Int. Conf. Intell. Data Acquisition Adv. Comput. Syst., Technol. Appl. (IDAACS)*, vol. 1, Sep. 2015, pp. 91–101.
- [104] Y. P. Zhang, "Indoor radiated-mode leaky feeder propagation at 2.0 GHz," *IEEE Trans. Veh. Technol.*, vol. 50, no. 2, pp. 536–545, Mar. 2001.
- [105] K. Carter, "Predicting propagation loss from leaky coaxial cable terminated with an indoor antenna," in *Wireless Personal Communications*. Boston, MA, USA: Kluwer, 2006, pp. 71–82.
- [106] J. A. Seseña-Osorio, A. Aragón-Zavala, I. E. Zaldívar-Huerta, and G. Castañón, "Indoor propagation modeling for radiating cable systems in the frequency range of 900-2500 MHz," *Prog. Electromagn. Res. B*, vol. 47, no. 47, pp. 241–262, 2013.
- [107] P. Kyösti, "IST-4-027756 WINNER II," Wireless World Initiative New Radio, WINNER II Channel Models, Tech. Rep. IST-4-027756 WINNER II D1.1.2 v1.2, 2008.
- [108] *Study on Channel Model for Frequencies From 0.5 to 100 GHz*, 3GPP, document TR 38.901, Group Radio Access Network, 2019.
- [109] K. Haneda et al., "Indoor 5G 3GPP-like channel models for office and shopping mall environments," in *Proc. IEEE Int. Conf. Commun. Workshops (ICC)*, May 2016, pp. 694–699.
- [110] C. Muller, H. Georg, M. Putzke, and C. Wietfeld, "Performance analysis of radio propagation models for smart grid applications," in *Proc. IEEE Int. Conf. Smart Grid Commun. (SmartGridComm)*, Oct. 2011, pp. 96–101.
- [111] S. Hosseinzadeh, H. Larjani, K. Curtis, A. Wixted, and A. Amini, "Empirical propagation performance evaluation of LoRa for indoor environment," in *Proc. IEEE 15th Int. Conf. Ind. Informat. (INDIN)*, Jul. 2017, pp. 26–31.
- [112] G. Castro, R. Feick, M. Rodríguez, R. Valenzuela, and D. Chizhik, "Outdoor-to-Indoor empirical path loss models: Analysis for Pico and Femto cells in street canyons," *IEEE Wireless Commun. Lett.*, vol. 6, no. 4, pp. 542–545, Aug. 2017.
- [113] Z. Latinovic and H. Huang, "A channel model for indoor time-of-arrival ranging," *IEEE Trans. Wireless Commun.*, vol. 19, no. 2, pp. 1415–1428, Feb. 2020.
- [114] J. Lee, K.-W. Kim, M.-D. Kim, and J.-J. Park, "32-GHz outdoor-to-indoor channel measurement of propagation losses and delay spread," in *Proc. IEEE Int. Symp. Antennas Propag. USNC-URSI Radio Sci. Meeting (APSURSI)*, Jul. 2019, pp. 2071–2072.
- [115] A. M. Al-Samman, T. Abd. Rahman, T. Al-Hadhrani, A. Daho, M. N. Hindia, M. H. Azmi, K. Dimiyati, and M. Alazab, "Comparative study of indoor propagation model below and above 6 GHz for 5G wireless networks," *Electronics*, vol. 8, no. 1, p. 44, Jan. 2019.
- [116] *Guidelines for Evaluation of Radio Interface Technologies for IMT-Advanced*, document Rep. ITU-R M.2135-1, 2009.
- [117] *Standard for Low-Rate Wireless Networks*, IEEE Standard 802.15.4, 2020.
- [118] *Coexistence of Wireless Personal Area Networks With Other Wireless Devices Operating in Unlicensed Frequency Bands*, IEEE Standard 802.15.2, 2003.
- [119] *Standard for Information Technology—Local and Metropolitan Area Networks*, IEEE Standard 802.11n, 2009.

- [120] J. Bi, Y. Wang, Z. Li, S. Xu, J. Zhou, M. Sun, and M. Si, "Fast radio map construction by using adaptive path loss model interpolation in large-scale building," *Sensors*, vol. 19, no. 3, p. 712, Feb. 2019.
- [121] S. Aguirre, L. H. Loew, and Y. Lo, "Radio propagation into buildings at 912, 1920, and 5990 MHz using microcells," in *Proc. 3rd IEEE Int. Conf. Universal Pers. Commun.*, Oct. 1994, pp. 129–134.
- [122] S. Saunders and A. Aragón-Zavala, *Antenna and Propagation for Wireless Communication Systems*, 2nd ed. Hoboken, NJ, USA: Wiley, 2007.
- [123] A. Purohit, Z. Sun, S. Pan, and P. Zhang, "SugarTrail: Indoor navigation in retail environments without surveys and maps," in *Proc. IEEE Int. Conf. Sens., Commun. Netw. (SECON)*, Jun. 2013, pp. 300–308.
- [124] D. Plets, W. Joseph, K. Vanhecke, E. Tanghe, L. Martens, S. Bouckaert, I. Moerman, and P. Demeester, "Validation of path loss by heuristic prediction tool with path loss and RSSI measurements," in *Proc. IEEE Antennas Propag. Soc. Int. Symp.*, Jul. 2010, pp. 1–4.
- [125] D. Plets, W. Joseph, K. Vanhecke, E. Tanghe, and L. Martens, "Simple indoor path loss prediction algorithm and validation in living lab setting," *Wireless Pers. Commun.*, vol. 68, no. 3, pp. 535–552, Feb. 2013.
- [126] J. Li and A. D. Heap, "A review of comparative studies of spatial interpolation methods in environmental sciences: Performance and impact factors," *Ecol. Informat.*, vol. 6, nos. 3–4, pp. 228–241, Jul. 2011.
- [127] A. Konak, "A kriging approach to predicting coverage in wireless networks," *Int. J. Mob. Netw. Des. Innov.*, vol. 3, no. 2, pp. 65–71, Jan. 2009.
- [128] D. Denkovski, V. Atanasovski, L. Gavrilovska, J. Riihijärvi, and P. Maehoenen, "Reliability of a radio environment map: Case of spatial interpolation techniques," in *Proc. 7th Int. Conf. Cognit. Radio Oriented Wireless Netw. (CROWNCOM)*, 2012, pp. 248–253.
- [129] K. Sato, K. Inage, and T. Fujii, "On the performance of neural network residual kriging in radio environment mapping," *IEEE Access*, vol. 7, pp. 94557–94568, 2019.



MELISSA EUGENIA DIAGO-MOSQUERA

received the B.Sc. degree in electronics and telecommunications engineering from the University of Cauca, Colombia, in 2014, and the M.Sc. degree in informatics and telecommunications from Icesi University, Colombia, in 2018. She is currently pursuing the Ph.D. degree with the School of Information Technology and Electronics, Tecnológico de Monterrey Campus Querétaro. From 2015 to 2019, she joined the Sugarcane Research Center, CENICAÑA, as a Networks and Telecommunications Engineer facility working on the Internet of Things (IoT) projects, specifically focused on hybrid radiocommunication networks. Her research interests include indoor radio propagation, vehicular technologies, and channel modeling.



ALEJANDRO ARAGÓN-ZAVALA received the B.Sc. degree in electronics and communications engineering from the Tecnológico de Monterrey Campus Querétaro, Mexico, in 1992, the M.Sc. degree in satellite communication engineering from the University of Surrey, U.K., in 1997, and the Ph.D. degree in antennas and propagation from the Centre for Communication System Research, University of Surrey, in 2003. He worked as a Senior In-Building Radio Consultant with Cellular

Design Services Ltd., U.K., from 1998 to 2003, and as the Program Chair and the Head of the Electronics Department, Tecnológico de Monterrey Campus Querétaro, from 2003 to 2011. He is currently a Titular Professor and the Head of the Regional Department of Computing, School of Engineering and Science, Tecnológico de Monterrey Campus Querétaro, and a Wireless Expert Consultant with Real Wireless Ltd., U.K. He is the author of more than 40 research articles, two e-books, and three books on wireless communications. His research interests include indoor radio propagation, high-altitude platforms (HAPS), antenna design, vehicular technologies, satellite communications, and channel modeling.



GERARDO CASTAÑÓN received the B.Sc. degree in physics engineering from the Monterrey Institute of Technology and Higher Education (ITESM), Mexico, in 1987, the M.Sc. degree in physics (optics) from the Ensenada Research Centre and Higher Education, Mexico, in 1989, and the master's and Ph.D. degrees in electrical and computer engineering from the State University of New York at Buffalo, in 1995 and 1997, respectively. He was supported by the Fulbright

Scholarship through his Ph.D. studies. From 1998 to 2000, he was a Research Scientist with the Alcatel USA Corporate Research Center, Richardson, TX, USA, where he was doing research on IP over WDM, dimensioning and routing strategies for next generation optical networks, and the design of all-optical routers. From 2000 to 2002, he was a Senior Researcher with Fujitsu Network Communications, doing research on ultrahigh speed transmission systems. He has been working with the Department of Electrical and Computer Engineering, ITESM, since 2002. He is an Associate Professor. He has over 90 publications in journals and conferences and four international patents. He frequently acts as a Reviewer for IEEE journals. He is a Senior Member of the IEEE Communications and Photonics Societies. He is a member of the Academy of Science in Mexico and the National Research System in Mexico.

• • •

Chapter 3

The performance of in-building measurement-based path loss modeling using kriging

3.1 Summary of the Chapter

In this chapter, a measurement-based model which includes Kriging as part of the post-processing analysis is proposed. To ensure a suitable methodology, the selection of the variogram function in the variography stage, tuning dataset method and tuning dataset size must be understood due to these selections are an open topic that had not been addressed in the available literature in channel modeling. Thus, and considering a typical indoor scenario, from a measurement bench available in the research group, signal-strength measurements at the frequency bands of 800 and 1900 MHz in the library of campus Queretaro were employed, to achieve these three pre-tests. Once the selection of these approaches is clear, it is possible to ensure accurate predictions.

Additionally, and in order to validate the accuracy of the proposed model, 57 indoor scenarios in campus Queretaro, such as a congress hall, a gym, an auditorium, buildings, and offices were considered to validate if ordinary Kriging is the best linear unbiased predictor, as is reported by linear geostatistics theory [22]. In addition to comparing, the accuracy of the mathematical measurement-based model proposed, which predicts the unmeasured shadowing according to the ordinary Kriging technique, against a classic linear interpolation and the traditional assumption of shadowing as a normally distributed variable.

3.2 Full Article

The performance of in-building measurement-based path loss modelling using kriging

M. E. Diago-Mosquera¹  | A. Aragón-Zavala¹ | C. Vargas-Rosales²

¹Tecnologico de Monterrey, Escuela de Ingeniería y Ciencias, Queretaro, Mexico

²Tecnologico de Monterrey, Escuela de Ingeniería y Ciencias, Monterrey, Mexico

Correspondence

M. E. Diago Mosquera, Tecnológico de Monterrey, Escuela de Ingeniería y Ciencias, Queretaro 76130, Mexico.

Email: a00829220@itesm.mx

Funding information

Consejo Nacional de Ciencia y Tecnología-A, Grant/Award Number: 746015

Abstract

An accuracy evaluation analysis of a novel in-building measurement-based path loss prediction narrowband model is presented here, comparing the performance of Kriging-aided shadowing prediction against the most traditional assumption of slow fading as a random variable and a classical estimation derived from linear interpolation. Extensive radio measurements were employed using distinct samples to calibrate (tuning dataset) and validate (testing dataset) the model. Path loss predictions are made over the testing dataset locations to compare it against the measured values, thus obtaining an error in the prediction from the difference between measurements and predictions. The results in the seven buildings evaluated show the potential of Kriging-aided channel modelling with a higher level of confidence than other modelling approaches compared hereafter.

1 | INTRODUCTION

Channel modelling can enhance communication efficiency through an accurate design to deliver higher quality to mobile users inside buildings. Clear processes and methodologies that can provide a high level of confidence in the design of indoor radio propagation systems are thus required. With the deployment of 5G wireless communication and the need to accommodate for the shorter signal range, mmWave-enabled networks will have a high density of base stations. In such a dense network, interference is an important factor affecting network performance [1]. In this way, an efficient radio access—constructed by accurate channel modelling—combined with more spectrum availability is essential to achieve the ongoing demands faced by wireless carriers [2]. Therefore, it is important to explore suitable in-building mathematical propagation modelling approaches that can accurately make predictions, avoiding undesirable effects—for example, interference, which may result in a low Signal to Interference plus Noise Ratio (SINR), throughput, and in some cases, a total disruption of service [3]—and support ever-growing consumer data rate demands of modern 5G communication systems.

Since hybrid approaches employ solid reference models based on physical principles and are complemented with

measurements to tune up relevant model parameters [4, 5], they look promising towards higher accuracy predictions. Such measurement-based modelling approaches have been used in the past with encouraging results [6–9], taking into consideration that radio measurements are always required even on physical models for validation purposes.

The possibility to collect large amounts of data from measurement campaigns can be very limited for practical designs. Venues often permit data collection campaigns having restrictions on measurement areas, test antenna location placements, available times, and dates to conduct the measurements, etc.

Nevertheless, with a careful design of the measurement campaign, valuable information can be extracted and used in our modelling approach. Linear geostatistics show potential to estimate measurements in such situations, by significantly improving the results with few available samples. In addition, it allows us to extract as much information as possible from the existing sources and to explore the accuracy and efficacy trade-off of the designed model.

The path loss consists of three major components: median path loss, shadowing, and fast fading [10]. These components depend on both the relative position of the elements of a wireless system and the obstructions in the channel. The

This is an open access article under the terms of the Creative Commons Attribution-NonCommercial-NoDerivs License, which permits use and distribution in any medium, provided the original work is properly cited, the use is non-commercial and no modifications or adaptations are made.

© 2021 The Authors. *IET Microwaves, Antennas & Propagation* published by John Wiley & Sons Ltd on behalf of The Institution of Engineering and Technology.

median path loss is predicted by any standard path loss model, such as the classical single slope path loss model. Fast fading results from rapid signal variations on the scale of half-wavelength and is often removed by filtering. For indoor channels, shadowing occurs due to the large variability of obstructions present in the venue, which results in a received power that fluctuates randomly over time. Median path loss modelling cannot only be used to estimate shadowing, but it is empirically known that shadowing has a spatial correlation. Therefore, it can be estimated by applying an appropriate weighted average to the observation dataset in the framework of spatial statistics or by including a method of linear geostatistics that minimises the variance of estimation errors under the constraint of unbiased estimation [11].

Kriging is an interpolation technique based on the methods of geostatistics, where the subject is concerned with spatial data. Geostatistics assumes that there is an implied connection between the measured data value at a point and its location in space. Therefore, it is possible to estimate unknown values from the best set of available sample points, which consider the singularities and the characteristics associated with the selected scenario. An outstanding influence of Kriging interpolation on the construction of radio environment map (REM) has also been observed in various works [12–17]. REM is a tool for analysing radio propagation, which is typically defined as a map that stores the received signal power. Several of these works reported that Kriging is employed to interpolate the received signal power over unknown locations, simplifying the design of REM-based systems. El-friakh et al. [18] suggest that when building indoor Wi-Fi REMs via spatial interpolation methods, in practice, less complex spatial interpolation methods may be preferred over more computationally demanding methods such as Kriging variants. However, for indoor scenarios, the spatial interpolation methods based solely on the estimation error over all rooms analysed in [18] is not sufficient to fully characterise Wi-Fi REMs. Therefore, it is a promising approach to use spatial interpolation methods to estimate only an individual variable and not a global one that depends on others, for example, shadowing instead of received power. Related works on the radio propagation analysis, for example, [19–21], attempt to characterise and estimate shadowing as a variable that follows a normal distribution with zero mean and standard deviation σ . However, few efforts have been taken to predict and extract shadowing from other assumptions and lot less work from spatial statistics.

In channel modelling, the accuracy and efficacy trade-off of the designed model are essential. Purely empirical models are not sufficiently accurate to be employed in all types of buildings and purely deterministic models still need a good amount of computational resources, requiring a large quantity of building details and therefore becoming unviable for practical radio prediction work. Therefore, the model proposed in this study is inspired by the most promising approach of measurement-based method, besides, it is intended primarily for narrowband modelling to estimate path loss inside buildings. The use of Kriging for wideband channel modelling has not been tested yet and somehow is out of the scope of this

work, leaving it as a possibility for future research related to this topic.

Additionally, the contributions presented hereafter are the comparisons of path loss results when spherical and exponential variogram models are selected, showing the most suitable variogram function and the shadowing spatial correlation according to an exponential model; the analysis of different methods to select a tuning dataset towards choosing the best method for taking full advantage of Kriging; and the recommendation about the effective tuning dataset samples to be selected from measurements for obtaining the best goodness of fit, and finding the best trade-off between accuracy and sample size.

2 | MEASUREMENT PROCEDURE AND SCENARIOS

Radio signal measurements were performed within typical in-building propagation in seven buildings at Tecnológico de Monterrey, campus Querétaro, Mexico, as shown in Figure 1.

Extensive measurements were made on each building, in at least three different floors, F_{tx} . The buildings have classrooms, laboratories, offices, general areas of entrance, rooms, and corridors where interior and exterior walls were built with drywall and block, respectively. Ceilings were built of steel decks and metallic beams while the floors were built of ceramic tile. Ceilings are 4 m high with false ceilings which are 3 m high. The measurements were carefully calibrated and filtered for tuning and model validation, included in the so-called tuning and testing dataset.

The transmitter system was placed on different floors in each building, F_{tx} , the overall description of the measurement campaign is shown in Table 1. This system consisted of two types of antennas at different heights, h_{tx} : a Kathrein tri-band omnidirectional indoor antenna, model 800–10,249 for 869.6 MHz with 2 dBi gain, and a Kathrein tri-band directional indoor antenna, model 800–10,248 for 1930.2, 2400, and 2500 MHz with 7 dBi gain; and a Rohde and Schwarz Signal Generator, model SMB100A, 9 KHz–3.2 GHz with 30 dBm of max power. The receiver comprises an omnidirectional monopole 0 dBi antenna plugged into a Rohde and Schwarz Vector Network Analyser (VNA), model ZVL6 for 2400 and 2500 MHz. In addition, a dual-band whip 0 dBi antenna with a portable SeeGull LX dual-band radio scanner was used to perform measurements at 869.6 and 1930.2 MHz.

To avoid an overly transmitter, system pictures Figures 2–5 illustrate the external view of some buildings and the transmitter system used during measurement campaigns.

The measurements were collected by using different walk routes at a constant speed and recorded by means of the radio scanner as well as using the spectrum analyser option of the VNA. Sample locations were recorded with the software InSite v3.1.0.19, from PCTEL, and with a special programme developed in Matlab for the radio scanner and the spectrum analyser, respectively. Afterwards, data post-processing is required to be carried out on the raw collected data to remove

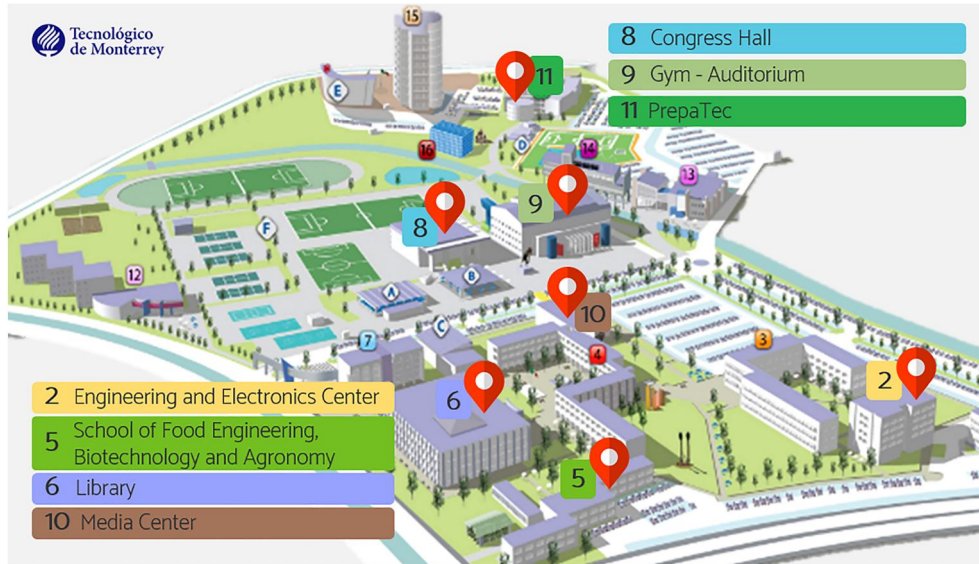


FIGURE 1 Buildings for measurement campaign

TABLE 1 Measurement campaign specifications

| Building | f [MHz] | P_{tx} [dBm] | Orientation [°] | h_{tx} [m] | Antenna location | |
|----------|-----------|----------------|-----------------|--------------|------------------|------------|
| | | | | | F_{tx} | F_{rx} |
| B2 | 869.6 | 11 | 0 | 2.6 | 2 | 1; 2; 3; 4 |
| | 1930.2 | 25 | 90 | 2 | 3 | |
| | 2400 | 25 | 90 | 2 | 2 | 1; 2; 3 |
| B5 | 869.6 | 11 | 0 | 2.6 | 3 | 1; 2; 3 |
| | 1930.2 | 25 | 90 | 2.2 | 1 | |
| B6 | 869.6 | 11 | 0 | 2.3 | 1 | 1; 2; 3 |
| | 1930.2 | 25 | 270 | 2 | | |
| B8 | 869.6 | 11 | 0 | 2.6 | | |
| | 1930.2 | 25 | 90 | 2.2 | 1 | 0; 1; 2 |
| B9 | 869.6 | 11 | 0 | 2.54 | 0 | 0; 1; 2; 3 |
| | 1930.2 | 25 | 235 | 2.2 | 2 | |
| B10 | 869.6 | 11 | 0 | 2.6 | 1 | 0; 1; 2 |
| | 1930.2 | 25 | 180 | 2 | 2 | |
| | 2500 | | | | 1 | |
| B11 | 869.6 | 11 | 0 | 2.6 | 1 | 1; 2; 3 |
| | 1930.2 | 25 | 169 | 2.2 | 2 | |

fast fading by averaging the instantaneous signal strength measurements and samples that either are beyond the noise floor of the receiver or are clipped due to very strong field strength at short distances from a strong transmitter antenna to the receiver. This process should be performed carefully to preserve the shadowing variations and avoid filtering it out. Considering that fast fading is on the scale of half-wavelength,

the entire layout of each scenario was segmented in a grid of $\lambda \times \lambda$ squares, where λ is the wavelength for each measurement frequency—described in Table 1. All the samples inside each square were averaged through (1), removing the fast fading from the sampled signal measured without causing smooth shadowing variations.

$$\overline{P_{rx}} = 10 \log \left(\frac{1}{s} \sum_{i=1}^s 10^{P_{rx_i}/10} \right), \quad (1)$$

where P_{rx_i} is the received power in dBm, and s is the number of samples inside a square of the grid. The averaged measurements were divided into two datasets as follows: one set chosen to perform model fitting, denoted as *tuning dataset*, and the rest of the data considered as a second set called the *testing dataset*. The measurements over the testing dataset were used to evaluate the accuracy of the predictions at those measured locations.

3 | CHANNEL MODEL DESCRIPTION

To improve confidence for in-building radio design, an optimum combination of carefully calibrated and filtered radio measurements with simple path loss models to predict complete system coverage performance was employed. Our overall channel model description is illustrated in Figure 6.

From the tuning dataset, the path loss L is extracted in dB as follows

$$L = P_{tx} + G - P_{rx}, \quad (2)$$

where P_{tx} denotes the transmission power in dBm and G is the transmission gain in dBi. The effects of the antenna radiation pattern are considered to calculate G in a specific location

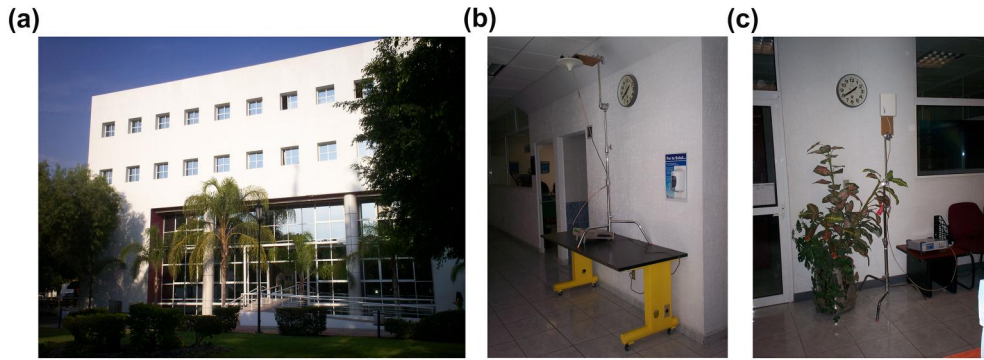


FIGURE 2 Measurement campaign at B2 (a) External view, (b) omnidirectional antenna, (c) directional antenna

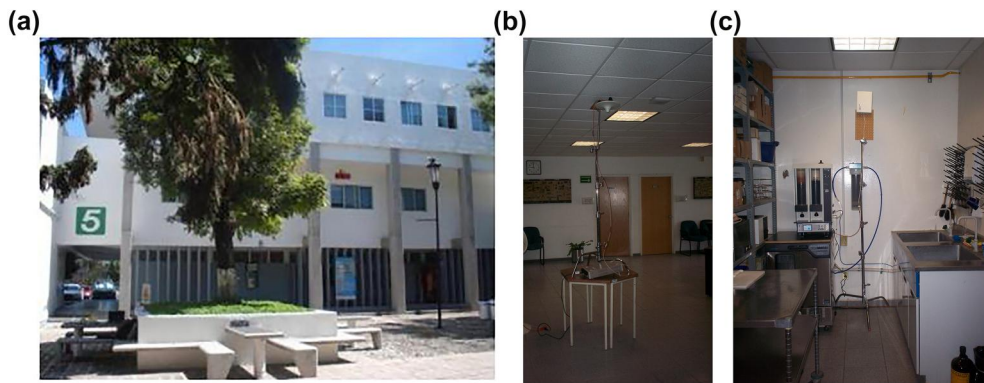


FIGURE 3 Measurement campaign at B5 (a) External view, (b) omnidirectional antenna, (c) directional antenna

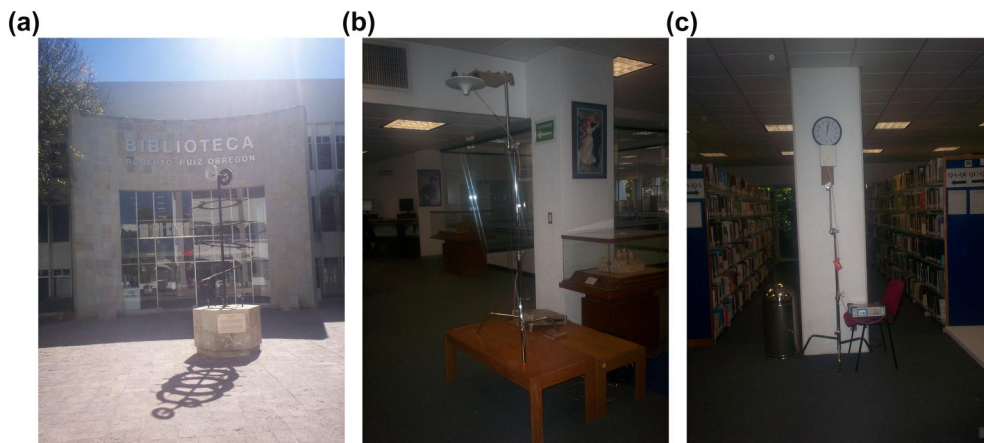


FIGURE 4 Measurement campaign at B6 (a) External view, (b) omnidirectional antenna, (c) directional antenna

point, $G(\theta, \phi)$. For this, the manufacturer's radiation patterns are used, provided in two planes: azimuth θ and elevation ϕ . To estimate gain values at any location from manufacturer's data, the pattern interpolation method proposed by Vasiliadis et al. in [22] was employed as follows:

$$G(\theta, \phi) = \frac{G_H(\theta) \cdot w_1 + G_V(\phi) \cdot w_2}{\sqrt{w_1^2 + w_2^2}}, \quad (3)$$

where, $G_H(\theta)$ and $G_V(\phi)$ are the horizontal and vertical gain in dBi, respectively. w_1 and w_2 are the weight functions described in [22]. To continue with the model tuning process, two components are defined as median path loss L_{50} in dB and shadowing L_s in dB. The median path loss describes a distance-dependent relation, which considers both free space path loss L_{fs} at a reference distance $d_0 = 1$ m and the characteristics of the propagation medium. The median path loss is given by

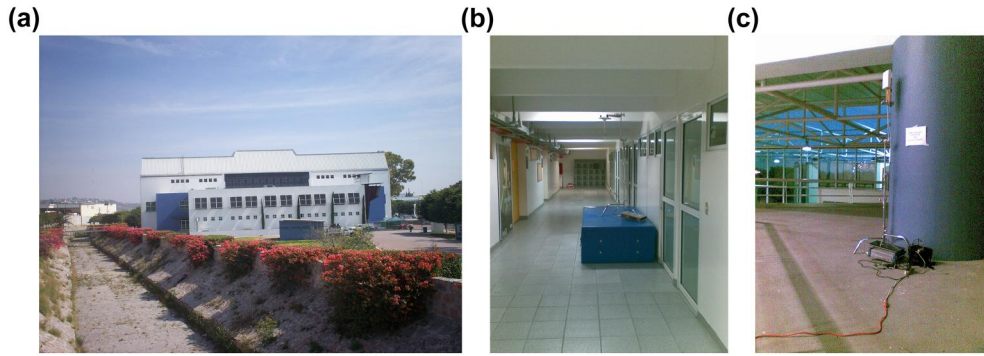


FIGURE 5 Measurement campaign at B9 (a) External view, (b) omnidirectional antenna, (c) directional antenna

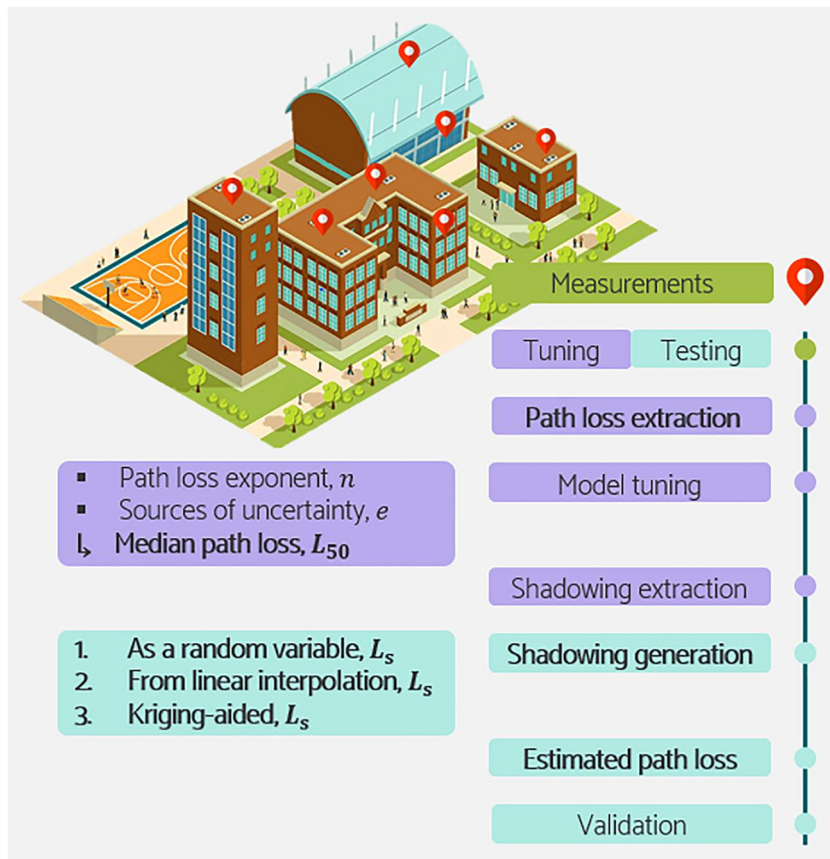


FIGURE 6 Channel model methodology

$$L_{50} = L_{fs} + 10n \log_{10} \left(\frac{d}{d_0} \right) + e, \quad (4)$$

$$L_{fs} = 20 \log_{10} (d_0) + 20 \log_{10} (f) - 28, \quad (5)$$

where n denotes the path loss exponent, d is the Euclidean distance in a three-dimensional space in m , e is a variable accounting for specific sources from floor and walls attenuations and waveguiding gain due to multiple reflections in corridors, and f is the frequency in MHz. To fit the variables in Equation (4), n and e are tuned by linear regression, using the path loss extracted in Equation (2) as L_{50} .

In seeking to optimise the model and to continue with the second component for path loss, shadowing, or slow fading, it depends on the characteristics of the nearby—local clutter—propagation environment, and this is given by

$$L_s = L - L_{50}, \quad (6)$$

Three facts are considered as follows:

1. Kriging, as a spatial predictor, does not require that data follows a normal distribution since it is considered the best linear unbiased predictor. However, if data does follow a

normal distribution, then Kriging becomes the best unbiased spatial predictor of all [23].

2. Shadowing can be modelled as a random variable in dB, normally distributed with zero-mean and standard deviation σ , resulting in a log-normal distribution of the received power in watts.
3. The spatial correlation of the random process from the shadowing datasets is estimated through the *variography* described in Section 4.1.

Thus, a Kriging-aided channel modelling approach was selected to predict shadowing in specific locations and needs to be validated. Equation (6) yields shadowing extracted behaviour, necessary for Kriging processes.

To sum up, the channel model proposed here estimates the path loss as follows

$$L = L_{fs} + 10n \log_{10} \left(\frac{d}{d_0} \right) + e + L_s, \quad (7)$$

where L_s will be extracted from a shadowing grid that is using Kriging, as is presented in the next section. Towards comparing the proposed method accuracy, two more shadowing approaches were considered as follows: an estimate of L_s in dB as a random variable with zero-mean and a standard deviation σ extracted from the tuning dataset in Equation (6) labelled as ‘R’; and an estimate of L_s in dB from a shadowing grid generated by Matlab *griddata* function, that is, a triangulation-based linear interpolation from the tuning dataset in Equation (6), this approach is labelled as ‘LP’. The Kriging-aided method is labelled ‘K’ in the results presented here.

4 | MODELLING KRIGING-AIDED SHADOWING

In geostatistics, the autocorrelation of one or more variables is described to make estimations of a specific parameter for unobserved locations. The main tool in linear geostatistics is known as a *variogram*, which quantifies and describes squared differences between observations, that is, the spatial variability. Thus, the autocorrelated component suggests that, on average, closer observations—distances smaller than a half-wavelength—are more similar to each other than more widely separated observations. For this reason, it is expected to observe that semivariances are smaller at shorter distance and then they stabilise at some distance within the extent of a study area, where the differences between the pairs are approximately equal to the global variance (plotted in a variogram) [24].

To determine the amount of influence that neighbouring observations have when predicting values for unobserved locations, Kriging employs the variogram to make the interpolation. In brief, linear geostatistics include the following:

- variography for modelling the variogram, and
- Kriging for interpolation.

4.1 | Shadowing variography

Since the true variogram of the spatial process is usually unknown, it must be estimated through shadowing extracted from the tuning dataset—given by Equation (6)—as follows:

1. Experimental variogram $\gamma(h)$: calculate the differences between pairs of observed shadowing values,

$$\gamma(h) = \frac{1}{2} (z_x - z_{x+h})^2, \quad (8)$$

where z_x is the shadowing value at the cartesian coordinates given by the vector x and z_{x+h} is the shadowing at another point at a distance h from x .

2. Summarise the experimental variogram by the variogram estimator $\gamma_E(h)$,

$$\gamma_E(h) = \frac{1}{2N(h)} \sum_{i=1}^{N(h)} (z_{x_i} - z_{x_i+h})^2, \quad (9)$$

where $N(h)$ is the number of pairs within the lag interval h and x_i the cartesian coordinates given by vector x at location i .

3. Fit a variogram model function to the variogram estimator, spherical and exponential models provide good results for most datasets in the available published works [25, 26], these functions can be modelled as,

$$\gamma_{sph}(h) = \begin{cases} c_0 + c \left(1.5 \frac{h}{a} - 0.5 \left(\frac{h}{a} \right)^3 \right), & 0 \leq h \leq a \\ c_0 + c, & h > a \end{cases}, \quad (10)$$

$$\gamma_{exp}(h) = c_0 + c \left(1 - e^{-3\frac{h}{a}} \right), \quad (11)$$

where c is the sill, a is the range, and c_0 is the nugget effect of the variogram estimator. The nugget, sill and range of the variogram models are fitted according to weighted least square error, considering that this is a convenient method for fitting a model to an experimental variogram [27].

4.2 | Kriging

Once the model is selected to describe the variogram behaviour, the next step is to employ *ordinary Kriging* to interpolate the shadowing known values onto a regular grid, which is the most popular Kriging method. Ordinary Kriging uses a weighted average of the neighbouring points to estimate the value \hat{z} of an unobserved point x_0 as follows:

$$\hat{z}_{x_0} = \sum_{i=1}^N w_i \cdot z_{x_i}, \tag{12}$$

where w_i denotes the weights that must be estimated, N the number of observations and z_{x_i} the known shadowing values. To guarantee that the estimates are unbiased, this method determines the weights under the constraint $\sum_{i=1}^N w_i = 1$, where the expected average error must be minimised, that is, $E(\hat{z}_{x_i} - z_{x_i}) = 0$.

Satisfying the condition that the sum of the weights should be equal to one. This optimisation problem can be solved using a Lagrange multiplier, resulting in a linear Kriging system of $N + 1$ equations. The Kriging system can be presented in a matrix notation

$$K_v \cdot E = K_R, \tag{14}$$

where K_v is the matrix of the coefficients; these are the modelled variogram values for the pairs of observations, E is the vector of the unknown weights w_i and the Lagrange multiplier v and K_R is the right-hand-side vector. The process to calculate the shadowing regular grid estimates is described by the following steps:

1. Create a grid with the locations where the shadowing is unknown to compute the Euclidean distance with the known locations.
2. Calculate K_R , as follows

$$K_R = \begin{bmatrix} \gamma(x_1, x_0) \\ \gamma(x_2, x_0) \\ \vdots \\ \gamma(x_N, x_0) \\ 1 \end{bmatrix}, \tag{13}$$

where $\gamma(x_i, x_0)$ is the variogram between the data points and the unobserved points. $\gamma(x_i, x_0)$ is calculated from Equation (10) or Equation (11) with h as the values obtained in the previous step.

3. Obtain the weights w_i and the Lagrange multiplier v contained in the matrix $E = [w_1 \ w_2 \ \dots \ w_N \ v]'$, the matrix K_v must be inverted

$$E = K_v^{-1} \cdot K_R, \tag{14}$$

$$K_v = \begin{bmatrix} 0 & \gamma(x_1, x_2) & \dots & \gamma(x_1, x_N) & 1 \\ \gamma(x_2, x_1) & 0 & \dots & \gamma(x_2, x_N) & 1 \\ \vdots & \vdots & \vdots & \vdots & \vdots \\ \gamma(x_N, x_1) & \gamma(x_N, x_2) & \dots & 0 & 1 \\ 1 & 1 & \dots & 1 & 0 \end{bmatrix}, \tag{15}$$

where $\gamma(x_i, x_j)$ are the modelled variogram values for the pairs of observations that are calculated from Equation (10) or

Equation (11) with h as the Euclidean distance between the known locations.

4. Calculate the Kriging shadowing estimations for the grid through Equation (12), where w_i values are in the E matrix obtained through Equation (14). The Kriging variance is given by

$$\sigma^2 = K_R^{-1} \cdot E, \tag{17}$$

5 | MODEL VALIDATION

To justify our Kriging selection and the assumptions that it implies—the shadowing can be modelled as a zero-mean Gaussian random variable; this is usually only tested by visual inspection of the histogram—the histogram of shadowing from tuning datasets was computed. By fitting a Gaussian curve to the histograms, we obtained a goodness of fit metric of R-squared (R^2) for each measurement campaign y_i , which are described in Table 2 and calculated as follows

$$R^2 = 1 - \frac{\sum_{i=1}^N (y_i - \hat{y}_i)^2}{\sum_{i=1}^N (y_i - \bar{y}_i)^2}, \tag{18}$$

TABLE 2 Goodness of fit for shadowing histograms

| Building | F_{tx} | F_{rx} | | | | |
|----------|----------|----------|------|------|------|------|
| | | 0 | 1 | 2 | 3 | 4 |
| B2 | 2 | - | 0.94 | 0.98 | 0.98 | 0.87 |
| | 3 | - | 0.89 | 0.98 | 0.89 | 0.97 |
| | 2 | - | 0.68 | 0.88 | 0.99 | - |
| B5 | 3 | - | 0.96 | 0.95 | 0.99 | - |
| | 1 | - | 0.96 | 0.78 | 0.89 | - |
| B6 | 1 | - | 0.72 | 0.99 | 0.99 | - |
| | - | - | 0.30 | 0.99 | 0.97 | - |
| B8 | 1 | 0.98 | 0.77 | 0.89 | - | - |
| | - | 0.96 | 0.41 | 0.17 | - | - |
| B9 | 0 | 0.99 | 0.89 | 0.99 | 0.90 | - |
| | 2 | 0.99 | 0.97 | 0.98 | 0.97 | - |
| B10 | 1 | 0.96 | 0.93 | 0.99 | - | - |
| | 2 | 0.94 | 0.96 | 0.96 | - | - |
| | 1 | 0.99 | 0.91 | 0.97 | - | - |
| B11 | 1 | - | 0.99 | 0.82 | 0.77 | - |
| | 2 | - | 0.94 | 0.87 | 0.95 | - |

where $(y_i - \hat{y}_i)$ is the difference between measured values and predicted values for the N measures and $(y_i - \bar{y}_i)$ is the difference between measured values and the mean of the predicted values. Indeed, the R^2 coefficient measures how well the prediction explains the measurements, it is in the range $(0, 1)$, where a value close to one means that the prediction efficiently explains the observations.

Based on the results from Table 2, we conclude that in most cases, our Kriging model assumption on the shadowing part is valid. Nevertheless, in the cases where R^2 is below 0.9, we want to analyse how Kriging behaves; therefore, it is further reviewed in Section 5 (Table 5).

The understanding of the selection of the variogram function, tuning dataset method, and tuning dataset size, is an open issue that has been almost not addressed in the available literature. Moreover, the adequate selection of these three approaches results in a reliable model tuning process. Thus, the following three pre-tests were conducted in the B6 to detail the statements considered to validate the model proposed herein:

- *Variogram function selection*: for successful Kriging estimation, it is necessary to choose the most suitable variogram between spherical and exponential fitting functions.
- *Tuning dataset method selection*: it is necessary to analyse what happens when the selection of tuning dataset method varies, to select the right one to get the most out of Kriging.
- *Tuning dataset size*: to select the least amount of tuning dataset to obtain the best goodness of fit, it is necessary to analyse what percentage of data should be selected for this dataset. In all the previous tests, 1 and 2, it is considered at a rate of 70% for tuning and 30% for testing datasets, 70/30, from the whole samples.

5.1 | Pre-test 1: Variogram function selection

Path loss results for spherical and exponential variogram models were analysed. To extract the tuning dataset, the floor layout was divided into nine classification zones each of a width of 5m describing rings around the transmitting antenna, where a 70/30 rate extracted from each classification zone is ensured to carry out an accurate fitting process that considers data from all zones.

For this test and to verify the goodness of fit of the variogram function selected, the metric of R^2 was selected. According to Figure 7, in this case, it seems that the spherical function has a better goodness of fit than the exponential with an $R^2 = 0.75$.

Once the shadowing is predicted over the testing dataset locations through the methodology described in Section 3, the estimations are compared to the real values with a spherical and an exponential function, Figure 8 shows Kriging-aided shadowing estimations and its variance. The kriging variance observed with an exponential function as a fitting variogram model presents a better fit of closer locations to measurement

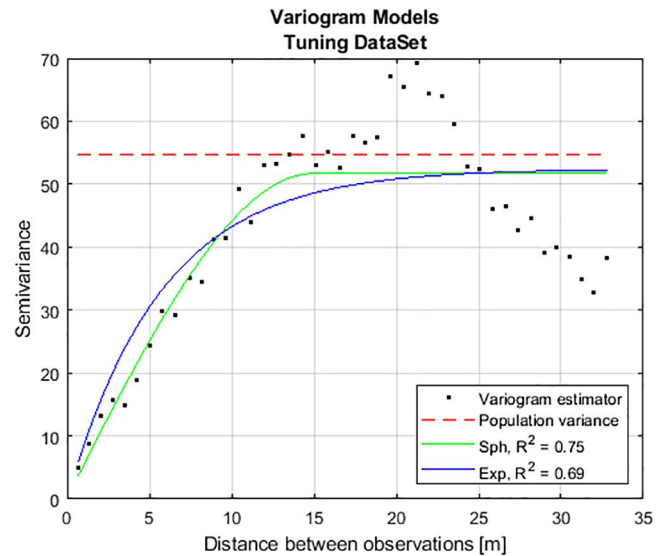


FIGURE 7 Variogram models for shadowing semivariance in B6 (TxL1_RxL1)

samples (black dots—tuning dataset—plus blue dark values of the shadowing variance). Besides, when root mean square errors (RMSE) of both cases were compared, both were small. However, in all cases, the exponential function has a lower value of RMSE.

For B6, Table 3 overviews the goodness of fit metric of R^2 given by (18) and the RMSE defined by

$$\text{RMSE} = \sqrt{\frac{1}{N} \sum_{i=1}^N (y_i - \hat{y}_i)^2}, \quad (19)$$

From the results presented in Table 3, when the exponential function was selected to represent the experimental variogram obtained from tuning dataset, the path loss modelled has a better fit—with a RMSE of 3.03 dB—than the spherical selection.

Therefore, shadowing can be modelled as a zero-mean Gaussian random variable that is spatially correlated according to an exponential correlation model. Besides, shadowing can be estimated through Kriging with a higher level of confidence—with the best goodness of fit of $R^2 = 0.96$ —than the other two approaches: R and LI.

5.2 | Pre-test 2: Tuning dataset method selection

To select the most appropriate tuning dataset from all available measurements, different methods were validated to efficiently divide the samples into two datasets namely tuning and testing. Four classification methods are proposed, each method will divide the measurements into zones under different considerations, where a 70/30 rate from all zones is ensured according

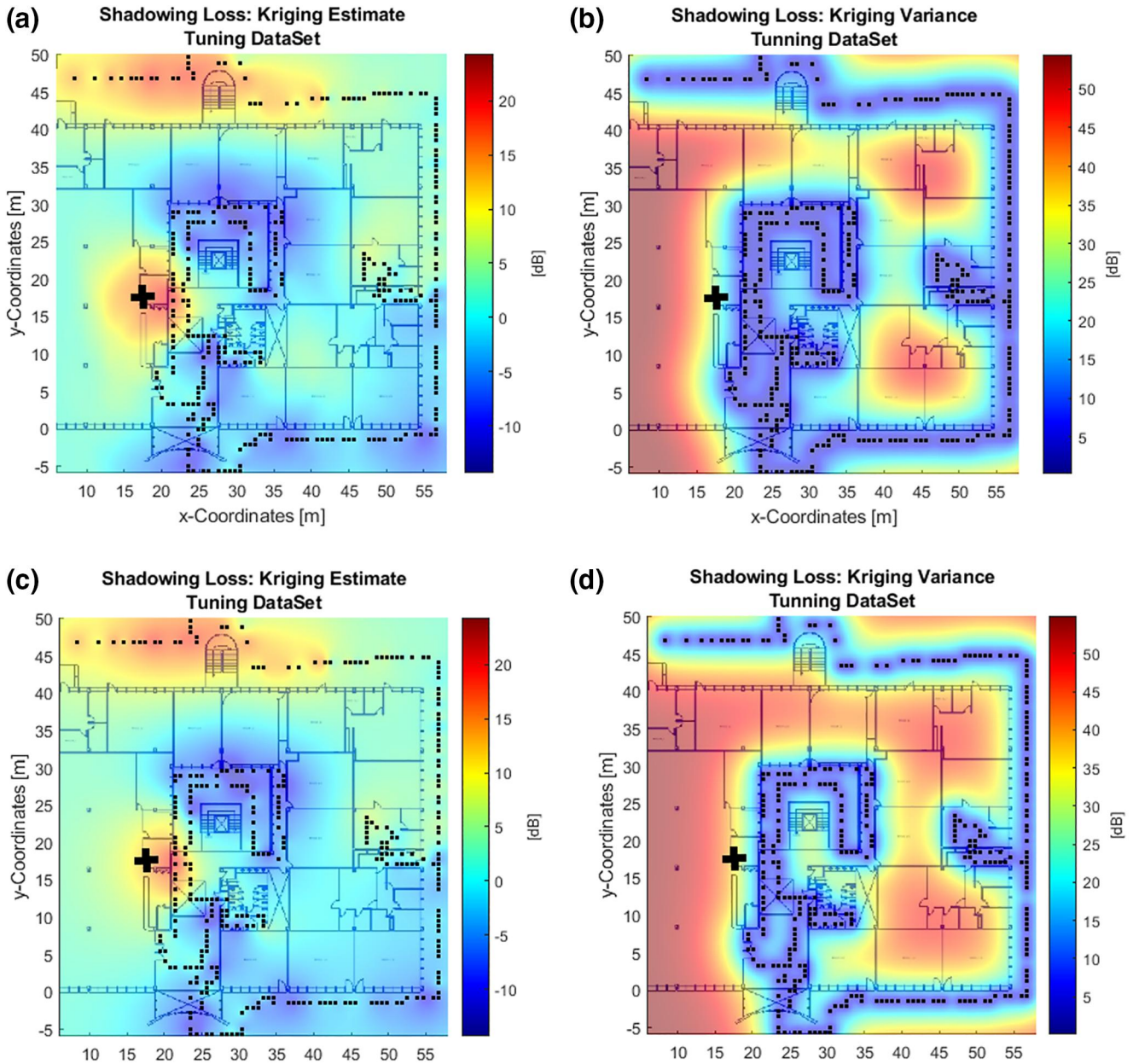


FIGURE 8 Kriging estimates and variance for the tuning shadowing dataset in B6 (a) and (b) with spherical function, (c) and (d) with exponential function

to the classification method. These methods are described as follows:

- Measurements are assigned to areas defined by concentric circles with radius $r = 5k \text{ m}$, where $k = 1, 2, \dots, n$, centred at the position of the transmitting antenna. n depends on the maximum separation distance between transmitter and receiver.
- Measurements are zoned every 5 dBm of received power.
- Measurements are divided according to x coordinates every 3m.
- Measurements are divided into two datasets in a random process that only considers extracting 70% for tuning and 30% for testing from total measurements.

TABLE 3 Results for variogram selection for B6 (TxL1_RxL1)

| Shadowing approaches | R | LI | K (sph) $R^2 = 0.68$ | K (exp) $R^2 = 0.61$ |
|----------------------|-------|-------|----------------------|----------------------|
| R^2 shadowing | -0.93 | -9.81 | 0.82 | 0.81 |
| R^2 path loss | 0.62 | -1.12 | 0.96 | 0.96 |
| RMSE [dB] | 9.79 | 23.16 | 3.06 | 3.03 |

Table 4 shows an overview of the results in terms of R^2 given by Equation (18) and the mean absolute error (MAE) given by

TABLE 4 Results for zones classification

| Method | Parameter | R | LI | K |
|--------|--------------------------|-------|-------|------|
| 1 | R ² shadowing | -1.24 | 0.01 | 0.86 |
| | R ² path loss | 0.47 | 0.77 | 0.97 |
| | MAE [dB] | 8.50 | 3.81 | 2.16 |
| 2 | R ² shadowing | -1.08 | -1.17 | 0.84 |
| | R ² path loss | 0.49 | 0.46 | 0.96 |
| | MAE [dB] | 8.99 | 6.16 | 2.30 |
| 3 | R ² shadowing | -0.63 | -1.20 | 0.82 |
| | R ² path loss | 0.59 | 0.45 | 0.95 |
| | MAE [dB] | 7.96 | 5.64 | 2.40 |
| 4 | R ² shadowing | -0.61 | -1.54 | 0.73 |
| | R ² path loss | 0.58 | 0.33 | 0.93 |
| | MAE [dB] | 8.31 | 6.85 | 2.62 |

Abbreviation: MAE, mean absolute error.

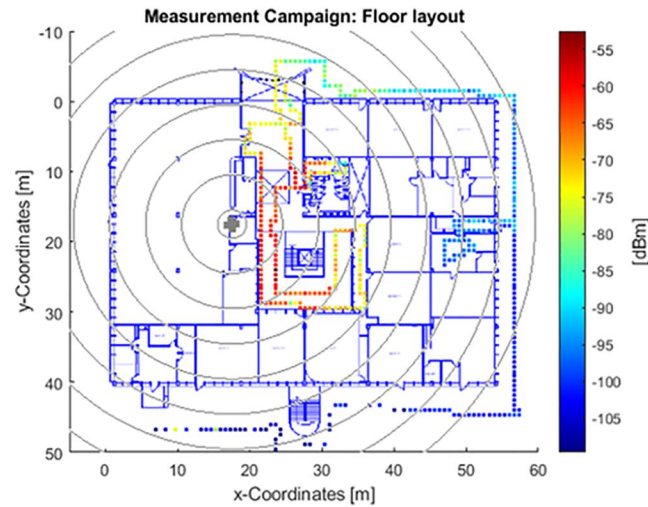


FIGURE 9 Zones to extract tuning and testing dataset. B6 TxL1_RxL1

$$MAE = \frac{1}{N} \sum_{i=1}^N |y_i - \hat{y}_i|, \quad (20)$$

where $|y_i - \hat{y}_i|$ is the absolute value of the difference between measured and predicted values for the N measures. The first method shows the best error performance with the least mean absolute error of 2.16 dB for shadowing estimations; it describes the rings around the transmitting antenna location (see Figure 9).

5.3 | Pre-test 3: Tuning dataset size

To select the least amount of tuning dataset obtaining the best goodness of fit, the size of this dataset was analysed. Tests with 100% to 60% of tuning dataset were carried out, where the 100% is extracted from an initial rate of 70/30.

Figure 10 presents the results of three tests that were performed for each approach (100, 90, 80, 70 and 60), in order to have a sufficient number of outcomes to derive a more solid conclusion.

From Figure 10, it is clear that a 100% to 80% of tuning dataset lets the least error of ≈ 2.2 dB—obtained as the mean error for the three tests—for Kriging-aided model approach. The percentages of 100, 90 and 80 represent a rate of 70/30, 63/37 and 56/44, respectively, for tuning/testing dataset. Consequently, a 60/40 rate to divide the measurement campaign is recommended, considering the first method to classify samples into zones and an exponential function as a fitting variogram model for Kriging process.

5.4 | Results: Path loss predictions

A validation that follows the procedure in Sections 2 and 3 was performed for seven buildings at Tecnológico de Monterrey, campus Querétaro, yielding 57 scenarios described in Table 1. Due to previous three pre-tests, the following approaches are considered to validate the model proposed herein:

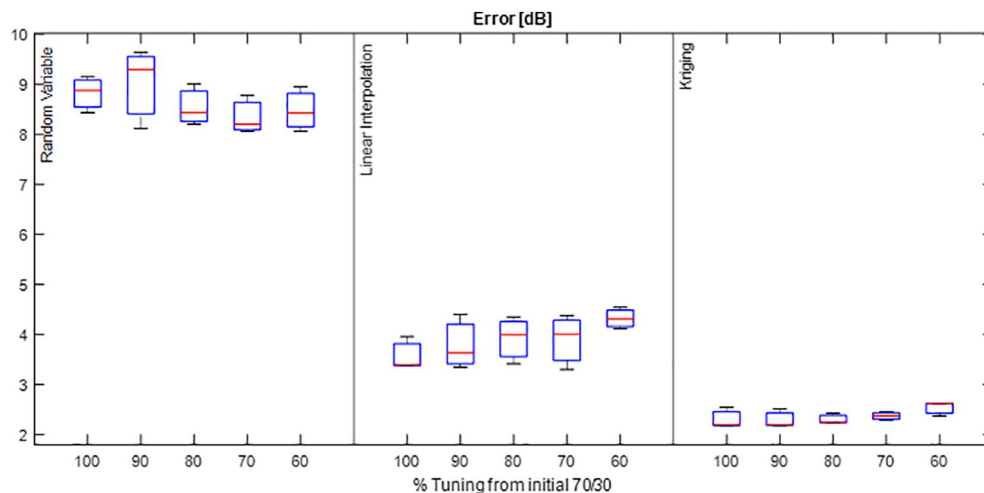


FIGURE 10 Boxplot: Error in path loss for different tuning rates

| No. | F_{tx} | F_{rx} | | | | | |
|-----|----------|---------------------------|---------------------------|---------------------------|---------------------------|-------------|--|
| | | 0 | 1 | 2 | 3 | 4 | |
| B2 | 2 | - | 0.94 0.86 | 0.98 0.19 | 0.98 0.77 | 0.87 0.84 | |
| | 3 | - | 0.89 0.89 | 0.98 0.57 | 0.89 0.79 | 0.97 0.82 | |
| | 2 | - | 0.68 0.89 | 0.88 0.84 | 0.99 0.8 | - | |
| B5 | 3 | - | 0.96 0.61 | 0.95 0.77 | 0.99 0.7 | - | |
| | 1 | - | 0.96 0.94 | 0.78 0.91 | 0.89 0.9 | - | |
| B6 | 1 | - | 0.72 0.96 | 0.99 0.93 | 0.99 0.68 | - | |
| | - | - | 0.30 0.93 | 0.99 0.93 | 0.97 0.84 | - | |
| B8 | 1 | 0.98 0.84 | 0.77 0.93 | 0.89 0.67 | - | - | |
| | - | 0.96 0.82 | 0.41 0.94 | 0.17 0.88 | - | - | |
| B9 | 0 | 0.99 0.85 | 0.89 0.89 | 0.99 0.62 | 0.90 0.47 | - | |
| | 2 | 0.99 0.9 | 0.97 0.75 | 0.98 0.77 | 0.97 0.7 | - | |
| B10 | 1 | 0.96 0.86 | 0.93 0.92 | 0.99 0.65 | - | - | |
| | 2 | 0.94 0.62 | 0.96 0.78 | 0.96 0.84 | - | - | |
| | 1 | 0.99 0.87 | 0.91 0.9 | 0.97 0.73 | - | - | |
| B11 | 1 | - | 0.99 0.95 | 0.82 0.94 | 0.77 0.65 | - | |
| | 2 | - | 0.94 0.92 | 0.87 0.96 | 0.95 0.67 | - | |

TABLE 5 Goodness of fit (R^2) for shadowing histograms and path loss estimations

1. shadowing will be modelled as a zero-mean Gaussian random variable that is spatially correlated according to an exponential correlation model,
2. measurements will be divided into classification zones defined by concentric circles every 5 m from the position of the transmitting antenna, and
3. a 60/40 rate will be extracted from each classification zone to divide samples into tuning and testing dataset.

In Table 5, the goodness of fit for both extracted shadowing fitting with a Gaussian curve (R_1^2) and path loss estimation with the model presented here (R_2^2), are given in the form $R_1^2 | R_2^2$. Through the results highlighted in bold in Table 5, the veracity of Kriging, as the best linear unbiased predictor is clear and validated; these results indicate that the extracted shadowing values that did not follow a normal distribution— $R_1^2 < 0.9$ —did not condition the Kriging process to obtain accurate path loss predictions. In the cases where $R_2^2 < 0.9$, the floors where the transmitting and receiving antenna are located should be observed since this indicates that the mathematical model should include in-building attenuations, and characterise those caused by walls and floors; it provides an opportunity of future work.

Figure 11 shows RMSEs for all the scenarios evaluated. In all cases, the shadowing can be estimated through Kriging with a higher level of confidence than the other two approaches: R and LI. From the 57 validated scenarios, 16 scenarios have the transmitting antenna located on the same floor as the receiving antenna (bold values in Table 5), of which 56.3% have an accurate goodness of fit of the model with $R_2^2 > 0.9$. Besides, in-building measurement-based path loss modelling using

Kriging is an attractive method when performing path loss prediction, as it offers a good trade-off between estimation quality and the number of measurements required for model tuning. In Figure 11, it can be seen that the methodology and the model proposed here improve the prediction accuracy, including cases where the transmitting antenna is located at a different floor from that of the receiving antenna. Moreover, the proposed combined path loss and shadowing model are more accurate and flexible compared with the conventional linear path loss plus log-normal shadowing model. In future work, we expect to compare in-building hybrid propagation models against the model validated here.

6 | CONCLUSIONS

This paper proposes Kriging-aided shadowing for modelling path loss in an indoor scenario based on measurements. It was validated through different approaches that the prediction accuracy, expressed in terms of a goodness of fit metric of R^2 and the RMSEs between estimations and measurements, was significantly better when Kriging is included as part of the tuning process.

As a result of the approaches in testing stages, it was validated that shadowing can be modelled as a zero-mean Gaussian random variable that is spatially correlated according to an exponential correlation model. Besides, in order to capitalise the benefit of using higher confidence predictions minimising cost, we recommend using a 60/40 rate to divide samples into tuning and testing datasets—considering the methodology presented here—with the objective to select the

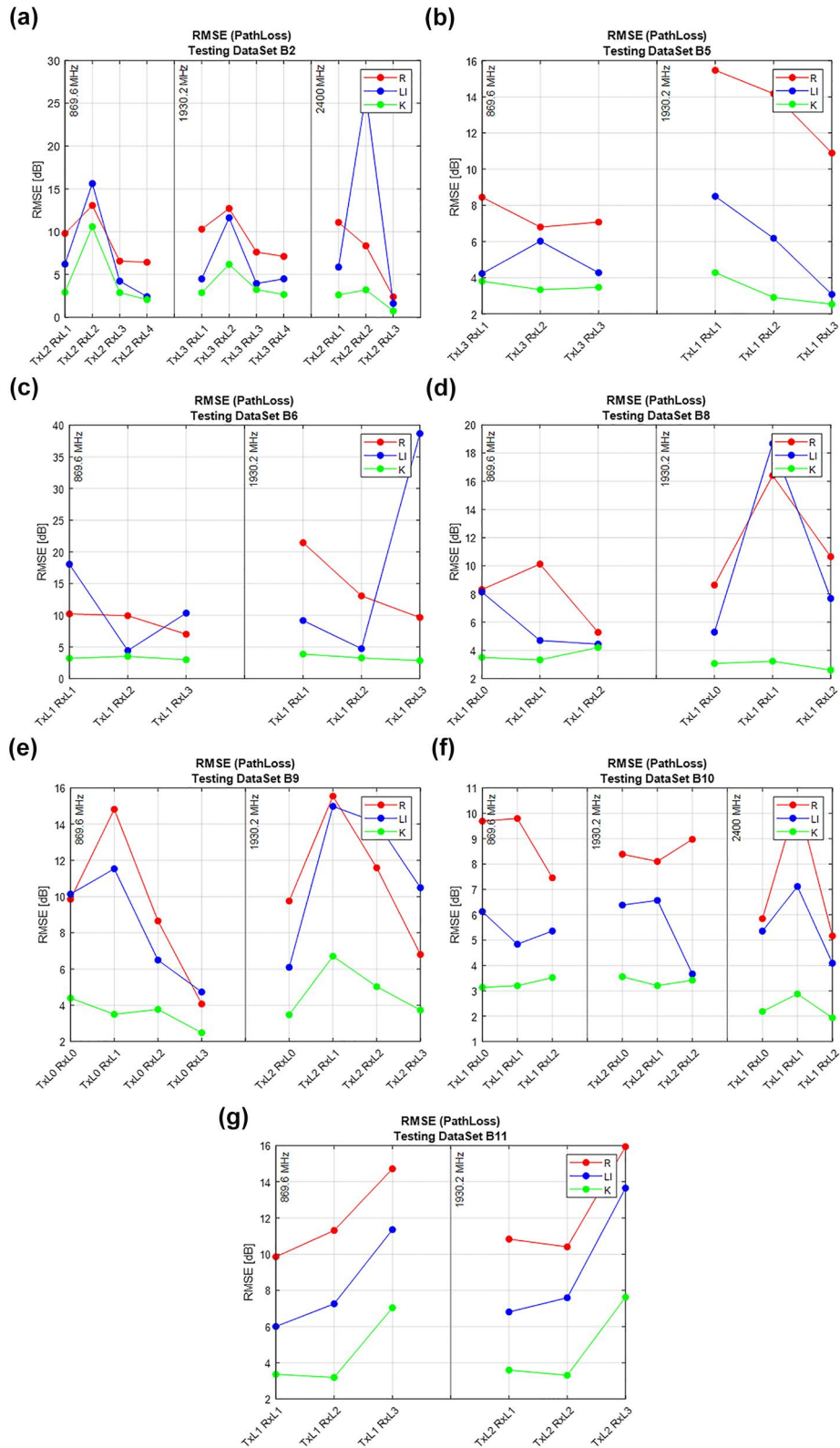


FIGURE 11 Root mean square error (RMSE) over 57 scenarios (a) B2, (b) B5, (c) B6, (d) B8, (e) B9, (f) B10, (g) B11

smallest tuning dataset to obtain the best goodness of fit for modelling Kriging-based shadowing.

ACKNOWLEDGEMENTS

M. E. Diago-Mosquera wishes to thank the National Council of Science and Technology CONACYT, for the student scholarship number 746015.

CONFLICT OF INTEREST

No.

PERMISSION TO REPRODUCE MATERIALS FROM OTHER SOURCES

None.

ORCID

M. E. Diago-Mosquera  <https://orcid.org/0000-0001-8215-3593>

REFERENCES

- Alizadeh, A., Vu, M., Rappaport, T.S.: A study of interference distributions in millimetre wave cellular networks. In: IEEE International Conference on Microwaves, Antennas, Communications and Electronic Systems, COMCAS 2019. Institute of Electrical and Electronics Engineers Inc, Tel-Aviv, Israel (2019)
- Rappaport, T.S., et al.: Wireless communications and applications above 100 GHz: Opportunities and challenges for 6g and beyond. *IEEE Access*. 7, 78729–78757 (2019)
- Kpojime, H.O., Safdar, G.A.: Interference mitigation in cognitive-radio-based femtocells. *IEEE Commun. Surv. Tutorials*. 17(3), 1511–1534 (2015)
- Khatun, M., et al.: Millimetre-wave path loss at 73 GHz in indoor and outdoor airport environments. In: IEEE Vehicular Technology Conference. Institute of Electrical and Electronics Engineers Inc. (2019)
- Faruk, N., et al.: Path loss predictions in the VHF and UHF bands within urban environments: experimental investigation of empirical. Heuristics and Geospatial Models. *IEEE Access*. 7, 77293–77307 (2019)
- Oyic, N.O., Afullo, T.J.O.: Measurements and analysis of large-scale path loss model at 14 and 22 GHz. in *Indoor Corridor*. *IEEE Access*. 6, 17205–17214 (2018)
- Erden, F., Ozdemir, O., Guvenc, I.: 28 GHz mmWave channel measurements and modeling in a library environment. In: IEEE Radio and Wireless Symposium, RWS, pp. 52–55. IEEE Computer Society (2020)
- Zhang, P., et al.: Measurement-based 5G millimeter-wave propagation characterization in vegetated suburban macrocell environments. *IEEE Trans. Antennas Propag.* 68(7), 5556–5567 (2020)
- Chizhik, D., et al.: Path loss and directional gain measurements at 28 GHz for non-line-of-sight coverage of indoors with corridors. *IEEE Trans. Antennas Propag.* 68(6), 4820–4830 (2020)
- Aragon-Zavala, A.: Radio propagation. In: *Indoor Wireless Communications*, pp. 77–112. John Wiley & Sons, Ltd (2017)
- Sato, K., Inage, K., Fujii, T.: On the performance of neural network residual kriging in radio environment mapping. *IEEE Access*. 7, 94557–94568 (2019)
- Bi, J., et al.: Fast radio map construction by using adaptive path loss model interpolation in large-scale building. *Sensors*. Switzerland. 19(3) (2019)
- Sato, K., Fujii, T.: Kriging-based interference power constraint: integrated design of the radio environment map and transmission power. In: *IEEE Transactions on Cognitive Communications and Networking*, pp. 13–25. Institute of Electrical and Electronics Engineers Inc. (2017)
- Sato, K., Inage, K., Fujii, T.: Modelling the kriging-aided spatial spectrum sharing over log-normal channels. *IEEE Wirel. Commun. Lett.* 8(3), 749–752 (2019)
- Achtzehn, A., Riihijarvi, J., Mahonen, P.: Improving accuracy for TVWS geolocation databases: results from measurement-driven estimation approaches. In: *IEEE International Symposium on Dynamic Spectrum Access Networks*, pp. 392–403. IEEE Computer Society, 2014 (2014)
- Phillips, C., et al.: Practical radio environment mapping with geostatistics. In: *IEEE International Symposium on Dynamic Spectrum Access Networks*, pp. 422–433. (2012)
- Sato, K., et al.: Space-frequency-interpolated radio map. *IEEE Trans. Veh. Technol.* 70(1), 714–725 (2021)
- El-Friakh, Z., et al.: Crowdsourced indoor wi-fi REMs: does the spatial interpolation method matter? In: *IEEE International Symposium on Dynamic Spectrum Access Networks*. Institute of Electrical and Electronics Engineers Inc. 2019 (2018)
- Vallet García, J.: Characterisation of the log-normal model for received signal strength measurements in real wireless sensor networks. *J. Sens. Actuator Networks*. 9(1), 12 (2020)
- Morocho-Yaguana, M., et al.: An optimized propagation model based on measurement data for indoor environments. *J. Telecommun. Inf. Technol.* 2018(2), 69–75 (2018)
- Castro, G., et al.: Outdoor-to-Indoor empirical path loss models: analysis for pico and femto cells in street canyons. *IEEE Wirel. Commun. Lett.* 6(4), 542–545 (2017)
- Vasiliadis, T.G., Dimitriou, A.G., Sergiadis, G.D.: A novel technique for the approximation of 3-D antenna radiation patterns. *IEEE Trans. Antennas Propag.* 53(7), 2212–2219 (2005)
- Negreiros, J., et al.: Geographical information systems principles of ordinary kriging interpolator. *J. Appl. Sci* 10(11), 852–867 (2010)
- Hengl, T.: Statistical spatial prediction models. In: *A Practical Guide to Geostatistical Mapping*, pp. 15. (2009)
- Mutlu, T.M., Canberk, B.: A spatial estimation-based handover management for challenging femtocell deployments. In: *IEEE International Black Sea Conference on Communications and Networking, Black-SeaCom 2014*, pp. 144–148. IEEE Computer Society, 2014 (2014)
- Konak, A.: A kriging approach to predicting coverage in wireless networks. *Int. J. Mob. Netw. Des. Innov.* 3(2), 65–71 (2009)
- Jian, X., Olea, R.A., Yu, Y.S.: Semivariogram modelling by weighted least squares. *Comput. Geosci.* 22(4), 387–397 (1996)

How to cite this article: Diago-Mosquera, M.E., Aragón-Zavala, A., Vargas-Rosales, C.: The performance of in-building measurement-based path loss modelling using kriging. *IET Microw. Antennas Propag.* 15(12), 1564–1576 (2021). <https://doi.org/10.1049/mia2.12163>

Chapter 4

Testing a 5G Communication System: Kriging-Aided O2I Path Loss Modeling Based on 3.5 GHz Measurement Analysis

4.1 Summary of the Chapter




In indoor venues with high-density user volumes such as hotels, supermarkets and congress halls, among others, the deployment of indoor radio cells is a common solution, however considering the availability of outdoor radio cells, this would become a hasty solution. Regarding these conditions, outdoor-to-indoor (O2I) models become very relevant. As a consequence, this chapter describes the performance of the proposed model in Chapter 3 when it is employed in O2I scenarios at 3.5 GHz. Two different cases of non-line-of-sight (NLOS) links are considered when the transmitter system is located on the same side of the street where the receiver is located and on the opposite side in two different universities.

Continuing with the validation purposes and based on the fact that a typical O2I path loss model usually follows the most widely used standard equations provided by the projects COST231, WINNER+, ITU-R and 3GPP. The error of the predictions achieved by the proposed model is compared against those obtained when the standard models are employed.

4.2 Full Article

Article

Testing a 5G Communication System: Kriging-Aided O2I Path Loss Modeling Based on 3.5 GHz Measurement Analysis

Melissa Eugenia Diago-Mosquera ^{1,*}, Alejandro Aragón-Zavala ¹ and Mauricio Rodríguez ²

¹ Escuela de Ingeniería y Ciencias, Tecnológico de Monterrey, Av. Epigmenio González 500, Fracc. San Pablo, Querétaro 76130, Mexico; aaragon@tec.mx

² Escuela de Ingeniería Eléctrica, Pontificia Universidad Católica de Valparaíso, Valparaíso 2362804, Chile; mauricio.rodriguez.g@pucv.cl

* Correspondence: a00829220@itesm.mx

Abstract: Deep knowledge of how radio waves behave in a practical wireless channel is required for the effective planning and deployment of radio access networks in outdoor-to-indoor (O2I) environments. Using more than 400 non-line-of-sight (NLOS) radio measurements at 3.5 GHz, this study analyzes and validates a novel O2I measurement-based path loss prediction narrowband model that characterizes and estimates shadowing through Kriging techniques. The prediction results of the developed model are compared with those of the most traditional assumption of slow fading as a random variable: COST231, WINNER+, ITU-R, 3GPP urban microcell O2I models and field measured data. The results showed and guaranteed that the predicted path loss accuracy, expressed in terms of the mean error, standard deviation and root mean square error (RMSE) was significantly better with the proposed model; it considerably decreased the average error for both scenarios under evaluation.

Keywords: Kriging; outdoor-to-indoor (O2I); path loss; radio propagation; shadowing



Citation: Diago-Mosquera, M.E.; Aragón-Zavala, A.; Rodríguez, M. Testing a 5G Communication System: Kriging-Aided O2I Path Loss Modeling Based on 3.5 GHz Measurement Analysis. *Sensors* **2021**, *21*, 6716. <https://doi.org/10.3390/s21206716>

Academic Editor: Dima Bykhovskiy, Yoram Haddad and Yosef Pinhasi

Received: 24 August 2021

Accepted: 20 September 2021

Published: 9 October 2021

Publisher's Note: MDPI stays neutral with regard to jurisdictional claims in published maps and institutional affiliations.



Copyright: © 2021 by the authors. Licensee MDPI, Basel, Switzerland. This article is an open access article distributed under the terms and conditions of the Creative Commons Attribution (CC BY) license (<https://creativecommons.org/licenses/by/4.0/>).

1. Introduction

In recent years, there is a clear need to supply a sufficiently high data rate for areas with elevated user volume such as venues, hotels, and conference centers, etc., where a lack of signal is evident. Usually, in these situations the deployment of a new indoor radio cell is unnecessary considering outdoor radio cell availability. Under these conditions, outdoor-to-indoor (O2I) models become very relevant. These models characterize signal propagation inside buildings coming from external mobile radio base stations (BSs), which are mounted across a network of outdoor sites, occupying towers on hilltops, rooftops in built-up areas, and other promising outdoor structures. O2I radio propagation has become a challenging work, according to Small Cell Forum [1] some reasons for this are:

- Due to the lower operating frequencies becoming exhausted, higher frequencies are being deployed. However, they are not as effective for range and building penetration.
- O2I signal propagation is affected because the building fabric is more eco-friendly and noise-free, using low-emissivity glass which reflects the radiation from cellular antennas, and soundproof materials which attenuate radio waves.
- There are large increases in demand for mobile cellular services which densify available networks with more sites and an increase in the size of the spectrum that mobile network operators (MNOs) can deploy on those sites. This produces localized congestion; the service may be available, but it may not always be satisfactory.

Therefore, the scientific community is encouraged to understand O2I radio wave propagation [2–5] to help radio network engineers to achieve efficient radio coverage estimation, determine the optimal BS location, and perform interference feasibility studies. In seeking to understand those links, the applicability of standard urban microcell O2I path loss models such as COST231, WINNER+, ITU-R, and 3GPP are empirically tested [6].

The COST 231 project is based on adjusted models such as the one-slope model (1SM), the multi-wall model (MWM) and the linear attenuation model (LAM), that are based on propagation measurements [7]. The final O2I model proposed by the COST231 project is based on empirical data acquired for NLOS links, where the model relates the loss inside a room to the loss measured outside of it on the side nearest to the wall of interest, i.e., multi-floor propagation. The WINNER+ channel model followed a geometry-based stochastic channel modeling approach [8]. The channel parameters were determined stochastically, based on statistical distributions extracted from channel measurements. The ITU-R model [9] provided guidelines for both the procedure and the criteria (technical, spectrum and service) to be used in evaluating the proposed IMT-Advanced radio interface technologies (RITs) or sets of RITs (SRITs) for a number of test environments and deployment scenarios for the evaluation of the band of frequencies between 2 and 6 GHz. The NLOS model proposed by the 3GPP is based on measurement campaigns, for O2I building penetration loss. This model considered the material penetration losses for two types of models: low loss and high loss. The composition of low and high loss is dependent on the use of metal-coated glass in buildings and the deployment scenario characteristics. The study reported for the 3GPP project considered not only O2I building penetration losses but also O2I car penetration losses for the frequency range of 0.6 to 60 GHz [10].

According to [11], through an accurate channel modeling: the in-building radio propagation phenomena, complex by nature, can be characterized; the range of a wireless communication system can be calculated by assessing the expected coverage inside a building; signal strength/path loss can be predicted more accurately everywhere in a building; and channel performance predictions can be made quickly.

There are essentially three approaches for propagation models: physical, empirical and hybrid. The majority of physical models are simple to use but their assumptions are based on many simplifications. Generally, for this reason, they are employed to describe the phenomenon within a given error, whereas empirical models take valuable and building-specific information into account. As a result of combining the previous approaches, hybrid models include the accuracy of physical models and the suitability of measurement-based tuning perform in empirical models. On this basis, measurement-based methods are promising to achieve accurate and practical predictions, even in situations where there are not enough samples to carry out a rigorous characterization. To address the shortcoming of samples from measurement campaigns, linear geostatistics demonstrate their usefulness to predict unknown data with few available samples for practical designs.

To quantify the reliability of coverage provided by any radio cell it is imperative to understand and to characterize median path loss, shadow fading, and fast fading as the main path loss components [12]. As is surveyed in [11], the estimation of median path loss is deterministic, mathematical models describe it in terms of how path loss changes as a function of some factors, such as frequency and specific distance, etc. Nevertheless, these models need to account for the shadowing process, including it as an additional variable which describes the dispersion with respect to the nominal value given by the path loss models. Therefore, due to the normal distribution that shadowing produces in the signal measured, the most traditional action is to characterize it by a zero-mean Gaussian random variable, such as in [6]. Other wireless studies include nonconstant shadowing variance and non-lognormal shadowing, and predict the variance by considering the correlation between paths [13,14]. However, in [15] the authors validate a more accurate method to estimate the spatial correlation of shadowing by including Kriging, a linear geostatistics technique that is based on the regionalized theory, which states that there is a variance rate between samples over space in a physical continuity context, i.e., the spatial dependence stated by Tobler in [16]: spatial samples taken close to each other may be expected to have more similar values than samples taken farther apart. There are different types of Kriging techniques, ordinary Kriging is the most common method; however, if there is a spatial trend then this technique is no longer the appropriate to model the spatial variability. There are other alternatives of Kriging, for instance, universal Kriging and simple Kriging, among

others. The properly selection of the Kriging technique is focused on the data characteristics. To summarize, the aim of Kriging is to minimize the variance of estimation errors under the constraint of unbiased estimation [17]. The spatial prediction of Kriging does not require that data to be interpolated follow a normal distribution since Kriging describes the best linear unbiased estimator in the sense of least variance. However, if the data follow a normal distribution, then Kriging becomes the best unbiased spatial predictor. Therefore, telecommunications studies include Kriging to realize a highly accurate radio environment map (REM) [18–20] or to enrich the training dataset (to produce a large amount of data) for channel modeling, as is reported in [21].

Additionally, in [15], Kriging was employed to estimate shadowing only in indoor scenarios at 869.6 MHz, 1930.2 MHz, 2400 MHz and 2500 MHz without considering O2I non-line-of-sight (NLOS) links. Unlike the links studied in [15], in [6], the authors considered O2I NLOS; nevertheless, they only focused their study on comparing the performance of standard model predictions. To the best of our knowledge, this is the first time such novel modelling for estimating shadowing through Kriging in O2I links at 3.5 GHz for 5G communication systems has been presented.

The findings of this study engage students in wireless telecommunications, professionals in the industry, and readers with new Kriging-applied insights and help them to effectively reduce the time and costs involved in measurements campaigns to achieve efficient radio coverage estimations.

2. Methodology and Data Collection

As an optimum combination of carefully measurements, Kriging and simple path loss models were employed to predict complete system coverage performance in two types of O2I NLOS links. The methodology, measurement equipment, scenarios and procedure are described as follows.

2.1. Measurements and Data Collection Procedure

In order to represent typical O2I links, received signal-strength measurements were carried out in two universities in Chile with similar scenarios: the engineering campus of Universidad Diego Portales (UDP) in Santiago, and the main campus of Universidad Técnica Federico Santa María (USM) in Valparaíso. This measurement campaign was employed in [6] to research a completely different objective than the one addressed in this study; here we only employ the NLOS O2I samples. In seeking to analyze NLOS links, the samples collected in the measurement campaigns described two types of links reported in Table 1. Table 2 details the scenarios for measurement campaigns and the NLOS O2I samples collected.

Table 1. Measurement Campaign non-line-of-sight (NLOS) Links.

| NLOS Link | Description |
|--------------------|--|
| Same side (SS) | The transmitter and receiver system share the same street |
| Opposite side (OS) | The transmitter and receiver system are placed on opposing sides of the street |

Table 2. Measurement Campaign Scenarios.

| Scenario | Outdoor ¹ | | | Indoor | |
|----------|----------------------|---------------|---|-----------|-------------|
| | Street Width | Street Length | Surroundings | No. Rooms | Rooms Width |
| UDP | 21 m | 89 m | Concrete buildings with different floor heights and a few trees with ≈6 m in height | 2 | 6 m |
| USM | 8.5 m | 70 m | Three-story concrete buildings of uniform shape with 6 m ² windows | 5 | 6 m |

¹ There is an empty space on the opposite side of the university buildings.

In Figure 1, a basic layout of both scenarios is illustrated; for same side (SS) links, the transmitter system was always placed on the sidewalk 0.7 m away from the building wall, and for opposite side (OS) links, it was moved directly across the street from its previous location. Throughout the different transmitter system settings, it was located at a 5 m height with a 60° depression angle to the wall. The transmitter power of the system was 17.8 dBm (P_{tx}) at a 3.5 GHz continuous wave (CW) and it consisted of a vertically polarized directional patch antenna with 10.2 dB gain (G_{tx}), 60° azimuth and elevation half-power beamwidths. The received power was recorded by a narrowband receiver connected to a vertically polarized half-wavelength dipole with a 2.4 dB gain (G_{rx}). The receiver bandwidth of 200 KHz allowed it to capture any frequency dispersion affecting the CW transmission. In all field measurements the received power was at least 20 dB above the receiver noise floor of -123 dB.

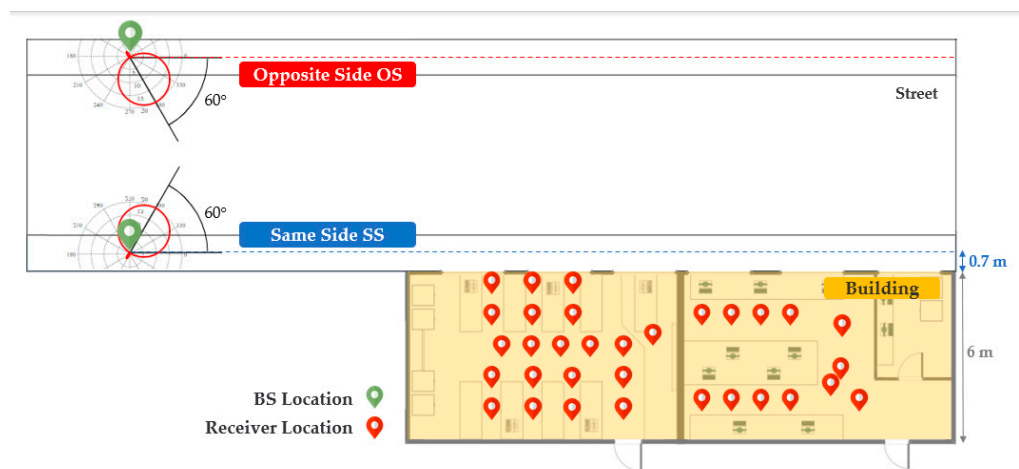


Figure 1. An example of the measurement layout.

For the sampling process the receiver antenna was placed on a computer-controlled rotating arm involving measurements of 6° (or 0.105 rad) angular increments on circles of radius 0.4 m at each receiver placement. For each angular position 25 consecutive power samples were collected, in order to verify consistency and averaging, and to remove residual temporal fades, which did not fluctuate by more than ± 0.5 dB due to the narrowband static environment. Then, these consecutive samples were averaged to account for the first power sample value and to continue to the next angular position until 60 possible angular positions were completed in a 360° circle. Finally, 60 received signal power samples were collected at each receive location, as illustrated in Figure 2. Regarding receiver locations, a total of 308 and 108 sample locations were reported for the O2I NLOS USM and UDP scenarios, respectively.

Considering the angular increments as θ and the circle radius as r in Figure 3 the resulting separation distance is illustrated. In each location, this method yields a circle with $\lambda/2$ separation distance between successive antenna positions because $0.04 \text{ m} \equiv \lambda/2$. According to [22], the spatial average of $\lambda/2$ is in accordance with the shadow-fade correlation distance.

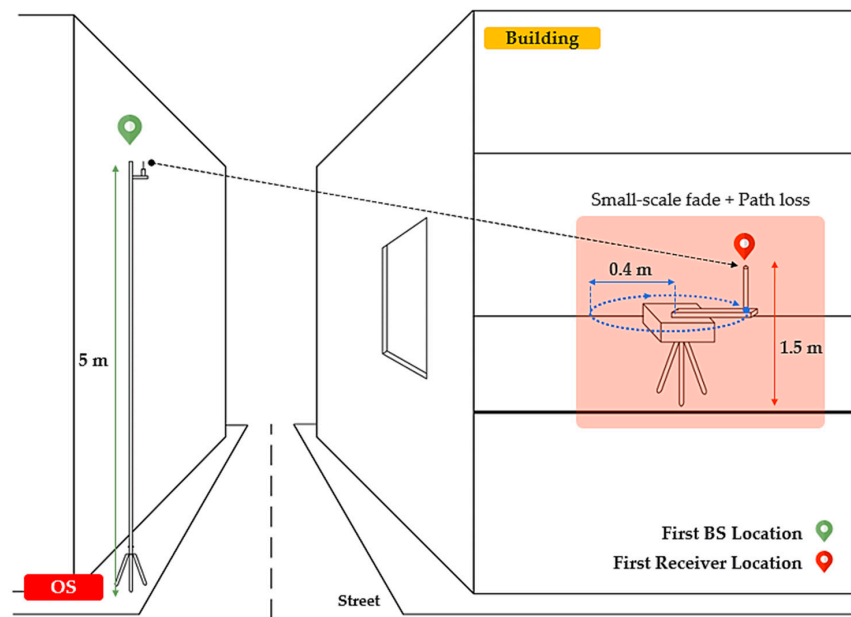


Figure 2. An example of the OS NLOS measurement configuration with the on-axis 0.4 m rotating system.

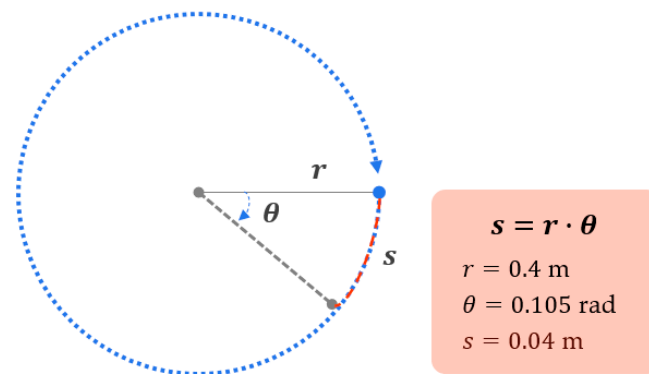


Figure 3. Separation distance according to the angular increment.

Thus, to average out the small-scale fades, the resulting average power ($\overline{P_{rx}}$) at specific locations corresponded to the mean of the 60 samples recorded, which was calculated as follows:

$$\overline{P_{rx}} = 10 \log \left(\frac{1}{60} \sum_{i=1}^{60} 10^{P_{rx_i}/10} \right), \quad (1)$$

where P_{rx_i} is the received power measured in dBm and i is the number of the sample recorded. An overview of the measurement conditions is presented in Table 3.

Table 3. Measurement Parameters.

| Parameter | Description |
|--|---------------------|
| Type of O2I links | OS NLOS and SS NLOS |
| Frequency, f | 3.5 GHz |
| Transmit power, P_{tx} | 17.8 dBm |
| Transmit gain, G_{tx} | 10.2 dB |
| Receive gain, G_{rx} | 2.4 dB |
| Receive distance range, d | 5–40 m |
| Receiver noise floor | −123 dBm |
| Number of spatial positions at each receive location | 60 |
| Number of O2I NLOS links at USM | 308 |
| Number of O2I NLOS links at UDP | 108 |

2.2. Kriging-Based Channel Model Development

The overall methodology for both SS and OS channel modelling links is illustrated in Figure 4 and described as follows. As a first step, from the resulting O2I measurements, SS and OS NLOS links, the path loss L is extracted in dB as a classical link budget:

$$L = P_{tx} + G_{tx} + G_{rx} - \overline{P_{rx}}. \quad (2)$$

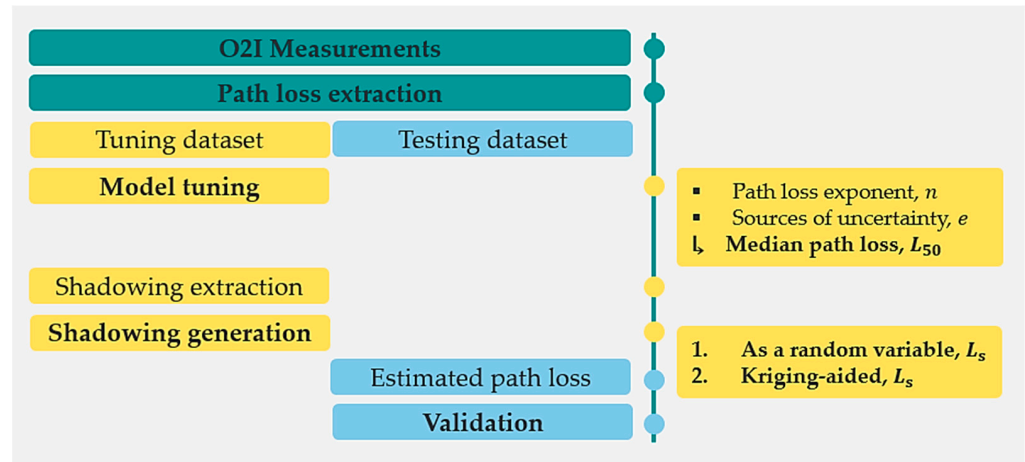


Figure 4. Channel model methodology.

To properly choose tuning samples that accurately reflected the characteristics of the larger measurement campaign, the selections suggested by the authors in [15] about the method and dataset size for tuning selection were considered: first, four classification methods were addressed and compared in terms of the mean absolute error (MAE); the results showed the first method as the most accurate with the lowest MAE of 2.16 dB. This method divided the target area of each scenario into representative zones bounded by concentric circles every 5 m from the position of the BS; and second, five approaches were addressed in order to select the least amount of tuning dataset, obtaining the best goodness of fit. The conclusion for this test was to recommend the rate of 60/40 to extract tuning and testing datasets. Considering both suggestions, the measurements were divided into areas defined by rings with radius $r = 5k$ in m (where $k = 1, 2, \dots, n$, and n depends on the maximum separation distance between transmitter and receiver) centered at the position of the BS. Then, a 60/40 rate was extracted from each zone: 60% exclusively used for driving the measurement-based prediction process using Kriging (tuning dataset), and 40% to perform the validation of the estimated path loss at those testing placements (testing dataset). For the model tuning process, the path loss extracted in (2) was defined by two components [22]: median path loss L_{50} and shadowing L_s in dB:

$$L = L_{50} + L_s. \quad (3)$$

The median path loss described how the transmitted signal was attenuated during the path, in terms of the free space path loss $L_{fs} = 20 \log_{10}(d_0) + 20 \log_{10}(f \text{ [MHz]}) - 28$ [23], the distance-dependent relation, and specific sources from wall attenuations. In this channel modeling proposal, the median path loss was calculated as:

$$L_{50} = L_{fs} + 10n \log_{10}\left(\frac{d}{d_0}\right) + e, \quad (4)$$

where $L_{fs} = 42.9$ dB, d_0 is the reference distance of 1 m, n denotes the path loss exponent, d is the Euclidean distance in a three-dimensional space in m, and e is strictly related to attenuation sources such as floor and walls attenuations. The variables n and e are found

by fitting a linear equation to the path loss extracted in (2); the linear regression results are shown in Table 4.

Table 4. Median Path Loss.

| O2I Link | n | e |
|----------|------|-------|
| SS | 1.93 | 24.73 |
| OS | 2.41 | 15.64 |

In Figure 5 the path loss extracted from (2) is illustrated in blue circles markers for the SS links and in red cross markers for the OS links (where the marker points are already averaged over all 60 samples per received position) along with the median path loss calculated by (4) with the values presented in Table 4 for the SS and OS NLOS O2I links.

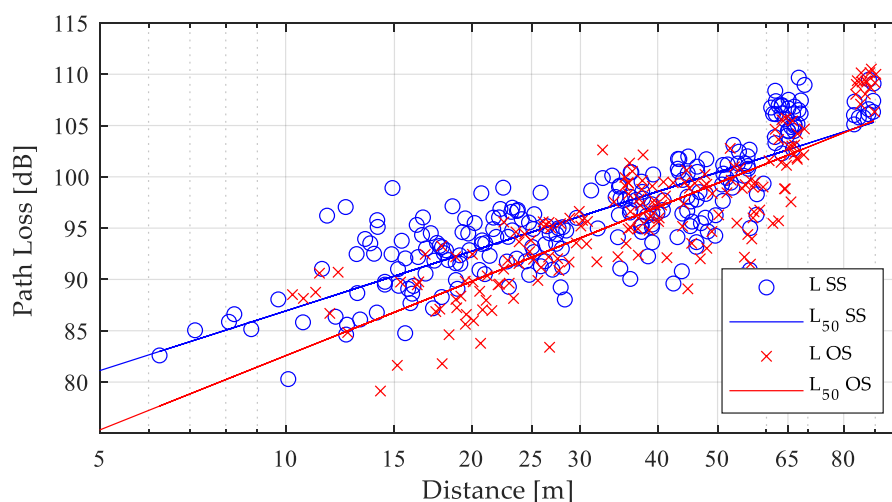


Figure 5. O2I path loss measurements.

For shadowing extraction and continuing with the second component for path loss, the shadowing is extracted from (3) as follows:

$$L_s = L - L_{50}. \quad (5)$$

The shadowing generation process employs the shadow values previously obtained in (5) to interpolate the known data $L_s(c_i)$ in unknown locations c_0 , achieving the accurate shadowing values through the Kriging-aided channel. In other words, from the N shadowing tuning samples at the coordinates c_i , the dataset vector defined by (6) is extracted, leading Kriging to estimate an unknown shadowing value $L_s(c_0)$ at a random location c_0 from the known samples $L_s(c_i)$:

$$L_s(c_i) = (L_s(c_1), L_s(c_2), \dots, L_s(c_N))^T. \quad (6)$$

To provide these predictions, Kriging employs the variography to understand and find a pertinent threshold of neighboring samples to the interpolation. In order to summarize the central shadowing tendency, an exponential model function is fitted to the variogram estimator to further visualize the shadowing spatial process. The selection of the exponential function is focused on both theoretical reasons, which highlight the properties that a function selected as a variogram model must fulfil, and practical reasons, for which evidence from multiple studies [15,24,25] demonstrates that the exponential function provides the best fits.

In Figure 6, it is possible to observe that the parametric curve (exponential function, Exp) fits reasonably well over the first three 5 m lags for both SS and OS NLOS links.

According to geostatistics [26], this is appropriate for Kriging due to near points, such as shadowing neighboring samples, carry more weight than more distant ones to the unknown shadowing values. Thereby, considering the characteristics of the data, ordinary Kriging is employed to interpolate and then predict shadowing at each grid location in the scenario area. Ordinary Kriging uses a weighted average of the neighboring points to estimate the value of an unobserved point. To guarantee that the estimates are unbiased this Kriging determines the weights under the constraint described below in Algorithm 1. As is illustrated in Figure 4, at the end of the methodology proposed, the estimated path loss is assessed by (3) at the testing locations in order to proceed with the validation of the shadowing measured at those points.

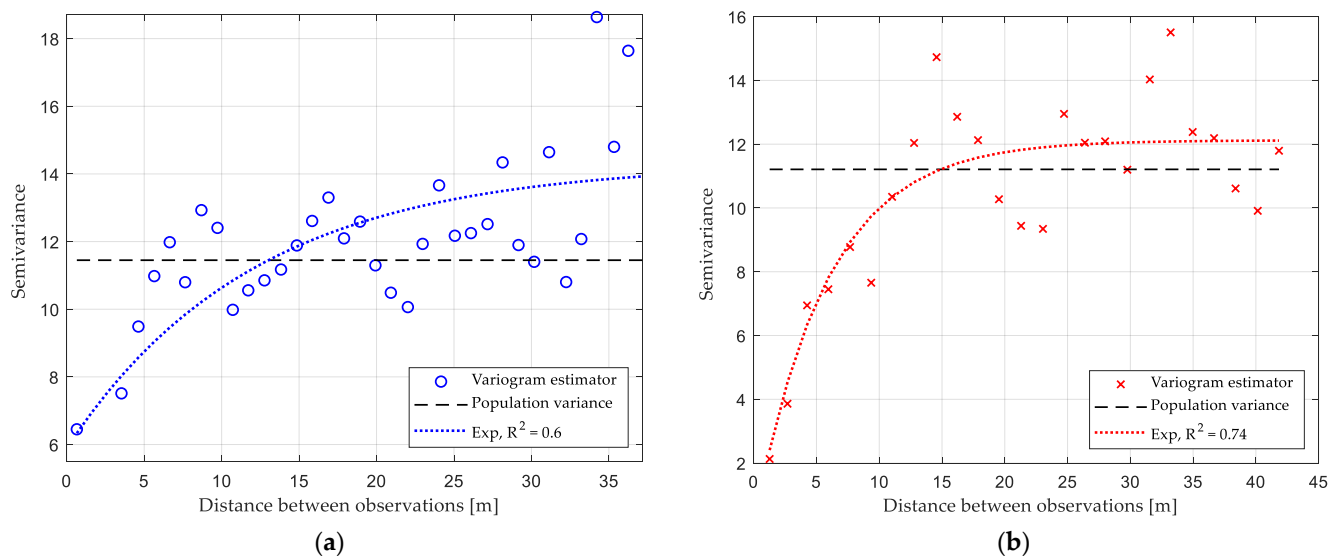


Figure 6. Variography results. (a) SS UDP & USM O2I link. (b) OS UDP & USM O2I link.

All the supporting information for the Kriging-aided method was analyzed and described in greater depth in [15]; however, an overview is presented in the algorithm below.

Algorithm 1. Kriging-aided process.

Designing the path loss:

- 1: Tune the parameters n and e in (4) from the tuning dataset.
- 2: Extract shadowing from (5).
- 3: Generate shadowing through the Kriging-aided process: variogram and interpolation.

Modeling the variogram:

- 4: Calculate the experimental variogram.
- 5: Summarize the experimental variogram.
- 6: Fit a parametric curve.
- 7: **if** variogram fits to the first 3 lags **then**

Kriging interpolation:

- 8: Create the scenario through a grid.
- 9: **Ordinary Kriging** constraint: $\sum_{i=1}^N w_i = 1$
- 10: Calculate the weights w_i and the Lagrange multiplier.
- 11: Estimate L_s through the weighted average of the neighboring points.

Estimating the path loss:

- 12:
$$L = L_{fs} + 10n \log_{10} \left(\frac{d}{d_0} \right) + e + L_s$$

3. Results

The developed model described in Section 2.2 is labeled as K with $L = L_{50} + L_s$ where L_s is extracted from the shadowing grid generated by Kriging. In order to validate the performance and the accuracy of the prediction results of the model, it is evaluated based

on the mean error, standard deviation and root mean square error (RMSE) of the predicted path loss values, \hat{L}_i , at the testing measured locations, t_N , relative to the corresponding testing measured path loss values, L_i . The mean error (ME), the standard deviation of the error (S) and the RMSE are given by:

$$ME = \frac{1}{t_N} \sum_{i=1}^{t_N} (L_i - \hat{L}_i), \quad (7)$$

$$S = \sqrt{\frac{1}{t_N - 1} \sum_{i=1}^{t_N} |(L_i - \hat{L}_i) - ME|^2}, \quad (8)$$

$$RMSE = \sqrt{\frac{1}{t_N} \sum_{i=1}^{t_N} (L_i - \hat{L}_i)^2}. \quad (9)$$

Furthermore, these results are compared with those of the most traditional assumption of $L = L_{50} + L_s$, where the shadowing, L_s , is a random variable with a zero mean and a standard deviation σ extracted from the tuning dataset behavior, labeled as R .

Based on the approach that a typical O2I path loss prediction model considers: the main large-scale propagation loss in line-of-sight (LOS) or NLOS up to the building wall, is a penetration factor that adds wall losses and an indoor path loss term, and that this structure is shared by the most widely used standard models for O2I: COST231 Building Penetration LOS model [7], WINNER+ O2Ia/LOS model [8], ITU-R O2I model [9] and 3GPP 3D-UMi O2I model [10]. The K model predictions are also compared with those of the standard models. The path loss estimated through the standard models is calculated using (7), where each component is in dB and is described in Table 5:

$$L_{sm} = L_1 + L_2 + L_3, \quad (10)$$

The path loss components, described in Table 5, were extracted from the setup and results of the O2I NLOS measurement campaign, i.e., the distances of the x , y , and z axes were given by the location of each measurement, the frequency f in Hz (3.5×10^9 Hz) and the room depth w in m by the measurement setup. In each room where the measurements were performed the receiver antenna was placed at three different room depths: around 1 m from the exterior university wall, in the center of the room, and around 1 m from the interior university wall.

Table 5. Standard Models.

| Standard Model | Path Loss Components ¹ |
|----------------|---|
| 3GPP | $L_1 = 22 \log(\sqrt{x^2 + y^2 + z^2}) + 28 + 20 \log f$ $L_2 = 20$ $L_3 = \frac{w}{2}$ |
| ITU-R | $L_1 = 22 \left(\log \sqrt{x^2 + (y-w)^2 + z^2} \right) + 28 + 20 \log f$ $L_2 = 14 + 15 \cdot (1 - \theta)^2$ $L_3 = \frac{w}{2}$ |
| WINNER | $L_1 = 22.7 \log(\sqrt{x^2 + (y-w)^2 + z^2}) + 27 + 20 \log f$ $L_2 = 17.64 + 14 \cdot (1 - 1.8 \log f) + 15 \cdot (1 - \theta)^2$ $L_3 = \frac{w}{2}$ |
| COST231 | $L_1 = 20 \log(\sqrt{x^2 + (y-w)^2 + z^2 + w}) + 32.4 + 20 \log f$ $L_2 = 7 + 20 \cdot \left(1 - \frac{y-w}{\sqrt{x^2 + (y-w)^2 + z^2 + w}} \right)^2$ $L_3 = 0.6 \cdot (w - 2) \cdot \left(1 - \frac{y-w}{\sqrt{x^2 + (y-w)^2 + z^2 + w}} \right)^2$ |

¹ $\theta = \tan^{-1}(\sqrt{x^2 + z^2}/y - w)$.

To make a robust analysis to the choice of the 60/40 rate for tuning and testing datasets, a uniform random sampling method was performed 2000 times to estimate the corresponding path loss according to the Kriging-aided model proposed. The average of the 2000 iterations for the mean error, the standard deviation of the error and the RMSE is presented in Table 6 for each link described in Table 2.

Table 6. Path Loss Models Accuracy.

| O2I Link | Model | Mean Error | Standard Deviation | RMSE |
|----------|---------|------------|--------------------|------|
| SS | R | −0.04 | 4.73 | 4.73 |
| | K | 0.30 | 2.82 | 2.85 |
| | 3GPP | 3.43 | 3.52 | 4.91 |
| | ITU-R | 5.26 | 3.82 | 6.49 |
| | WINNER+ | 1.29 | 3.91 | 4.11 |
| | COST231 | −3.81 | 3.31 | 5.04 |
| OS | R | 0.00 | 4.81 | 4.81 |
| | K | 0.47 | 2.78 | 2.84 |
| | 3GPP | 0.55 | 3.46 | 3.49 |
| | ITU-R | 5.20 | 3.02 | 6.00 |
| | WINNER+ | 1.16 | 3.03 | 3.23 |
| | COST231 | 1.14 | 3.02 | 3.21 |

In addition, after the 2000 iterations are performed to select a different 60/40 rate from measurements to estimate the path loss, the model-based results are presented in terms of the cumulative distribution function (CDF) of the mean error, the standard deviation of the error and the RMSE in Figures 7–9, respectively.

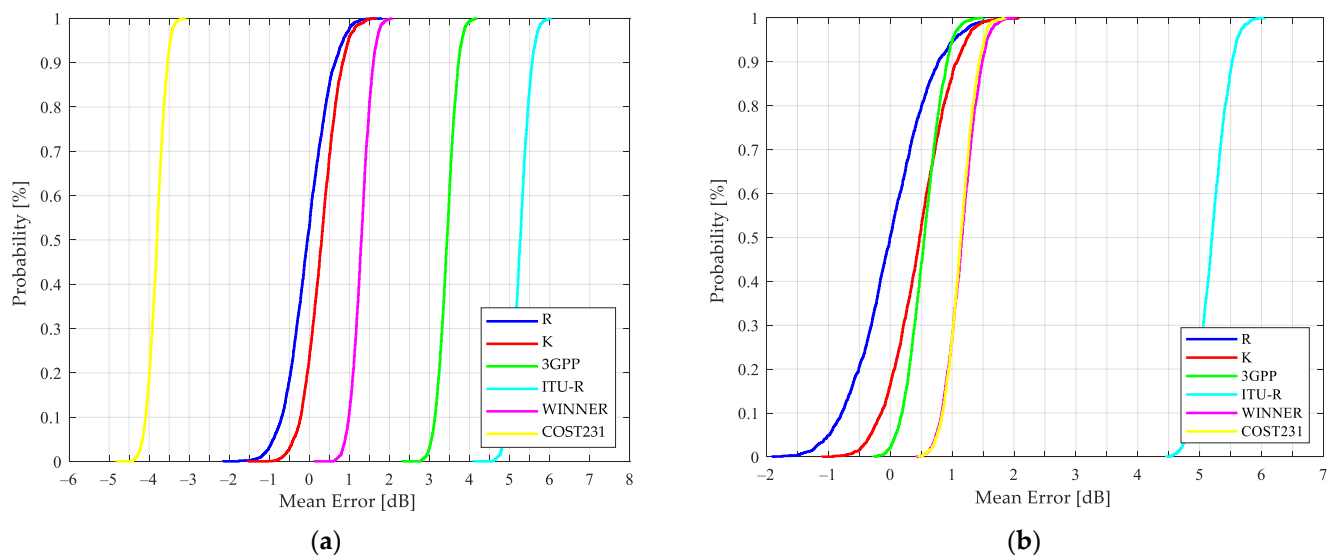


Figure 7. CDFs of mean error for path loss predictions based on different models: (a) SS O2I links; (b) OS O2I links.

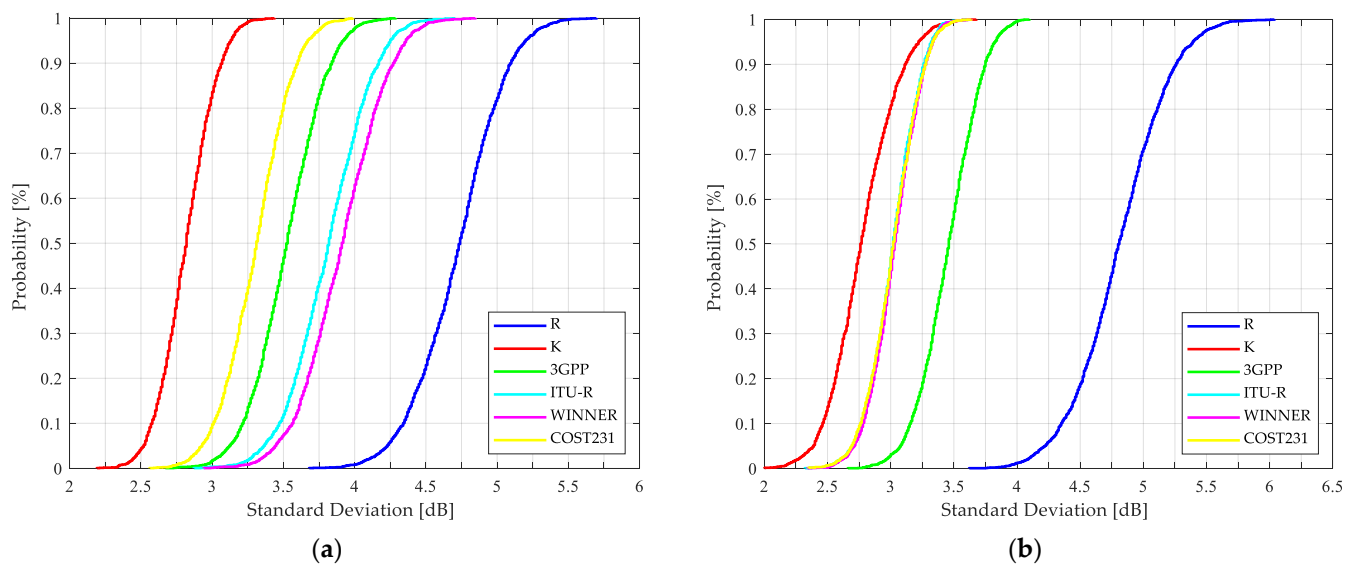


Figure 8. CDFs of standard deviation for path loss predictions based on different models: (a) SS O2I links; (b) OS O2I links.

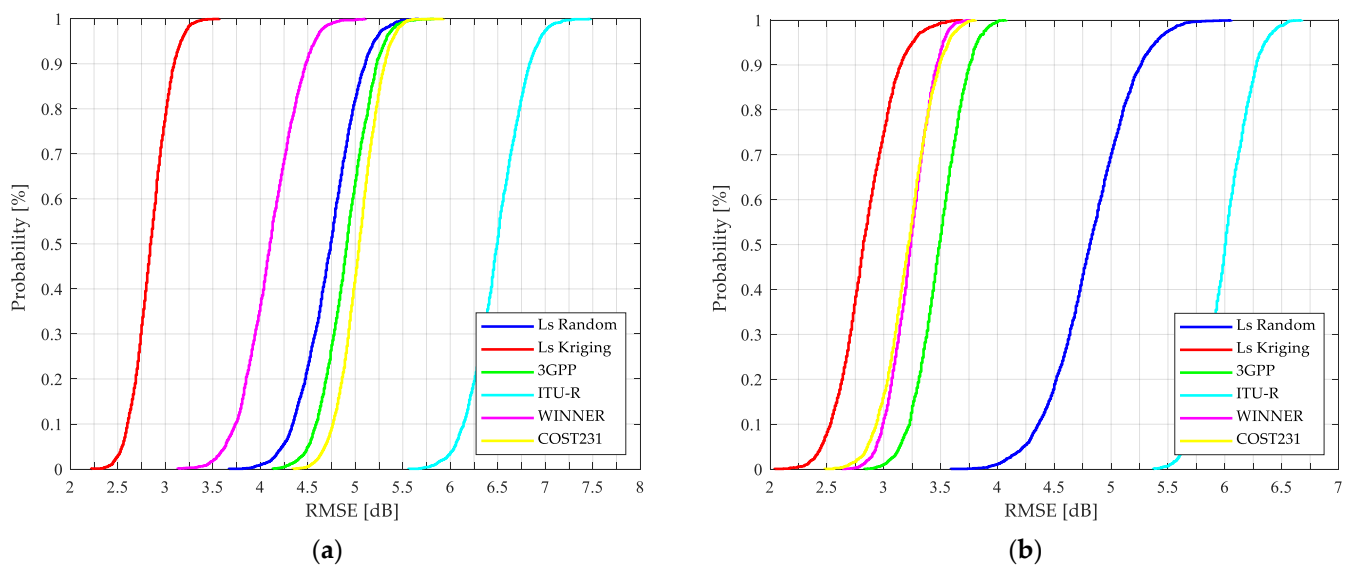


Figure 9. CDFs of RMSE for path loss predictions based on different models: (a) SS O2I links; (b) OS O2I links.

According to Table 6 and Figure 9, in both links, with an RMSE of 2.8 dB, the Kriging-aided model estimates the path loss with a higher level of confidence than the other approaches evaluated. Additionally, this novel technique provides the best fit to the measured data with respect to the standard models presented by Castro et al. in [6].

Kriging, as a geostatistical technique, assumes that there is an implied connection between the measured data value at a point and its location in space. Therefore, it was possible to estimate shadowing from the best set of available sample points (tuning dataset) yielding the K model as the most accurate of those exposed in Table 6, where the metrics and the CDFs illustrated in Figures 7–9 suggest the efficiency of the proposed model, since, unlike the others, it considers the characteristics of the selected link. Even though the R model tunes the parameters n , e and L_s from the tuning dataset and is considered in telecommunication society as the most traditional model, the WINNER+ is quite accurate for the SS link with an RMSE of 4.11 dB, and the COST231, WINNER+ and 3GPP for the OS case with an RMSE of no more than 3.4 dB.

In Figure 7 it is possible to validate the outstanding K model performance. From the 2000 tests that were carried out, it is possible to conclude that, when estimating the path

loss with Kriging-aided shadowing, there is a 95% probability that the mean error of the prediction is less than 1 dB and 1.3 dB for SS and OS links, respectively. Regarding Figure 9, the stability and the confidence to predict the path loss more accurately is guaranteed when the K model is used, with a 95% probability that the RMSE is less than 3.1 dB and 3.25 dB for SS and OS links, respectively.

The applicability of the standard model results presented in Figures 7–9 is discussed as follows: the COST231, 3GPP, and WINNER+ models are more accurate for the OS than for SS links, with median errors less than or equal to 1.16 dB and RMSEs of no more than 3.49 dB. The results presented in Table 6 demonstrate the WINNER+ model as the most consistent and the ITU-R as the least accurate compared to the other standard models for both types of links. Regarding SS results and considering the resulting scenario geometry by locating the BS as low as 0.7 m from the building wall, the standard models present higher standard deviations compared to the OS deviations. By taking into account these results and the following two considerations: the standard models were based on measurements at different frequencies: 850 MHz, 1.8 and 1.9 GHz for COST 231; 450 MHz to 6 GHz for WINNER; 2 to 6 GHz for ITU-R; and 0.5 to 100 GHz for 3GPP. Additionally, the formulation of each standard model was originally conceived for cells of up to 1 Km radius. It is important to improve the accuracy of the standard models for a specific application, in this case, for O2I NLOS links at the 3.5 GHz band, one of the candidate frequencies considered for 5G communications.

In [15] it was validated through different indoor approaches that the path loss prediction accuracy was significantly better when Kriging was included as part of the tuning process for frequencies in the ultra-high-frequency (UHF) band. This study validated the potential of this geostatistical technique for O2I scenarios at 3.5 GHz against standard models. Therefore, it is an interesting future line of research to consider other setups to validate and compare Kriging performance against the existing standard models at difference frequencies.

4. Conclusions

It was validated that the methodology and the model proposed in this paper for O2I applications such as 5G communications at 3.5 GHz, with a proposed accurate combined path loss and shadowing-aided model, were more accurate and versatile compared to both the conventional linear path loss plus log-normal shadowing model and the existing standard models.

The results and the methodology proposed in this study will help students in wireless telecommunications, professionals in the industry, and engineers to achieve efficient radio coverage estimation; estimate measurements in situations where the possibility to collect large amounts of data from measurement campaigns is very limited, reducing time and costs in practical campaigns; and to encourage them to perform Kriging-aided channel design, considering its accuracy to predict path loss in O2I NLOS links.

Author Contributions: Conceptualization, M.E.D.-M. and M.R.; methodology, M.E.D.-M. and A.A.-Z.; software, M.E.D.-M.; validation, M.E.D.-M. and M.R.; formal analysis, M.E.D.-M.; investigation, M.E.D.-M.; resources, M.E.D.-M. and M.R.; writing—original draft preparation, M.E.D.-M.; writing—review and editing, M.E.D.-M., A.A.-Z. and M.R.; supervision, A.A.-Z. and M.R. All authors have read and agreed to the published version of the manuscript.

Funding: M.E.D.-M. wishes to acknowledge the support received from the National Council of Science and Technology CONACYT, through the student scholarship number 746015 and M.R. wishes to acknowledge the support received from the Chilean Research Agency ANID, through research grants ANID FONDECYT 1211368 and ANID PIA/APOYO AFB180002, and from the project VRIEA-PUCV 039.437/2020.

Data Availability Statement: The data presented in this study are available on request from the corresponding author.

Conflicts of Interest: The authors declare no conflict of interest.

References

1. Small Cell Forum. *SCF231 Options for Indoor Cellular*; Small Cell Forum: London, UK, 2020.
2. Zhang, P.; Zhang, J.; Peppas, K.P.; Ng, D.W.K.; Ai, B. Dual-hop Relaying Communications Over Fisher-Snedecor F-Fading Channels. *IEEE Trans. Commun.* **2020**, *68*, 2695–2710. [[CrossRef](#)]
3. Dahal, S.; Ahmed, S.; King, H.; Bharatula, G.; Campbell, J.; Faulkner, M. Slant-Path Building Entry Loss at 24 GHz. *IEEE Access* **2019**, *7*, 158525–158532. [[CrossRef](#)]
4. Byeon, C.W.; Hossain, A.; Lee, Y.C. Building Entry Loss Measurements and Analysis on Non-Line-of-Sight and Line-of-Sight Paths at 6 GHz. *IEEE Antennas Wirel. Propag. Lett.* **2020**, *19*, 253–256. [[CrossRef](#)]
5. Zhang, P.; Yi, C.; Yang, B.; Wang, C.X.; Wang, H.; You, X. In-building Coverage of Millimeter-Wave Wireless Networks from Channel Measurement and Modeling Perspectives. *Sci. China Inf. Sci.* **2020**, *63*, 1–16. [[CrossRef](#)]
6. Castro, G.; Feick, R.; Rodríguez, M.; Valenzuela, R.; Chizhik, D. Outdoor-to-Indoor Empirical Path Loss Models: Analysis for Pico and Femto Cells in Street Canyons. *IEEE Wirel. Commun. Lett.* **2017**, *6*, 542–545. [[CrossRef](#)]
7. European Commissions. *COST Action 231: Digital Mobile Radio towards Future Generation Systems*; European Commissions: Brussels, Belgium, 1999.
8. Meinilä, J.; Kyosti, P.; Hentilä, L.; Jämsä, T.; Suikkanen, E.; Kunnari, E.; Narandzić, M. *D5.3: Winner+ Final Channel Models*; WINNER: Delray Beach, FL, USA, 2010.
9. ITU. *Report ITU-R M.2135-1: Guidelines for Evaluation of Radio Interface Technologies for IMT-Advanced*; ITU: Geneva, Switzerland, 2009.
10. 3rd Generation Partnership Project 3GPP. *Study on 3D Channel Model for LTE. Release 12*; 3GPP: Valbonne, France, 2018.
11. Diago-Mosquera, M.E.; Aragon-Zavala, A.; Castanon, G.A. Bringing It Indoors: A Review of Narrowband Radio Propagation Modeling for Enclosed Spaces. *IEEE Access* **2020**, *8*, 103875–103899. [[CrossRef](#)]
12. Aragon-Zavala, A. Radio Propagation. In *Indoor Wireless Communications*; John Wiley & Sons, Ltd.: Hoboken, NJ, USA, 2017; pp. 77–112.
13. Beaulieu, N.C.; Naseri, M. A Circuit Theory Model for Shadow Fading Autocorrelation in Wireless Radio Channels. *IEEE Wirel. Commun. Lett.* **2019**, *8*, 161–164. [[CrossRef](#)]
14. Szyszkowicz, S.S.; Yanikomeroğlu, H.; Thompson, J.S. On the Feasibility of Wireless Shadowing Correlation Models. *IEEE Trans. Veh. Technol.* **2010**, *59*, 4222–4236. [[CrossRef](#)]
15. Diago-Mosquera, M.E.; Aragón-Zavala, A.; Vargas-Rosales, C. The Performance of In-Building Measurement-Based Path Loss Modelling Using Kriging. *IET Microw. Antennas Propag.* **2021**, *15*, 1564–1576. [[CrossRef](#)]
16. Negreiros, J.; Painho, M.; Aguilar, F.; Aguilar, M. Geographical Information Systems Principles of Ordinary Kriging Interpolator. *J. Appl. Sci.* **2010**, *10*, 852–867. [[CrossRef](#)]
17. Sato, K.; Inage, K.; Fujii, T. On the Performance of Neural Network Residual Kriging in Radio Environment Mapping. *IEEE Access* **2019**, *7*, 94557–94568. [[CrossRef](#)]
18. Sato, K.; Inage, K.; Fujii, T. Modeling the Kriging-Aided Spatial Spectrum Sharing over Log-Normal Channels. *IEEE Wirel. Commun. Lett.* **2019**, *8*, 749–752. [[CrossRef](#)]
19. Bi, J.; Wang, Y.; Li, Z.; Xu, S.; Zhou, J.; Sun, M.; Si, M. Fast Radio Map Construction by Using Adaptive Path Loss Model Interpolation in Large-Scale Building. *Sensors* **2019**, *19*, 712. [[CrossRef](#)] [[PubMed](#)]
20. Sato, K.; Fujii, T. Kriging-Based Interference Power Constraint: Integrated Design of the Radio Environment Map and Transmission Power. *Trans. Cogn. Commun. Netw.* **2017**, *3*, 13–25. [[CrossRef](#)]
21. Mezhoud, N.; Oussalah, M.; Zaatri, A.; Hammoudi, Z. Hybrid Kriging and Multilayer Perceptron Neural Network Technique for Coverage Prediction in Cellular Networks. *Int. J. Parallel Emergent Distrib. Syst.* **2020**, *35*, 682–706. [[CrossRef](#)]
22. Aragón-Zavala, A. *Indoor Wireless Communications: From Theory to Implementation*, 1st ed.; Wiley: Chichester, UK, 2017; ISBN 9780470741160.
23. ITU. *Recomendación UIT-R P.525-4*; Ginebra: Sharm El-Sheikh, Egypt, 2019.
24. Mutlu, T.M.; Canberk, B. A Spatial Estimation-Based Handover Management for Challenging Femtocell Deployments. In Proceedings of the 2014 IEEE International Black Sea Conference on Communications and Networking, BlackSeaCom 2014, Odessa, Ukraine, 27–30 May 2014; IEEE Computer Society: Piscataway, NJ, USA, 2014; pp. 144–148.
25. Konak, A. A Kriging Approach to Predicting Coverage in Wireless Networks. *Int. J. Mob. Netw. Des. Innov.* **2009**, *3*, 65–71. [[CrossRef](#)]
26. Trauth, M.H. Spatial Data. In *MATLAB Recipes for Earth Sciences*, 4th ed.; Springer: Berlin/Heidelberg, Germany, 2015; pp. 1–427. ISBN 9783662462447.

Chapter 5

Tuning Selection Impact on Kriging-Aided In-Building Path Loss Modeling

5.1 Summary of the Chapter

The aim of this chapter is to understand if you select enough tuning dataset from measurements to guarantee the best accuracy in path loss predictions. The last pre-test achieved in [16] is similar to this objective, but in this case this study aims to select tuning dataset from a grid of measurements instead a random path. For that purpose, the available measurements in the frequency band of 800 MHz in the congress hall of campus Queretaro have been selected. However, to have a set of grids with different separation distances between two consecutive measured points Ray Launching (RL) has been included to provide samples in all the spatial points of the scenario.

Towards providing results for practical campaigns, where the time and the number of available samples are limited. In this part of the research, a cost function has been proposed in terms of the Euclidean distance to select the minimum cost of the mean absolute error (MAE), tuning samples and the sampling distance.

5.2 Full Article

Tuning Selection Impact on Kriging-Aided In-Building Path Loss Modeling

Melissa Eugenia Diago-Mosquera [✉], Alejandro Aragón-Zavala [✉], *Senior Member, IEEE*,
 Fidel Alejandro Rodríguez-Corbo [✉], Mikel Celaya-Echarri [✉], *Student Member, IEEE*,
 Raed M. Shubair [✉], *Senior Member, IEEE*, and Leyre Azpilicueta [✉], *Senior Member, IEEE*

Abstract—How do you know you select enough tuning dataset from measurements to guarantee model prediction accuracy? Tuning datasets are often selected based on simple random sampling with predefined rates. Usually, these rates are determined as a/b , where $a\%$ of the data goes to training and the remaining $b\%$ goes to testing. But it is not clear to what extent tuning dataset in order to minimize the estimation path loss errors. It is, thus, required to analyze the performance of channel modeling by selecting—among all measurement samples—appropriate tuning dataset. Using radio measurements and deterministic Ray Launching techniques to collect enough reliable samples, this letter analyzes the impact of tuning dataset selection—expressed in terms of the mean absolute error and cost—on a novel Kriging-aided in-building measurement-based path loss prediction model.

Index Terms—Indoor path loss model, Kriging, radio propagation, tuning dataset.

I. INTRODUCTION

ACCURACY and efficacy are the fundamental channel modeling features. Thus, it is important to strike a balance between them. Empirical models are useful for practical radio designs, but the similarity of the measured and predicted environment is a fundamental consideration to achieve accurate estimations; deterministic models are complex in terms of both computational resources and rigorous building details for channel modeling; but hybrid models represent good tradeoff between the empirical and deterministic models by including rigorous fitting and suitable validations [1]–[3].

Considering the restrictions during measurement campaigns, the opportunity to collect a useful quantity of samples can be very limited. However, with a precise measurement plan and Kriging-aided postprocessing, treasured data can be extracted for the accurate channel modeling, as is reported in [4]–[7]. The goal

of Kriging is to estimate missing values at a random location from the available measurement samples, which intrinsically contain the path loss singularities associated with the evaluated scenario. Measurement-based models employ radio measurements to perform model fitting and model validation through tuning and testing datasets, respectively. In most studies, these datasets are selected from the corresponding measurements according to a desired ratio a/b that is based on random sampling [8], [9], i.e., an $a\%$ for tuning the model and a $b\%$ for testing the model. In [10], Diago-Mosquera *et al.* analyze the following approaches: what happens when the method selection of tuning dataset varies in order to select the right one to get the most out of Kriging, and what percentage of data should be selected for tuning dataset to obtain the best goodness of fit; however, choosing a suitable approach for optimal tuning selection involves a deeper study that includes the analysis of the separation sampling distance and the cost function that minimizes the mean absolute error (MAE), the separation sampling distance, and the tuning dataset of the system.

The present letter is inspired by the fact that the impact of the tuning dataset selection on the accuracy of the model has not been thoroughly researched. Here, we carry out the accurate analysis of this approach with a novel Kriging-aided in-building measurement-based path loss prediction model. Besides, due to the possibility to collect large amount of data from measurement campaigns is very limited, we propose a methodology that includes a deterministic Ray Launching (RL) approach to account for valuable data in order to accomplish the characterization of samples related to missing points of the scenario where there is no spatial resolution from empirical measurements.

II. CHANNEL MODELING

An optimum combination of measurements, RL techniques, Kriging, and simple path loss models was employed to predict complete system coverage performance. The overall channel model description is illustrated in Fig. 1.

First, accurate measurement locations and signal strength levels are collected to account for the received power behavior in an indoor scenario. However, because the number of measurements and the area, where observations can be performed, are limited, full stored data are missing; therefore, and second, to address the shortcoming of the amount of data from measurement campaign, RL techniques described in Section III— are employed for the missing information. Besides, it is possible to obtain signal strength samples in the entire area of the scenario evaluated with an outstanding accuracy through RL as the RL predictions are calibrated with the measurements available. These complete samples are necessary due to the aim of this letter to analyze

Manuscript received August 20, 2021; accepted September 30, 2021. Date of publication October 7, 2021; date of current version January 12, 2022. This work was supported by the National Council of Science and Technology CONACYT, through the Student Scholarship under Grant 746015. (*Corresponding author: Leyre Azpilicueta.*)

Melissa Eugenia Diago-Mosquera and Alejandro Aragón-Zavala are with the Escuela de Ingeniería y Ciencias, Tecnológico de Monterrey, Querétaro 76130, Mexico (e-mail: a00829220@itesm.mx; aaragon@tec.mx).

Fidel Alejandro Rodríguez-Corbo, Mikel Celaya-Echarri, and Leyre Azpilicueta are with the Escuela de Ingeniería y Ciencias, Tecnológico de Monterrey, Monterrey 64849, Mexico (e-mail: fidel.rodriguez@tec.mx; mikel-celaya@tec.mx; leyre.azpilicueta@tec.mx).

Raed M. Shubair is with the Department of Electrical and Computer Engineering, New York University Abu Dhabi, Abu Dhabi 129188, UAE (e-mail: raed.shubair@nyu.edu).

Digital Object Identifier 10.1109/LAWP.2021.3118673

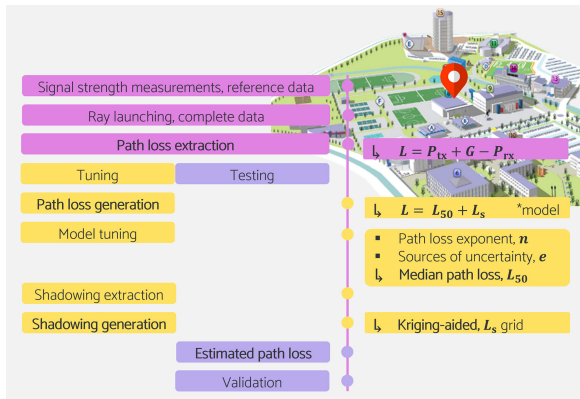


Fig. 1. Channel model methodology.

the impact of the tuning dataset selection-considering different amounts from available samples.

By querying communication system details, antenna gains G in dBi and transmission power P_{tx} in dBm along with the received signal strength values P_{rx} in dBm are processed to yield measurements of path loss L in dB against location, this process is named as *path loss extraction*, as shown in Fig. 1. As a fourth stage, the samples are divided into two datasets: a *tuning dataset*, which is exclusively used for driving the model fitting, and a *testing dataset*, which is used to evaluate the accuracy of the path loss predictions at those measured locations.

For *model tuning*, it is necessary to have the *path loss model generation*, which is made up of two components: a first distance-dependent d component named as median path loss L_{50} , which represents a typical propagation medium given by

$$L_{50} = L_{fs} + 10n \log_{10} \left(\frac{d}{d_0} \right) + e \quad (1)$$

where $L_{fs} = 20 \log_{10}(d_0) + 20 \log_{10}(f) - 28$ denotes the free space path loss at a reference distance d_0 (1 m) and a frequency f in MHz, n denotes the path loss exponent, d is the Euclidean distance in a three-dimensional (3-D) space in meter, and e accounts for specific sources from the floor and walls' attenuations and waveguiding gain due to multiple reflections in corridors. For model tuning, it is necessary to fit the variables in (1), n and e are tuned by linear regression, using the path loss extracted.

And a second component that depends on the characteristics of the nearby propagation environment. Resuming the concept of path loss by extracting the distance-dependent part (L_{50}) from the total loss, the value related to shadowing or slow fading L_s is obtained (in Fig. 1, this process is named as *shadowing extraction*) and this is given by

$$L_s = L - L_{50}. \quad (2)$$

The most conventional log-normal shadowing model is assumed in various studies; however, in seeking to enhance the model tuning and the *shadowing generation*, the aim of this letter validates the potential of Kriging-aided channel modeling to predict shadowing throughout the in-building area. From shadowing tuning samples (2), the dataset vector y is obtained $y = (z_{x_1}, z_{x_2}, \dots, z_{x_N})^T$, where N is the number of samples, and z_{x_i} is the known shadowing at the location given by x_i . Kriging minimizes the variance of estimation errors under the constraint of unbiased estimation; in fact, it is considered the best linear unbiased predictor [11]. To quantify and describe the



Fig. 2. Congress hall, Tecnológico de Monterrey, campus Queretaro.

spatial variability, Kriging preliminary employs the *variogram* as part of the variography process; afterward, Kriging interpolates the shadowing values at a random location x_0 from y to obtain unknown shadowing samples according to the variogram outcomes. Then, as a result of this postprocessing, a shadowing grid is generated for the target area; for a better understanding, this process is described in detail in [10]. Finally, the *estimated path loss* process is performed and is calculated as follows:

$$L = L_{fs} + 10n \log_{10} \left(\frac{d}{d_0} \right) + e + L_s \quad (3)$$

where L_s is extracted from the shadowing grid generated by Kriging; the variables L_{fs} , n , d_0 , and e are given from the process described and d is the location leading by testing dataset.

III. DATA COLLECTION

A. In-Building Radio Measurements

A series of carefully measurements were carried out at the first floor of the congress hall in the Tecnológico de Monterrey, campus Queretaro, Mexico. This building has a general area of entrance, two conference rooms, two bathrooms, and corridors. The congress hall is a two-story structure with interior and exterior walls that consist of glass, drywall, and block. Ceilings include building materials, such as steel roofing and metal beams, while the floors only include ceramic tile. Ceilings are 8 m high with false ceilings of 6 m high. Fig. 2 shows the inside and outside building views.

The transmitter system consisted of a Kathrein triband omnidirectional indoor antenna, model 800-10249 with 2 dBi gain plugged into a Rohde, and a Schwarz Signal Generator, model SMB100A with 11 dBm of electrical power at 869.6 MHz. Received signal strength values were supplied by the use of a dual-band whip 0 dBi antenna with a portable SeeGull LX radio scanner. The walk route visualized, as shown in Fig. 3, was followed at a constant speed to collect the measurements through the radio scanner, and to record location data, the software InSite v3.1.0.19, from PCTEL, was employed.

The aforementioned signal strength measurements should be filtered prior to using them in the RL fitting. Considering the fact that fast fading is on the scale of half-wavelength and filtering must be done carefully to remove it, avoiding delete the shadowing variations, this procedure consists of averaging all the signal strength measurements inside a $\lambda \times \lambda$ square, which belongs to the target area that previously was segmented in a grid of $\lambda \times \lambda$ squares, where λ is the wavelength for the measurement frequency. All the samples inside each square, represented by the path in Fig. 3, were averaged as follows:

$$\overline{P_{rx}} = 10 \log \left(\frac{1}{s} \sum_{i=1}^s 10^{P_{rx_i}/10} \right) \quad (4)$$

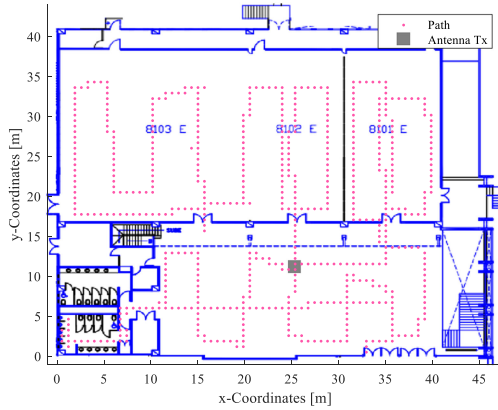


Fig. 3. First floor layout for each scenario.

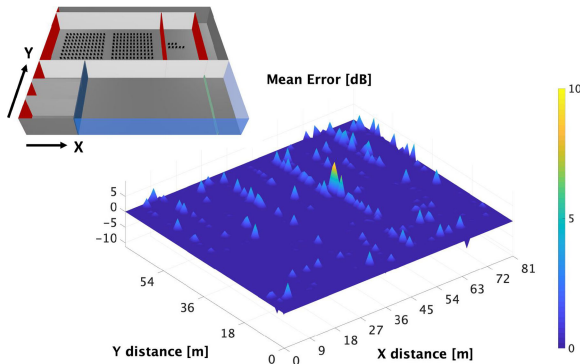


Fig. 4. Schematic view of the considered scenario for simulation and mean error comparison between simulation and measurement results.

where P_{rx_i} is the received power measured in dBm, and s is the number of samples inside a square of the grid.

B. RL Simulations to Obtain Propagation Data

An in-house deterministic RL algorithm has been used to obtain valuable data to analyze the tuning selection impact in Kriging-aided path loss modeling. The RL technique is a geometry-based deterministic model, which considers the 3-D morphology of the scenario taking into account all the material properties of all the obstacles in the scenario at the system frequency under analysis (with the conductivity and relative permittivity). Electromagnetic phenomena, such as reflection, refraction, or diffraction, are considered. Parameters, such as the operating frequency, number of ray reflections, or angular and spatial resolution, are initiated before the simulations. Thus, accurate received power levels can be obtained for all the spatial points of the considered scenario. A detailed description of the 3-D RL algorithm can be found in [12] and its validation for indoor/outdoor complex environments [13], [14].

In this letter, in order to validate the proposed RL algorithm in the in-building considered complex scenario where measurements have been performed, the same scenario with similar input parameters as the measurement campaign has been simulated. Fig. 4 presents the schematic recreated scenario, which corresponds with the same congress hall where the campaign of measurements was performed and the mean error comparison between the simulation results and measurements layout, as shown in Fig. 3, showing a

mean error less than 1.7 dB, thus, validating the RL technique. The main advantage of RL techniques is that valuable data are obtained for all spatial points of the scenario; therefore, once the RL has been validated, the next step has been to analyze the tuning selection impact in the Kriging-aided path loss modeling with these valuable data.

IV. RESULTS

Toward choosing an optimal tuning dataset to be representative of the extent of the target area, which is reasonable to perform in a practical situation, it is helpful to analyze and estimate the error when a different size of tuning dataset is selected to predict path loss in testing locations. Note that this letter defines an evaluation in the following procedure where the word “samples” refer to the 7495 path loss values contained into the complete RL grid when considering 0.5 m spatial resolution at the same height of the transmitter antenna (1.2 m).

- 1) Variogram results show that shadowing values are low at small separation distances, i.e., near the origin, but they increase with increasing distance until reaching a plateau, which is close to the shadowing variance. This indicates that the spatial process is correlated over short distances but there is no spatial dependence over longer distances, in this in-building case 5 m. Therefore, from samples and variogram analysis, seven new grids are generated to consider the separation-1 to 7 m-between two consecutive measurement points as a first approach to achieve an optimal tuning selection, e.g., the original RL grid consists of samples reported every 0.5 m, a new grid will contain the samples reported every 1 m instead of 0.5 m.
- 2) From the new grid generated, $a\%$ goes to the tuning dataset. This percentage varies from 10% to 100% in order to validate the optimal quantity to consider in model tuning. This percentage is extracted according to the method validated in [10], which limits the samples to classification zones defined by concentric circles every 5 m from the position of the transmitting antenna, and the corresponding $a\%$ is extracted from each classification zone.
- 3) Through the methodology described in Section II, the estimated path loss is calculated at each RL grid location.
- 4) The MAE is calculated as

$$\text{MAE} = \frac{1}{N} \sum_{i=1}^N |z_i - \hat{z}_i| \quad (5)$$

where $|z_i - \hat{z}_i|$ is the absolute value of the difference between the measured and predicted path loss for the N samples.

To report the results in Table I, the steps that select the tuning dataset percentage between 10 to 90 were iterated 100 times. In Table I, each scenario is clearly described in terms of tuning samples and MAE, considering both approaches distance separation and tuning dataset percentage. Fig. 5 describes the behavior of the MAE as the number of model tuning samples increases; the tendency is depicted in a red dashed line.

According to the article presented in [15], the aim of a cost function is to measure how optimal the model is in terms of its ability to estimate the relationship between desired variables. In this case, the cost function is used to optimize the MAE as well as the tuning samples (ts) and distance (sd). Due to the positive nature of the aforementioned variables, the Euclidean distance has been selected as the cost function in order to find a tradeoff between desired variables, allowing the tuning process optimization.

TABLE I
 PATH LOSS PREDICTIONS PERFORMANCE

| Result | Grid Separation [m] | Tuning dataset [%] | | | | | | | | | |
|----------------|---------------------|--------------------|------|------|------|------|------|------|------|------|------|
| | | 10 | 20 | 30 | 40 | 50 | 60 | 70 | 80 | 90 | 100 |
| Tuning samples | 1 | 189 | 376 | 567 | 755 | 945 | 1130 | 1318 | 1509 | 1697 | 1885 |
| | 2 | 49 | 96 | 146 | 193 | 242 | 289 | 338 | 386 | 435 | 482 |
| | 3 | 23 | 44 | 67 | 89 | 112 | 134 | 156 | 179 | 200 | 223 |
| | 4 | 15 | 27 | 40 | 52 | 67 | 79 | 93 | 104 | 118 | 131 |
| | 5 | 9 | 18 | 27 | 36 | 47 | 53 | 64 | 71 | 82 | 89 |
| | 6 | 5 | 11 | 18 | 23 | 29 | 32 | 38 | 44 | 51 | 55 |
| | 7 | 4 | 9 | 13 | 18 | 23 | 23 | 28 | 32 | 37 | 41 |
| MAE [dB] | 1 | 5.16 | 4.96 | 4.74 | 4.56 | 4.40 | 4.24 | 4.09 | 3.95 | 3.81 | 3.67 |
| | 2 | 5.63 | 5.49 | 5.39 | 5.29 | 5.26 | 5.18 | 5.16 | 5.09 | 5.06 | 5.01 |
| | 3 | 5.57 | 5.54 | 5.39 | 5.35 | 5.29 | 5.29 | 5.27 | 5.27 | 5.25 | 5.23 |
| | 4 | 5.45 | 5.40 | 5.36 | 5.34 | 5.33 | 5.33 | 5.33 | 5.33 | 5.33 | 5.32 |
| | 5 | 5.72 | 5.55 | 5.50 | 5.40 | 5.31 | 5.28 | 5.22 | 5.18 | 5.15 | 5.12 |
| | 6 | 6.15 | 5.86 | 5.63 | 5.54 | 5.49 | 5.49 | 5.39 | 5.29 | 5.28 | 5.23 |
| | 7 | 6.44 | 5.72 | 5.56 | 5.42 | 5.42 | 5.46 | 5.39 | 5.30 | 5.30 | 5.22 |

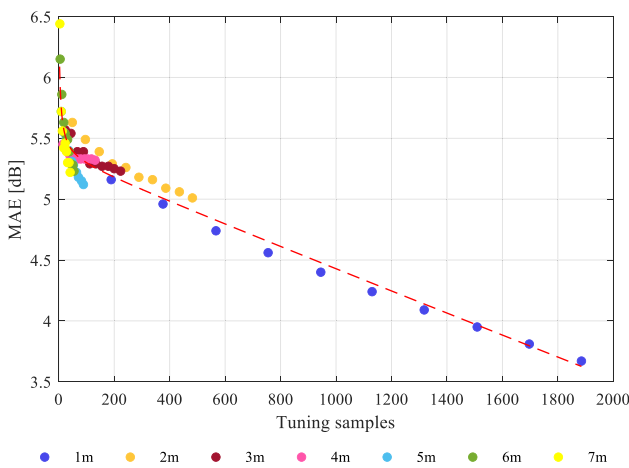
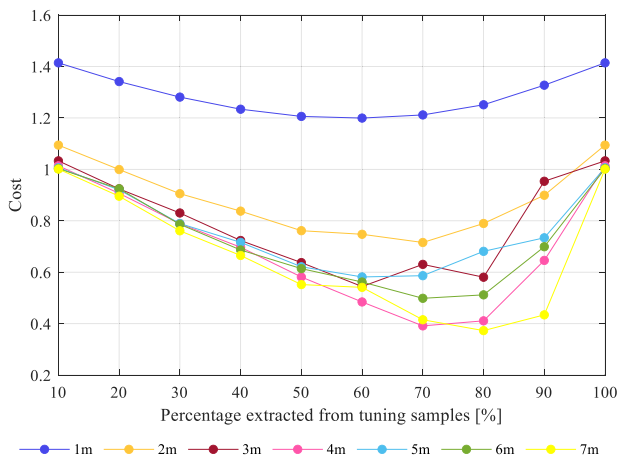


Fig. 5. MAEs considering the number of tuning samples.


 Fig. 6. Cost function in terms of *mae*, *ts*, and *sd*.

Therefore, in order to identify a feasible amount of tuning samples from a measurement campaign with practical separation sampling distance, Fig. 6 describes the cost function in terms of Euclidean distance [16] to select the minimum value of the curves—i.e., the minimum cost in terms of MAE, tuning samples

and separation distance—calculated as follows:

$$f_{\text{cost}} = \sqrt{\text{mae}^2 + ts^2 + \left(\frac{1}{sd}\right)^2} \quad (6)$$

where *mae*, *ts*, and *sd* were normalized in the range of data to [0, 1]. The *mae*, *ts*, and *sd* correspond to MAEs, number of tuning samples, and the inverse of the separation distance, respectively. To simplify the measurement campaign process, it is desirable to maximize the sampling distance, considering the MAEs and tuning samples. Thus, the invert of the variable *sd* has been used in the cost function weighting into the optimization process. Compared with direct observation, as shown in Fig. 5, the best accuracy is presented by the method proposed with the grid that reports samples every 1 m. However, the purpose of this study is to approach a channel modeling methodology without affecting estimated values accuracy for practical campaigns, considering the optimal *mae*, *ts*, and *sd*. Therefore, the proposed methodology allows to conclude that an optimal separation distance to perform practical indoor radio measurements is 7 m, taking into account the MAE of 5.3 dB with 32 samples—80% of the grid-employed for model tuning, which represents an outstanding 92% decrease of the 1509 samples used in the grid with 1 m of separation sampling distance. Resulting in a feasible reference to know and to understand the quantity of measurements that must be carried out in a measurement campaign toward characterizing the path loss in an in-building scenario, including Kriging, as an interpolation technique, in the postprocessing stage for shadowing generation. From these results, the dependence of the path loss exponent *n* and the MAE in a Kriging-aided in-building path loss model can be analyzed as a future research line, considering multiples scenarios.

V. CONCLUSION

This letter proposes Kriging-aided shadowing for modeling path loss in an indoor scenario based on measurements. It was validated through different approaches that this model is a powerful candidate for the radio propagation estimation, considering the reported prediction accuracy expressed in terms of MAEs between estimations and RL samples. Moreover, numerical results show that it is possible to consider an optimal tuning dataset, which reduces the extent of walk testing during measurement campaigns which are reasonable to perform in a practical situation with good tradeoff between enough tuning dataset and model prediction accuracy. Additionally, a hybrid method between RL and Kriging could be interesting future work, considering the possibility to increase the statistical precision and outperform Kriging.

REFERENCES

- [1] F. Erden, O. Ozdemir, and I. Guvenc, "28 GHz mmWave channel measurements and modeling in a library environment," in *Proc. IEEE Radio Wireless Symp.*, Jan. 2020, pp. 52–55, doi: [10.1109/RWS45077.2020.9050106](https://doi.org/10.1109/RWS45077.2020.9050106).
- [2] M. Khatun, C. Guo, L. Moro, D. Matolak, and H. Mehrpouyan, "Millimeter-wave path loss at 73 GHz in indoor and outdoor airport environments," in *Proc. IEEE Veh. Technol. Conf.*, Sep. 2019, pp. 1–5, doi: [10.1109/VTCTFall.2019.8891488](https://doi.org/10.1109/VTCTFall.2019.8891488).
- [3] N. O. Oyie and T. J. O. Afullo, "Measurements and analysis of large-scale path loss model at 14 and 22 GHz in indoor corridor," *IEEE Access*, vol. 6, pp. 17205–17214, 2018, doi: [10.1109/ACCESS.2018.2802038](https://doi.org/10.1109/ACCESS.2018.2802038).
- [4] J. Bi *et al.*, "Fast radio map construction by using adaptive path loss model interpolation in large-scale building," *Sensors*, vol. 19, no. 3, Feb. 2019, Art. no. 712, doi: [10.3390/s19030712](https://doi.org/10.3390/s19030712).
- [5] A. Konak, "A Kriging approach to predicting coverage in wireless networks," *Int. J. Mobile Netw. Des. Innov.*, vol. 3, no. 2, pp. 65–71, Jan. 2009, doi: [10.1504/IJMNDI.2009.030838](https://doi.org/10.1504/IJMNDI.2009.030838).
- [6] A. Dalla-Rosa, A. Raizer, and L. Pichon, "Deterministic tool based on transmission line modelling and Kriging for optimal transmitter location in indoor wireless systems," *Microw., Antennas Propag.*, vol. 5, no. 13, pp. 1537–1545, Oct. 2011, doi: [10.1049/iet-map.2010.0613](https://doi.org/10.1049/iet-map.2010.0613).
- [7] A. Dalla-Rosa, A. Raizer, and L. Pichon, "Optimal indoor transmitters location using TLM and Kriging methods," *IEEE Trans. Magn.*, vol. 44, no. 6, pp. 1354–1357, Jun. 2008, doi: [10.1109/TMAG.2007.916239](https://doi.org/10.1109/TMAG.2007.916239).
- [8] J. A. Seseña-Osorio, A. Aragón-Zavala, I. E. Zaldívar-Huerta, and G. Castañón, "Indoor propagation modeling for radiating cable systems in the frequency range of 900-2500 MHz," *Prog. Electromagn. Res. B*, vol. 47, pp. 241–262, 2013, doi: [10.2528/PIERB12102314](https://doi.org/10.2528/PIERB12102314).
- [9] A. Aragón-Zavala, B. Belloul, V. Nikolopoulos, and S. R. Saunders, "Accuracy evaluation analysis for indoor measurement-based radio-wave-propagation predictions," *IEE Proc. Microw., Antennas Propag.*, vol. 153, no. 1, pp. 67–74, Feb. 2006, doi: [10.1049/ip-map:20045131](https://doi.org/10.1049/ip-map:20045131).
- [10] M. E. Diago-Mosquera, A. Aragón-Zavala, and C. Vargas-Rosales, "The performance of in-building measurement-based path loss modelling using Kriging," *Microw., Antennas Propag.*, vol. 15, pp. 1564–1576, Oct. 2021, doi: [10.1049/mia2.12163](https://doi.org/10.1049/mia2.12163).
- [11] J. Negreiros, M. Painho, F. Aguilár, and M. Aguilár, "Geographical information systems principles of ordinary Kriging interpolator," *J. Appl. Sci.*, vol. 10, no. 11, pp. 852–867, 2010, doi: [10.3923/jas.2010.852.867](https://doi.org/10.3923/jas.2010.852.867).
- [12] L. Azpilicueta, M. Rawat, K. Rawat, F. Ghannouchi, and F. Falcone, "Convergence analysis in deterministic 3-D ray launching radio channel estimation in complex environments," *Appl. Comput. Electromagn. Soc. J.*, vol. 29, no. 4, pp. 256–271, 2014.
- [13] L. Azpilicueta, M. Rawat, K. Rawat, F. M. Ghannouchi, and F. Falcone, "A ray launching-neural network approach for radio wave propagation analysis in complex indoor environments," *IEEE Trans. Antennas Propag.*, vol. 62, no. 5, pp. 2777–2786, May 2014, doi: [10.1109/TAP.2014.2308518](https://doi.org/10.1109/TAP.2014.2308518).
- [14] L. Azpilicueta, C. Vargas-Rosales, and F. Falcone, "Intelligent vehicle communication: Deterministic propagation prediction in transportation systems," *IEEE Veh. Technol. Mag.*, vol. 11, no. 3, pp. 29–37, Sep. 2016, doi: [10.1109/MVT.2016.2549995](https://doi.org/10.1109/MVT.2016.2549995).
- [15] Probyto Data Science and Consulting Pvt. Ltd., *Data Science for Business Professionals: A Practical Guide for Beginners*. Noida, India: BPB PUBLN, 2020, pp. 2–19.
- [16] A. Del Corte-Valiente, J. M. Gómez-Pulido, O. Gutiérrez-Blanco, and J. L. Castillo-Sequera, "Localization approach based on ray-tracing simulations and fingerprinting techniques for indoor-outdoor scenarios," *Energies*, vol. 12, no. 15, Jul. 2019, Art. no. 2943, doi: [10.3390/en12152943](https://doi.org/10.3390/en12152943).

Chapter 6

A 3D Indoor Analysis of Path Loss Modeling Using Kriging Techniques

6.1 Summary of the Chapter

The methodology proposed in Chapter 3 is based on the geostatistical fact that there is an implied connection between the observed values, that in this research concern to the path loss extracted, specifically to the shadowing, and its location in the space, i.e., the corresponding coordinates where the measured was achieved. To predict shadowing at unmeasured locations two main procedures are considered: variography, for investigating the spatial structure of shadowing and Kriging for interpolation.

Usually, the spatial structure is analyzed considering the semivariogram, but the aim of this chapter is to provide a solid basis to select an accurate tool for the variography, taking into account that there are three possibilities: the semivariogram, the covariance function and the correlogram. For that purpose, signal-strength radio measurements have been carried out in the Library of campus Monterrey at 28 GHz. Besides, to provide the empirical basis for the 3D path loss model two different receiver heights have been considered.

6.2 Full Article

A 3-D Indoor Analysis of Path Loss Modeling Using Kriging Techniques

Melissa Diago-Mosquera [✉], Alejandro Aragón-Zavala [✉], *Senior Member, IEEE*,
Leyre Azpilicueta [✉], *Senior Member, IEEE*, Raed Shubair [✉], *Senior Member, IEEE*,
and Francisco Falcone [✉], *Senior Member, IEEE*

Abstract—This study proposes a novel measurement-based method to predict and model three-dimensional (3-D) path loss in indoor scenarios, which first regresses 28 GHz measurements via median path loss modeling and then includes ordinary Kriging to interpolate shadowing. The performance of this method is evaluated by investigating the spatial structure that follows shadowing through the semivariogram, covariance function, and correlogram as variography tools. It is shown that semivariogram outperforms the other statistics to describe shadowing spatial continuity in path loss modeling in terms of the mean absolute error.

Index Terms—Indoor path loss model, Kriging, three-dimensional (3-D), variography.

I. INTRODUCTION

TO QUANTIFY the reliability of coverage provided by any base station, it is essential to understand and characterize radio propagation factors, which consist of median path loss and shadowing as the main path loss components for indoor scenarios. When rigorous fit design and reliable predictions are the principal approaches, hybrid path loss models are the best method for estimating and analyzing radio propagation. Usually, in these models, measurement datasets are first regressed via linear median path loss modeling and then shadowing is generated as random variable. For accurate predictions in in-building modeling it is necessary to consider the variability of the signal path due to obstacles and scenario geometry. Therefore, shadowing should be predicted considering the singularities associated with the evaluated scenario.

Kriging is a powerful technique for this constraint, this analytical solution provides clear steps to go through when estimating unknown values at unmeasured locations. Besides, prior to the

interpolation to predict unmeasured from measured values, this technique employs variography to explore the spatial structure of the variable under study, in this case, to provide a suitable description of the dispersion with respect to the nominal value given by the in-building path loss model.

A. Related Works

In hybrid models, specifically measurement-based, measurement campaigns are carried out to gain a better understanding of path loss behavior, allowing an accurate fitting of the specific scenario. Kriging, as a geostatistical technique, takes advantage of these measurements to predict values at unmeasured locations forming weights from surrounding known measured values, considering that the closest samples have the most influence. By looking at the spatial structure of the samples, it is possible to calculate Kriging weights. This process is named variography and its main goal is to explore the spatial dependence in order to quantify it through a fitted model, which can be obtained by plotting the semivariogram, covariance, or correlogram.

Recent works in radio propagation have employed Kriging to interpolate path loss [1], shadowing [2]–[6], and received power [7], [8] as part of the modeling process. All these studies have been performed in two-dimensions and employed the semivariogram as part of the variography stage, however, none of these studies explain or justify such a choice. In consequence, it is necessary to address and understand if the semivariogram is the best choice to investigate graphically the spatial patterns of the samples.

B. Our Contributions

The aim of this study is encouraged by the need to provide and validate an accurate method to estimate three-dimensional (3-D) path loss in indoor scenarios including Kriging as a geostatistical technique to predict the shadowing component. Therefore, the main contributions are summarized as follows.

- 1) From a complete analysis of the variography process, it is demonstrated that the semivariogram outperforms the other statistics to describe shadowing spatial continuity in path loss modeling.
- 2) To achieve accurate predictions, Kriging strongly depends on the use of a suitable fitted model, which is provided by the variography results. Through the first contribution, the best performance of Kriging is guaranteed. Then, it is employed to predict shadowing to estimate the path loss in a 3-D indoor scenario. We validate the accuracy of the

Manuscript received March 2, 2022; accepted March 19, 2022. Date of publication March 24, 2022; date of current version June 2, 2022. This work was supported by the National Council of Science and Technology CONACYT, through the student scholarship number 746015, under Project RTI2018-095499-B-C31, funded by the Ministerio de Ciencia, Innovación y Universidades, Gobierno de España (MCIU/AEI/FEDER, UE). (*Corresponding author: Leyre Azpilicueta.*)

Melissa Diago-Mosquera and Alejandro Aragón-Zavala are with the Escuela de Ingeniería y Ciencias, Tecnológico de Monterrey, Querétaro 76130, Mexico (e-mail: a00829220@itesm.mx; aaragon@tec.mx).

Leyre Azpilicueta is with the Escuela de Ingeniería y Ciencias, Tecnológico de Monterrey, Monterrey 64849, Mexico (e-mail: leyre.azpilicueta@tec.mx).

Raed Shubair is with the Department of Electrical and Computer Engineering, New York University Abu Dhabi, Abu Dhabi 129188, UAE (e-mail: raed.shubair@nyu.edu).

Francisco Falcone is with the Department of Electric, Electronic and Communication Engineering and the Institute of Smart Cities, Public University of Navarre, 31006 Pamplona, Spain (e-mail: francisco.falcone@unavarra.es).

Digital Object Identifier 10.1109/LAWP.2022.3162160



Fig. 1. Indoor scenario within the library building at TEC Monterrey, employed for the measurement campaign.

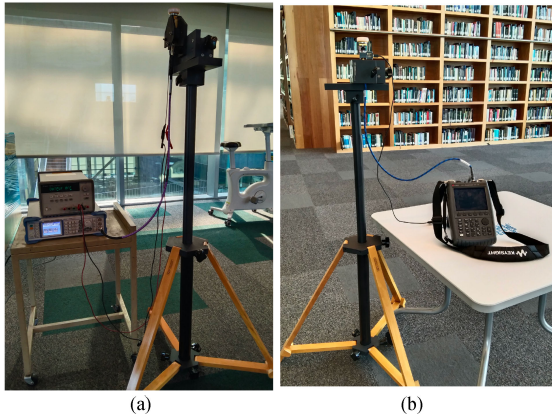


Fig. 2. Measurement equipment. (a) Transmitter. (b) Receiver.

methodology by comparing the results against measured data.

II. EXPERIMENTAL MEASUREMENT DESCRIPTION

A. Measurement Environment

To perform feasible in-building radio propagation modeling to proceed with confidence to the path loss predictions, radio measurements were carried out at 28 GHz in the 4th floor of the library of Tecnológico de Monterrey, campus Monterrey, as is illustrated in Fig. 1. This floor of the library is an open room that has three wooden bookcases evenly distributed in the target area, with exterior walls built with metallic beams and glass. Ceilings are built with drywall while the floor with concrete covered by a carpet material. This indoor scenario enables to carry out both line-of-sight and non-line-of-sight measurements. The transmitter system was located at a 1.5 m height and the receiver at 1 and 2 m heights. The measurement campaign was planned to collect samples on a grid (42 m long and 12 m wide) with squares of 2 m on each side, where the transmitter was located at the center of the grid at the low end. This setting yields 132 samples for each receiver height and a total of 264 measurements.

B. Measurement Equipment

To collect received power samples in the selected scenario, a complete radio propagation system was deployed, as is illustrated in Fig. 2. The transmitter system consisted of a Rohde & Schwarz microwave signal generator, model SMB100A, set at an operating frequency of 14 GHz. To access the frequency of 28 GHz, an up-converter (Farran Technologies, model FDA-K/28) with a multiplication factor of 2 was employed. It was

connected to an omnidirectional vertically polarized antenna with 3 dBi gain, G_{TX} , model SAO-2734030345-KF-S1. The transmitter power P_{TX} was 24 dBm.

The receiver system was composed of a vertically polarized omnidirectional antenna equipped with a low noise amplifier (LNA), model SAO-2734033045-KF-C1-BL, with 30 dB of receiver gain G_{RX} , of which 3 dBi were from the antenna and 27 dB from the integrated LNA. The receiver was plugged into a Keysight Field Fox N9952A microwave spectrum analyzer.

III. 3-D PATH LOSS MODELING

A. Path Loss Extraction

From the resulting power received measurements and considering the link budget of the radio propagation system, the path loss of the links is calculated in dB as follows:

$$L = P_{\text{TX}} + G_{\text{TX}} + G_{\text{RX}} - P_{\text{RX}} \quad (1)$$

where P_{TX} is the transmitted power, G_{TX} and G_{RX} the antenna gains employed to transmit and receive, respectively, and P_{RX} the measured power.

In the validation process it is necessary to quantify how well the model predicts the path loss at specific locations, locations which are obtained from testing dataset. Therefore, the path loss extracted is grouped into tuning and testing datasets. This process is based on radial sectors, where samples are extracted from each sector keeping a 60/40 rate, 60% for tuning and 40% for testing, following the methodology described in [5].

B. Model Tuning

For modeling median path loss L_{50} , it is considered the simplest form of power law model

$$L_{50} = 10n \log d + e \quad (2)$$

where d is the Euclidean distance between the transmitter and the receiver antenna, which have a 3-D coordinate system to represent their location in the target area. The path loss exponent n and the path loss intercept e are tuned with the tuning dataset of the path loss measurements extracted in (1), in order to adjust the model with specific characteristics and site details considered in the radio measurements carried out.

C. Shadowing Extraction and Generation

The path loss also depends on the shadowing L_s , which is the result of the sum between L_{50} and L_s . Therefore, it is possible to extract the shadowing component as follows:

$$L_s = L - L_{50}. \quad (3)$$

To predict and quantify the shadowing component in specific locations, ordinary Kriging is employed. Through this geostatistical technique, Kriging weights are generated for the known shadowing values to employ it to calculate a shadowing prediction for the location with the unknown value. To proceed, first, the spatial structure of (3) must be explored by variography in order to provide reliable Kriging weights.

IV. VARIOGRAPHY AND KRIGING INTERPOLATION

To investigate and quantify the spatial structure, empirical tools such as semivariogram, covariance function, and correlogram can be employed.

A. Variography: Spatial Modeling

The empirical semivariogram is computed as follows:

$$\gamma(h) = \frac{1}{2N(h)} \sum_{i=1}^{N(h)} (z_i - z_{i+h})^2 \quad (4)$$

where $N(h)$ is the number of pairs within the lag interval h , z_i is the known value at 3-D location i , and z_{i+h} is another known value separated by a lag h from i . In other words, h is a vector that represents the separation distance between two spatial locations.

The empirical covariance is calculated as follows:

$$C(h) = \frac{1}{N(h)} \sum_{i=1}^{N(h)} z_i \cdot z_{i+h} - m_i \cdot m_{i+h} \quad (5)$$

where m_i and m_{i+h} are given by the following:

$$m_i = \frac{1}{N(h)} \sum_{i=1}^{N(h)} z_i, \quad m_{i+h} = \frac{1}{N(h)} \sum_{i=1}^{N(h)} z_{i+h}. \quad (6)$$

And the empirical correlation is computed as follows:

$$\rho(h) = \frac{C(h)}{\sqrt{\sigma_i + \sigma_{i+h}}} \quad (7)$$

where σ_i and σ_{i+h} are given by the following:

$$\begin{aligned} \sigma_i &= \frac{1}{N(h)} \sum_{i=1}^{N(h)} (z_i - m_i)^2, \quad \sigma_{i+h} \\ &= \frac{1}{N(h)} \sum_{i=1}^{N(h)} (z_{i+h} - m_{i+h})^2. \end{aligned} \quad (8)$$

When the empirical functions (4), (5), and (7) are graphed versus the lag distance h , the semivariogram, the covariance function, and the correlogram tools are obtained. These tools provide information about the spatial correlation of the known data; however, all possible distances are not covered by the empirical functions, therefore, it is necessary to fit a theoretical model, which is what is actually used to develop the Kriging weights. This model must be a continuous function to guarantee positive Kriging variances.

Considering the accuracy of the results assessed for path loss modeling in [5], the exponential function is selected to provide a semivariogram fitting. Consequently, the semivariogram model is expressed as follows:

$$\gamma_{\text{exp}}(h) = s \cdot \left(1 - e^{-3h/r}\right) \quad (9)$$

where s is the sill, the semivariance value at which the semivariogram yields a plateau, and r is the range, the separation distance at which the semivariogram reaches s .

If the spatial dependency of the measured known values is analyzed by employing the covariance function, the fitting model, resulting from the variography, is calculated considering that the covariance function obeys the following relationship:

$$C(h) = \sigma^2 - \gamma_{\text{exp}}(h) \quad (10)$$

where σ^2 is the variance of the variable under consideration z , and $\gamma_{\text{exp}}(h)$ is the exponential function described in (9).

Therefore, the fitting model when covariance function tool is selected is as follows:

$$C_{\text{exp}}(h) = s \cdot e^{-3h/r}. \quad (11)$$

Similarly, when the correlogram tool is employed, it obeys the following relationship:

$$\rho(h) = \frac{C(h)}{\sigma^2} \quad (12)$$

where $C(h)$ is the function described in (11). Once the corresponding values are replaced in (12) the fitting model is calculated as follows:

$$\rho_{\text{exp}}(h) = e^{-3h/r}. \quad (13)$$

At this point, it is clear that there are three options of statistical tools for modeling the spatial patterns of measured samples through a fitted model $f(h)$ computed by (9), (11), or (13), depending on the tool selection, where s and r are calculated by fitting a least-squares regression analysis to the empirical values.

Going on the variography, the binning process is adopted for spatial modeling. Over this process, properly neighbor samples, as described in [5], will restrict how far and where to look for the samples to be used in the prediction, for this process a distance separation matrix between all measured locations is created as D . Toward selecting a suitable lag h and placing a maximum lag limit on the calculation of (4), (5), and (7), it is important to understand this process. Since the estimated values in the variography tend to become more erratic with increasing distances, boundaries are necessary to analyze D . The maximum lag limit is the maximum distance that is going to be considered and is calculated as the half of the maximum distances reported in D , while h determines the lag interval considered to find measured neighbors, which is calculated as the mean of the minimum distance extracted from D . For instance, $z_i - z_{i+h}$ in (4), is grouped based on their corresponding lag interval h —resulting in $N(h)$ pairs—up to the maximum lag to calculate (4) for each separation distance reported in D .

B. Ordinary Kriging for Shadowing Generation

Then, when the spatial patterns have been modeled by fitting a theoretical function $f(h)$, ordinary Kriging employs it to interpolate known data and predict values at unsampled locations by solving the following equation:

$$k = V^{-1} \cdot v \quad (14)$$

where the matrix V is composed by the values resulting from $f(h)$ with h as the distances between the pairs of measured points, the vector v contains the result of compute the distance of each measured locations to the prediction location and substituting it as the lag h in $f(h)$, and k is composed by the Kriging weights λ_i and the Lagrange multiplier l .

When calculating (14) the weights are found and the predicted value \hat{z}_0 at unmeasured place is provided by the following:

$$\hat{z}_0 = \sum_{i=1}^{N(h)} \lambda_i \cdot z_i. \quad (15)$$

Fig. 3 shows an example of shadowing-aided predictions employed by the variography tools when a random 60/40 is selected (considering the radial grouping process). In Fig. 3,

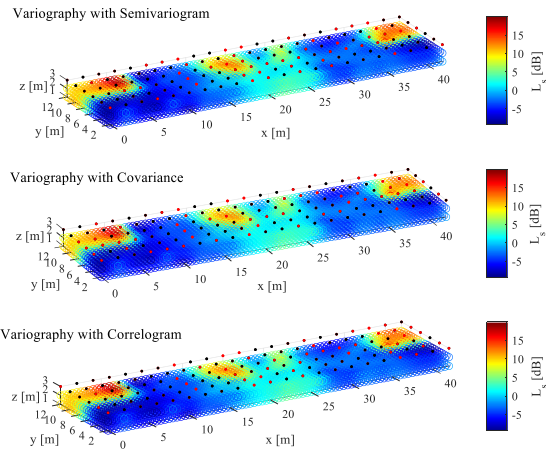


Fig. 3. Shadowing prediction results obtained by variography analysis.

TABLE I
PATH LOSS PREDICTIONS PERFORMANCE

| Tool | $\gamma(h)$ | $C(h)$ | $\rho(h)$ |
|------|-------------|--------|-----------|
| MAE | 2.70 | 2.81 | 2.72 |

tuning and testing dataset locations are plotted with black and red dots, respectively.

V. 3-D PATH LOSS PREDICTIONS

For 3-D indoor path loss predictions, particular data features are required, considering the aim of aided-shadowing Kriging, the variable z described in Section IV corresponds to the shadowing for the tuning dataset extracted in (3) from the measurements. Thus, to predict path loss at specific location in the 3-D indoor space, the next model is followed:

$$\hat{L} = 10n \log d + e + \sum_{i=1}^{N(h)} \lambda_i \cdot L_{si}. \quad (16)$$

One of the aims of this study is encouraged by the fact that on the performance of feasible and accurate Kriging interpolation processing, there is no explicit research to understand and correctly select the best statistical tool to be employed in the preliminary variography process. For this reason, the performance of the variogram, the covariance function and the correlogram is analyzed by comparing the predicted path loss values \hat{L}_i with the measured path loss L_i at the remaining test locations t_N , in terms of the mean absolute error (MAE), which is given by the following:

$$\text{MAE} = \frac{1}{t_N} \sum_{i=1}^{t_N} |L_i - \hat{L}_i|. \quad (17)$$

For a reliable analysis, 1000 iterations are assessed to extract different 60/40 groups for tuning and testing dataset through the radial algorithm described for the path loss extraction. Each value presented in Table I is obtained as the 1000-result average for each statistical tool employed in the variography process.

Furthermore, once the 1000-samples are performed the results of the Kriging-aided model is presented for the tools analyzed

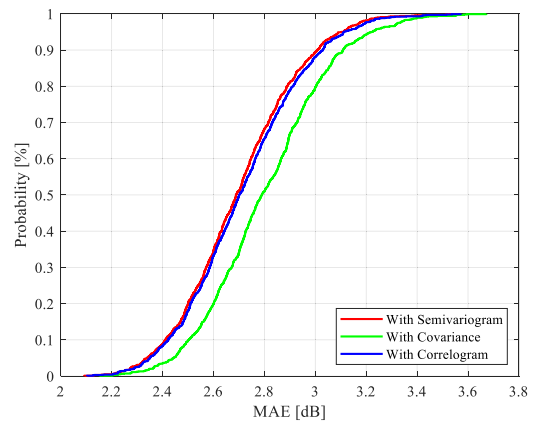


Fig. 4. CDFs of MAE over path loss predictions based on the three tools.

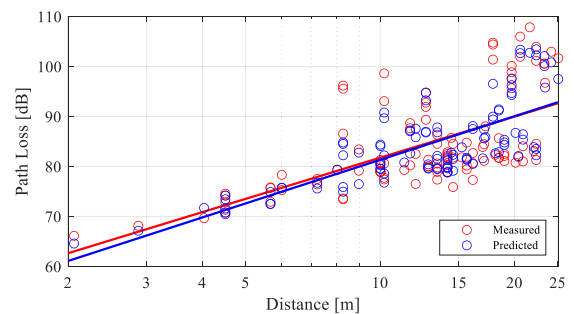


Fig. 5. Path loss prediction versus measurement results for the testing dataset.

in terms of the cumulative distribution function (CDF) for the MAE in Fig. 4.

According to Table I and Fig. 4, it can be seen that employing semivariogram and correlogram for shadowing spatial modeling improves the accuracy of Kriging at 28 GHz. With an MAE of 2.7 dB, the semivariogram guarantees the high level of confidence of the spatial modeling, thus, when it is employed, the proposed model achieves accurate path loss indoor predictions at 28 GHz. However, even though the covariance function has the highest MAE, it is still a small error of 2.81 dB for indoor path loss predictions compared to other hybrid models available in the literature [9].

Considering the profitable results when semivariogram is employed as a statistical tool for variography process in shadowing predictions, Fig. 5 shows the predicted path loss with the model here described and the path loss extracted from measurements at the testing locations, as well as the fitting lines for each case.

VI. CONCLUSION

The aim of this study seeks to evaluate the performance of the specific tool used in variography as part of the Kriging-aided shadowing predictions for indoor path loss modeling. Specifically, we focused on whether the choice of semivariogram, covariance function or correlogram as a statistical tool influences the improvement of the path loss estimation accuracy. The novel knowledge obtained through this work is that in an indoor scenario, correlogram achieves an almost equal performance of semivariogram, even though semivariogram is validated as the most accurate tool to describe shadowing spatial continuity in enclosed spaces for 3-D path loss modeling at 28 GHz.

REFERENCES

- [1] N. Faruk *et al.*, "Path loss predictions in the VHF and UHF bands within urban environments: Experimental investigation of empirical, heuristics and geospatial models," *IEEE Access*, vol. 7, pp. 77293–77307, 2019.
- [2] K. Sato, K. Inage, and T. Fujii, "Radio environment map construction with joint space-frequency interpolation," in *Proc. Int. Conf. Artif. Intell. Inf. Commun.*, Feb. 2020, pp. 051–054, doi: [10.1109/ICAII C48513.2020.9065217](https://doi.org/10.1109/ICAII C48513.2020.9065217).
- [3] K. Sato, K. Inage, and T. Fujii, "On the performance of neural network residual Kriging in radio environment mapping," *IEEE Access*, vol. 7, pp. 94557–94568, 2019.
- [4] M. E. Diago-Mosquera, A. Aragon-Zavala, F. A. Rodriguez-Corbo, M. Celaya-Echarri, R. Shubair, and L. Azpilicueta, "Tuning selection impact on Kriging-aided in-building path loss modeling," *IEEE Antennas Wireless Propag. Lett.*, vol. 21, no. 1, pp. 84–88, Jan. 2022, doi: [10.1109/LAWP.2021.3118673](https://doi.org/10.1109/LAWP.2021.3118673).
- [5] M. E. Diago-Mosquera, A. Aragón-Zavala, and C. Vargas-Rosales, "The performance of in-building measurement-based path loss modelling using Kriging," *Microw. Antennas Propag.*, vol. 15, no. 12, pp. 1564–1576, 2021, doi: [10.1049/mia2.12163](https://doi.org/10.1049/mia2.12163).
- [6] M. E. Diago-Mosquera, A. Aragón-Zavala, and M. Rodriguez, "Testing a 5G communication system: Kriging-aided O2I path loss modeling based on 3.5 GHz measurement analysis," *Sensors*, vol. 21, no. 20, Oct. 2021, Art. no. 6716, doi: [10.3390/S21206716](https://doi.org/10.3390/S21206716).
- [7] N. Mezhoud, M. Oussalah, A. Zaatri, and Z. Hammoudi, "Hybrid Kriging and multilayer perceptron neural network technique for coverage prediction in cellular networks," *Int. J. Parallel, Emergent Distrib. Syst.*, vol. 35, no. 6, pp. 682–706, Nov. 2020, doi: [10.1080/17445760.2020.1805609](https://doi.org/10.1080/17445760.2020.1805609).
- [8] K. Sato, K. Inage, and T. Fujii, "Modeling the Kriging-aided spatial spectrum sharing over log-normal channels," *IEEE Wireless Commun. Lett.*, vol. 8, no. 3, pp. 749–752, Jun. 2019.
- [9] M. E. Diago-Mosquera, A. Aragon-Zavala, and G. A. Castanon, "Bringing it indoors: A review of narrowband radio propagation modeling for enclosed spaces," *IEEE Access*, vol. 8, pp. 103875–103899, 2020.

Chapter 7

Towards Practical Path Loss Predictions in Indoor Corridors Considering 5G mmWave 3D Measurements

7.1 Summary of the Chapter

Reliable indoor path loss models for mmWave frequencies are essential to provide accurate predictions for the deployment of 5G wireless service in in-building scenarios. In this chapter, a long indoor corridor with a 90° break has been selected as a typical corridor to characterize the effect of waveguiding due to the reflections along walls, floor, and ceiling. Besides, radio measurements have been performed at three different receiver heights in order to provide the empirical basis of the 3D propagation geometry. The measurements have been achieved at two different mmWave frequencies, 28 and 60 GHz.

This chapter provides an additional example to ensure the effectiveness of the inclusion of Kriging as a tool to improve model accuracy and achieved the minimum error when it is compared against the most accurate single-slope segment-wise model presented in [23].

7.2 Full Article

Towards Practical Path Loss Predictions in Indoor Corridors Considering 5G mmWave Three-Dimensional Measurements

Melissa Eugenia Diago-Mosquera^{1b}, Alejandro Aragón-Zavala^{1b}, *Senior Member, IEEE*,
and Mauricio Rodríguez^{2b}, *Senior Member, IEEE*

Abstract—Theoretical and empirical foundations of how radio waves behave in practical wireless channels need to be fully revisited for millimeter-wave (mmWave) frequencies so that fifth-generation (5G) technologies may be successful. Kriging is an outstanding geostatistical interpolation technique that employs variography to understand the spatial variability of known samples at specific locations to predict unmeasured samples, based on the fact that there is an implied connection between the measured value and its location in space. The research we here report is aimed at validating the improvement in predictions when this tool is included for mmWave frequency path loss modeling in a long indoor corridor with break. In order to quantify the accuracy of the proposed methodology, it is compared with a well-established procedure described in the literature. Extensive path-loss measurements were collected through specialized narrowband sounders at 28 and 60 GHz. Spatially averaged power measurements using omnidirectional and directive antennas at different heights provided the empirical basis for the three-dimensional Kriging-aided model. It was found that this method significantly improves the accuracy as it considers all the singularities and site-associated features that are implicit in measured samples. This is important to obtain a reliable path loss model for planning and deployment of mmWave wireless communication systems in indoor scenarios.

Index Terms—Fifth-generation (5G) mmWave, indoor corridor, Kriging, path loss model.

I. INTRODUCTION

AS PROMISED by the fifth generation (5G) of radio communication networks, future wireless mobile systems will be inclusive, i.e., technologies for supporting wireless connectivity for any rates, type of communicating units, and scenarios [1]. To meet this ambitious aim, reliable path loss modeling for millimeter-wave (mmWave) frequencies is essential to provide

Manuscript received 9 June 2022; revised 30 June 2022; accepted 9 July 2022. Date of publication 12 July 2022; date of current version 6 October 2022. This work was supported in part by the National Council of Science and Technology CONACYT through the student scholarship 746015; in part by the Chilean Research Agency ANID under Grants ANID FONDECYT 1211368, ANID FONDEQUIP EQM190023, and ANID PIA/APOYO AFB180002; and in part by the Project VRIEA-PUCV 039.437/2020. (Corresponding author: Melissa Eugenia Diago-Mosquera.)

Melissa Eugenia Diago-Mosquera and Alejandro Aragón-Zavala are with the Escuela de Ingeniería y Ciencias, Tecnológico de Monterrey, Querétaro 76130, Mexico (e-mail: a00829220@tec.mx; aaragon@tec.mx).

Mauricio Rodríguez is with the Escuela de Ingeniería Eléctrica, Pontificia Universidad Católica de Valparaíso, Valparaíso 2362804, Chile (e-mail: mauricio.rodriguez.g@pucv.cl).

Digital Object Identifier 10.1109/LAWP.2022.3190324

accurate predictions for the deployment of 5G wireless service. These services are likely to be extensively used in indoor environments such as office spaces linked by long corridors. Propagation in corridors, whose structural geometry resembles a waveguide, has been reported to exhibit path losses lower than those observed in free space, attributable to the contributions of reflections along walls, floor, and ceiling. This has been referred to in the literature as “waveguide effect” [2]–[5], characterized by a path loss exponent (PLE) less than 2, as reported in [6].

Path loss models for indoor corridors at various frequencies have been reported in several previous studies. The model derived in [7] is easy to implement and has clear physical meaning for line-of-sight (LOS) in indoor corridors at 5.25 GHz. Batalha *et al.* [8] employed measurements to adjust path loss prediction models of radio propagation for indoor environments in the frequency band of 8 to 11 GHz. However, these studies have not explicitly discussed waveguiding, which is the reason for a PLE less than 2. Other research, such as those reported in [9], have included this effect through a modified method named effective wall loss model to estimate the path loss at 2.4, 5.3, 28, 60, and 73.5 GHz. In [10], motivated by the waveguiding effect, the authors have proposed a single-slope segmentwise path gain model for transmission along corridors at 28 GHz. In [11], to overcome channel complexity and time-consuming measurements, a novel methodology using an artificial neural network techniques in indoor corridors at 3.7 and 28 GHz has been studied. To improve path loss models for indoor corridors, in [12], the close-in free-space reference distance model and the floating-intercept model were studied and optimized considering 14, 18, and 22 GHz measurements. In total, 14 and 22 GHz were also considered in [5] where a dual slope large-scale path loss model was evaluated. Propagation measurements at 26 and 38 GHz have been conducted in [13] to investigate propagation characteristics of indoor corridors. Even though the works presented in [5] and [7]–[13] were suitable to predict path loss in indoor corridors, their validation was restricted to two-dimensional (2-D) since their models only accounted for one receiver height without considering the complete coverage in a three-dimensional (3-D) space.

Generally, for radio propagation predictions path loss has been modeled using the log-distance model, which includes normal distributed shadow fading [14], [15]. Other studies have taken advantage of the spatial correlation of shadowing to estimate it by including Kriging, which has minimized the variance of estimation errors, due to Kriging employs variography to restrict how far and where to look for the samples to be used in the

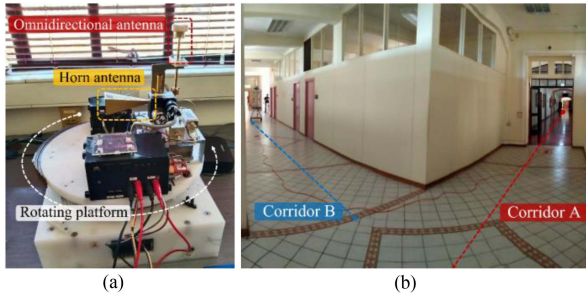


Fig. 1. Equipment and scenario. (a) Receiver system platform at 60 GHz. (b) Long corridor at the USM with break.

interpolation [16], yielding accurate shadowing predictions, as has been validated in [17] and [18]. However, these models have not considered the 3-D propagation geometry to predict the path loss at mmWave frequencies nor employed Kriging to estimate path loss.

The principal novelty in the work here reported is the inclusion of Kriging as an effective tool to improve modeling accuracy for mmWave indoor propagation as it considers all the singularities and site-associated features that are implicit in measured samples. To the best of our knowledge this has not been reported before despite the fact that its potential has been validated [19]–[21] in previous work. Therefore, this letter is focused on better understanding and modeling path loss considering long indoor corridors, the effect of corners and different receiver heights (i.e., 3-D) validating the benefits of using Kriging to ensure accurate path loss predictions.

II. MEASUREMENT CAMPAIGNS AND DATA COLLECTION PROCEDURE

A detailed description of the radio measurements conducted in typical indoor corridor scenarios is provided as follows.

A. Measurement Equipment

Universidad Técnica Federico Santa María (USM) in collaboration with Pontificia Universidad Católica de Valparaíso (PUCV) and Nokia Bell Laboratories constructed two narrowband sounders at 28 GHz [10] and 60 GHz.

The sounders transmit a—22.5 dBm at 28 GHz and 20.5 dBm at 60 GHz—continuous wave tone into vertically polarized horn antennas with 55° half-power beamwidths (HPBW) and 10 dBi of gain. In both cases, the power is recorded by narrowband receivers with the alternative of using horn and omnidirectional (omni) antennas. For 28 GHz the omni antenna has a 1.4 dBi gain. The horn antenna has a 25 dBi gain and 10° HPBW. At 60 GHz the omni antenna has a 2 dBi gain and a vertical HPBW of 30°. The horn antenna has 25 dBi of gain and 9° HPBW in the E-plane and 10° HPBW in the H-plane. The receiver is shown in Fig. 1(a).

The received signal is amplified by several adjustable gain low-noise amplifiers, mixed with a local oscillator and narrowband filtered at a 100 MHz intermediate frequency. A logarithmic-gain power meter generates 740 samples/second, which are transmitted to a laptop computer. The receiver is placed on a rotating 360° platform with the horn antenna rotating on its phase center and the omni antenna describing a circle of 20 cm radius. The path loss is calculated based on the spatially

averaged power measurements received at each location. Average power received by rotating the horn antenna is equivalent to spatial averaging of the omni antenna after compensating for elevation gain if all received multipath wavefronts are within the vertical beamwidth of either antenna, according to the radiation pattern analysis [10]. Using both types of antennas allowed us to verify if there is a significant contribution of received power that the narrower vertical-beamwidth horn antenna will miss.

B. Experimental Scenario and Data Acquisition

In order to represent typical long indoor corridors, received signal-strength measurements were carried out in a long corridor with one 90° break at 37 m from the transmitting antenna—dividing corridor A from corridor B, Fig. 1(b)—in the engineering school of the USM. Corridor A is 39 m long, 3.6 m high, and 2.74 m in width. Corridor B is 16 m long, 3.7 m high, and in 2.57 m width. Both corridors are lined with rooms. The walls and ceilings consist of brick and concrete, with a ceramic-tile floor. At 28 m from the transmitter position, there is a glass door with aluminum frame. The transmitter was always placed in the middle of the corridor at a 1.66 m height and the horn antenna of the transmitter system was manually aimed to get maximum averaged received power at the measured locations.

The first measurement was recorded at 2 m from the transmitter and subsequent samples were spaced every 1 m, resulting in 37 measurements for corridor A and 16 for corridor B, yielding 53 measurements for each system configuration, obtained when varying: 1) frequency, 28 and 60 GHz; 2) type of receiver antenna, horn and omni; 3) receiving height, 0.98 (h_1), 1.66 (h_2), and 2.03 m (h_3). Consequently, a total of 636 radio measurements were made.

Propagation in this scenario can be classified into two types of links: LOS, corridor A, and non-line-of-sight (NLOS), corridor B. NLOS results from reflected, dispersed, and/or diffracted paths after the break. For the sampling process the receiver platform is programmed to switch every ten turns between omnidirectional and horn antenna. This is done for 30 s with the platform rotating at 100 r/min. Small-scale fades are eliminated by averaging power over all angular positions for both types of antennas. Average power over successive rotations is compared to assure consistency in a static environment where no significant temporal variation is to be expected. This sampling process resulted in 636 links. The corresponding path losses are illustrated in Fig. 2, where as expected, we found that the spatially averaged path losses are very close for both types of antennas. This is further discussed in Section IV.

III. CHANNEL MODELING

As a benchmark for comparison to our results we use the most accurate single-slope segmentwise model presented in [10], for the specific case of one break, i.e., one LOS corridor followed by a 90° break and a NLOS corridor. This is described by

$$\hat{L} = \begin{cases} L(d_0) + 10n \log d, & \text{LOS} \\ L(d_0) - S + 10n \log(x_1(d - x_1)), & \text{NLOS} \end{cases} \quad (1)$$

where $L(d_0)$ is the free-space path loss at the reference distance $d_0 = 1$ m, n is the path loss exponent, d is the “Manhattan distance” of the path, i.e., the sum of the path lengths along the corridors from the transmitter to the receiver, S is the around-the-corner loss, and x_1 is the length of the LOS segment, 37 m after which the transition to NLOS causes an evident increase

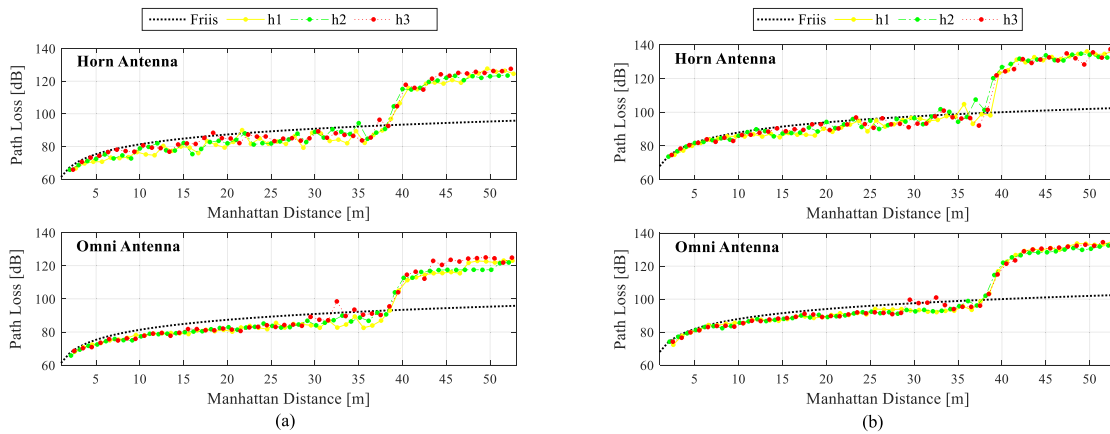


Fig. 2. Path loss measured at three-receiver heights. (a) 28 GHz. (b) 60 GHz.

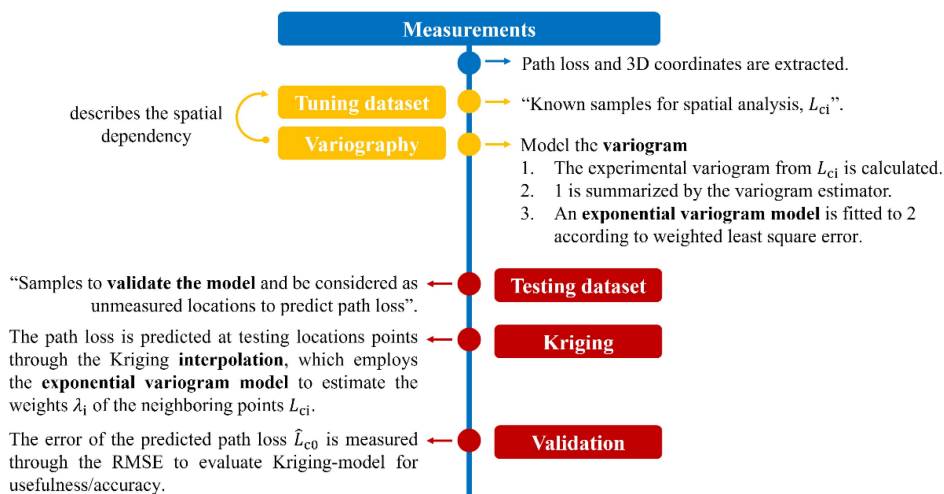


Fig. 3. Methodology for the Kriging-aided path loss predictions.

in path loss as seen in Fig. 2. The values of n and S are fitted from measurements according to the best fit of a classical linear regression.

Based on the fact that the closest samples to the unmeasured locations have the most influence, Kriging predicts path loss values at an unmeasured location with $c0$ 3-D coordinates, forming weights λ_i based on surrounding measured path loss L_{ci} , at known locations with ci 3-D coordinates, following the methodology described in Fig. 3. The path loss proposed is modeled as

$$\hat{L}_{c0} = \sum_{i=1}^{N(h)} \lambda_i L_{ci} \quad (2)$$

where $N(h)$ is the number of known measured pairs within the lag interval h , i.e., for the variography, the distance separation between all measured locations is computed to select neighbor samples by restricting how far (maximum lags) and where to look (in each lag) for the samples to be used in the interpolation through a matrix of Euclidean separation distances. This procedure is described in more detail in [22]. In (2), h is calculated as the mean of the minimum separation distance and $N(h)$ is the resulting number of pairs with h as the separation distance. An

extended explanation of the process to form the λ_i weights to interpolate and predict unmeasured values can be found in [17].

IV. RESULTS

The proposed mathematical model in (2) takes advantage of the spatial analysis of measured samples included in the variography process, which generates the principal boundary that Kriging considers for interpolations. The results we here present are aimed at two distinct objectives, first quantifying the benefit of including 3-D measurements and second, assessing the advantage of using the Kriging-aided model (2). To this effect, three different cases to select tuning and testing datasets are considered. A tuning dataset is used to train the models, in order to fit n and S in (1) and model the variogram to estimate λ_i in (2). The testing dataset allows us to predict the path loss when using the previously obtained model at the 3-D locations and compare them to the measured values. The first case aims to analyze the accuracy of the predictions at heights h_3 and h_1 , i.e., higher and lower than the transmitter antenna when the models are tuned using only measurements at the same transmitter height, h_2 ; The second case uses the samples at h_1 and h_3 to tune and test the models, from each height. In total, 60% of data is randomly selected for the tuning dataset and the remaining 40% from each

TABLE I
RESULTS FOR PATH LOSS PREDICTIONS EMPLOYING (1) AND (2)

| Frequency [GHz] | Receiver Antenna | Case | n | S [dB] | RMSE ₁ [dB] | RMSE _K [dB] |
|----------------------|------------------|------|------|----------|------------------------|------------------------|
| 28 | Horn | 1 | 1.77 | -15.0 | 3.6 | 3.1 |
| | | 2 | 1.70 | -18.1 | 3.6 | 2.9 |
| | | 3 | 1.73 | -17.1 | 3.6 | 3.0 |
| | Omni | 1 | 1.68 | -15.3 | 2.9 | 2.4 |
| | | 2 | 1.70 | -15.9 | 3.0 | 2.1 |
| | | 3 | 1.69 | -15.7 | 2.9 | 2.0 |
| all cases | | | 1.71 | -16.2 | 3.2 | 2.6 |
| 60 | Horn | 1 | 2.00 | -14.0 | 3.9 | 2.9 |
| | | 2 | 1.87 | -16.9 | 3.8 | 3.0 |
| | | 3 | 1.91 | -16.0 | 3.6 | 2.9 |
| | Omni | 1 | 1.78 | -16.5 | 2.5 | 2.0 |
| | | 2 | 1.82 | -16.9 | 2.7 | 1.6 |
| | | 3 | 1.81 | -16.8 | 2.5 | 1.6 |
| all cases | | | 1.87 | -16.2 | 3.2 | 2.3 |
| averaged RMSE | | | | | 3.2 | 2.5 |

height for the testing dataset. Finally, the third case tunes/tests the models considering a rate of 60/40 percentage randomly selected from the samples measured at each of the three-heights: h_1 , h_2 , and h_3 .

The accuracy and effectiveness of the predictions achieved with (2) are evaluated and compared against those calculated with (1) through the root-mean-square error (RMSE) metric considering all the three cases described. In Table I, the fitted values, n and S , are calculated with (1), RMSE₁ refers to the RMSE calculated when (1) is employed, and RMSE_K when (2) is used to predict the path loss at testing locations. These parameters depend on the specific case selected to tune/test (1) and (2), therefore, in Table I, the column “case” is included.

To analyze the results, it is important to bear in mind that the first case considers only same-height transmit and receive measurements for tuning, so the possible effect of dissimilar heights is not part of the model. Instead for the second and third cases possible 3-D effects are included, as transmitter and receiver are at different heights. For the second and third cases, the 60/40 rate is based on random sample selection, therefore, the variability of the tuning/testing dataset must be considered. Thus, 2000 iterations with a 60/40 rate were assessed to quantify n , S , and the RMSE. The results in Table I correspond to the average over the 2000 iterations, in contrast to the first case where all samples were used to obtain a single value. In order to overview the results listed for the horn and omni antennas at both frequencies, the values of n , S , RMSE₁, and RMSE_K are averaged and referred to as *all cases* in Table I. Also, the RMSE reported for *all cases* is averaged and listed at the end of Table I.

Table I, first, shows that both type of antennas yields very similar path loss parameters indicating that virtually all power is collected by the narrower vertical-beam horn antenna, i.e., most multipath wavefronts are close to the horizontal plane. We also note that the omni antenna measurements have a consistently lower RMSE. This suggests that although the omni antenna moves over a relatively short range this nevertheless contributes to reducing the shadowing that can affect the horn, which only spins on axis with no displacement.

As seen for both types of antennas at 28 and 60 GHz n was less than 2, suggesting a better scenario than free space, which is the effect of waveguiding due to walls, ceiling and floor.

On average, the value obtained for n in all cases at 28 GHz with the horn receiver antenna was 1.73, which is similar to the value reported in [10] when the first corner is at 37 m. The case reported in [10] only considered 2-D measurements at 28 GHz with a horn receiver antenna, where the RMSE for the similar indoor corridor was 2.7 dB. However, when the model (1) is employed for 3-D predictions the RMSE increases to 3.6 dB for the first case evaluated, where only the measurements obtained at h_2 are considered. The Kriging-aided model improves accuracy predicting path loss with 3.1 dB RMSE.

When comparing the second case with the first, an improvement is expected since the tuning data now includes power measurements at heights that correspond to those for which the model-predictions will be compared with measurements. However, when (1) is employed, the RMSEs remain essentially the same for both frequencies. Instead, when using Kriging, better accuracy is observed in virtually all cases.

All three cases allow us to validate the enhancement obtained when using the Kriging model instead of slope and intercept for 3-D predictions. The reduction in RMSE is clearly seen in Table I. For the third case, at 28 GHz, the RMSE indicates that with the horn receiver antenna there is an improvement of 17%, and a 31% with the omnidirectional when (2) is used to predict path loss. At 60 GHz, with the horn receiver antenna the RMSE decreases by 19%, and with the omnidirectional by 36% when using the Kriging-aided model. When the third case is tested considering all link configurations (both frequencies and receiver antennas), the advantage of Kriging is validated by employing only 60% of the measured data, providing an excellent tradeoff between the averaged accuracy and the number of tuning samples. We found the RMSE to be 2.4 dB using 95 tuning samples (from the 159 samples measured at the different heights).

Accurate 3-D coverage prediction of wireless links is an important consideration in assessing the quality of service. It follows from our results that the methodology here proposed for indoor corridors is a useful prediction tool to make effective use of a limited number of available measurements. Based on our extensive set of measurements and reviewing the results, we found that using only 60% of the data, the minimum prediction error of the Kriging-based model was up to 41% lower than that of the single-slope segmentwise model.

V. CONCLUSION

Careful and extensive measurements to obtain path loss after averaging small scale fades were collected using 28 and 60 GHz narrowband sounders in a long indoor corridor with break. We obtain a reliable 3-D Kriging-aided path loss model to plan and deploy mmWave wireless communication systems in indoor corridors, which effectively considers all the singularities and site-associated features that are implicit in measured samples.

ACKNOWLEDGMENT

The author M. E. Diago-Mosquera would like to thank the PUCV and USM during her doctoral stay, which allowed her to assess the outstanding results presented in this letter. The authors would like to thank A. R. Lopez, F. Torres, V. Díaz, and D. Orrego for all the help with the extensive measurement campaign, and Leonardo Guerrero for platforms improvements and his continuous support.

REFERENCES

- [1] S. Ruiz et al., "5G and beyond networks," in *Inclusive Radio Communications for 5G and Beyond*. New York, NY, USA: Academic, 2021, ch. 6, pp. 141–186, doi: [10.1016/B978-0-12-820581-5.00012-2](https://doi.org/10.1016/B978-0-12-820581-5.00012-2).
- [2] S. Salous et al., "IRACON channel measurements and models," in *nclusive Radio Communications for 5G and Beyond*. Jan. 2021, ch. 3, pp. 49–105, doi: [10.1016/B978-0-12-820581-5.00009-2](https://doi.org/10.1016/B978-0-12-820581-5.00009-2).
- [3] D. Porrat and D. C. Cox, "UHF propagation in indoor hallways," *IEEE Trans. Wireless Commun.*, vol. 3, no. 4, pp. 1188–1198, Jul. 2004, doi: [10.1109/TWC.2004.828023](https://doi.org/10.1109/TWC.2004.828023).
- [4] H. Xu, V. Kukshya, and T. S. Rappaport, "Spatial and temporal characteristics of 60-GHz indoor channels," *IEEE J. Sel. Areas Commun.*, vol. 20, no. 3, pp. 620–630, Apr. 2002, doi: [10.1109/49.995521](https://doi.org/10.1109/49.995521).
- [5] N. O. Oyie and T. J. O. Afullo, "Measurements and analysis of large-scale path loss model at 14 and 22 GHz in indoor corridor," *IEEE Access*, vol. 6, pp. 17205–17214, 2018, doi: [10.1109/ACCESS.2018.2802038](https://doi.org/10.1109/ACCESS.2018.2802038).
- [6] T. S. Rappaport, *Wireless Communications—Principles And Practice*. New York, NY, USA: Prentice-Hall, 2002.
- [7] X. Zhao, S. Geng, and B. M. Coulibaly, "Path-loss model including LOS-NLOS transition regions for indoor corridors at 5 GHz," *IEEE Antennas Propag. Mag.*, vol. 55, no. 3, pp. 217–223, Jun. 2013, doi: [10.1109/MAP.2013.6586668](https://doi.org/10.1109/MAP.2013.6586668).
- [8] I. D. S. Batalha et al., "Indoor corridor and office propagation measurements and channel models at 8, 9, 10 and 11 GHz," *IEEE Access*, vol. 7, pp. 55005–55021, 2019, doi: [10.1109/ACCESS.2019.2911866](https://doi.org/10.1109/ACCESS.2019.2911866).
- [9] H. A. Obeidat et al., "An indoor path loss prediction model using wall correction factors for wireless local area network and 5G indoor networks," *Radio Sci.*, vol. 53, no. 4, pp. 544–564, Apr. 2018, doi: [10.1002/2018RS006536](https://doi.org/10.1002/2018RS006536).
- [10] D. Chizhik, J. Du, R. Feick, M. Rodriguez, G. Castro, and R. A. Valenzuela, "Path loss and directional gain measurements at 28 GHz for non-line-of-sight coverage of indoors with corridors," *IEEE Trans. Antennas Propag.*, vol. 68, no. 6, pp. 4820–4830, Jun. 2020, doi: [10.1109/TAP.2020.2972609](https://doi.org/10.1109/TAP.2020.2972609).
- [11] F. D. Diba, M. A. Samad, and D. Y. Choi, "Centimeter and millimeter-wave propagation characteristics for indoor corridors: Results from measurements and models," *IEEE Access*, vol. 9, pp. 158726–158737, 2021, doi: [10.1109/ACCESS.2021.3130293](https://doi.org/10.1109/ACCESS.2021.3130293).
- [12] M. K. Elmezughi and T. J. Afullo, "An efficient approach of improving path loss models for future mobile networks in enclosed indoor environments," *IEEE Access*, vol. 9, pp. 110332–110345, 2021, doi: [10.1109/ACCESS.2021.3102991](https://doi.org/10.1109/ACCESS.2021.3102991).
- [13] Y. Shen, Y. Shao, L. Xi, H. Zhang, and J. Zhang, "Millimeter-Wave propagation measurement and modeling in indoor corridor and stairwell at 26 and 38 GHz," *IEEE Access*, vol. 9, pp. 87792–87805, 2021, doi: [10.1109/ACCESS.2021.3081822](https://doi.org/10.1109/ACCESS.2021.3081822).
- [14] H.-S. Jo, C. Park, E. Lee, H. K. Choi, and J. Park, "Path loss prediction based on machine learning techniques: Principal component analysis, artificial neural network, and Gaussian process," *Sensors*, vol. 20, no. 7, Mar. 2020, Art. no. 1927, doi: [10.3390/s20071927](https://doi.org/10.3390/s20071927).
- [15] K. Sato, K. Suto, K. Inage, K. Adachi, and T. Fujii, "Space-frequency-interpolated radio map," *IEEE Trans. Veh. Technol.*, vol. 70, no. 1, pp. 714–725, Jan. 2021, doi: [10.1109/TVT.2021.3049894](https://doi.org/10.1109/TVT.2021.3049894).
- [16] M. E. Diago-Mosquera, A. Aragón-Zavala, L. Azpilicueta, R. Shubair, and F. Falcone, "A 3D indoor analysis of path loss modeling using Kriging techniques," *IEEE Antennas Wireless Propag. Lett.*, vol. 21, no. 6, pp. 1218–1222, Jun. 2022, doi: [10.1109/LAWP.2022.3162160](https://doi.org/10.1109/LAWP.2022.3162160).
- [17] M. E. Diago-Mosquera, A. Aragón-Zavala, and M. Rodriguez, "Testing a 5G communication system: Kriging-aided O2I path loss modeling based on 3.5 GHz measurement analysis," *Sensors*, vol. 21, no. 20, Oct. 2021, Art. no. 6716, doi: [10.3390/S21206716](https://doi.org/10.3390/S21206716).
- [18] M. E. Diago-Mosquera, A. Aragón-Zavala, and C. Vargas-Rosales, "The performance of in-building measurement-based path loss modelling using Kriging," *Microw., Antennas Propag.*, vol. 15, Jun. 2021, Art. no. mia2.12163, doi: [10.1049/mia2.12163](https://doi.org/10.1049/mia2.12163).
- [19] M. E. Diago-Mosquera, A. Aragon-Zavala, F. A. Rodriguez-Corbo, M. Celaya-Echarri, R. Shubair, and L. Azpilicueta, "Tuning selection impact on Kriging-aided in-building path loss modeling," *IEEE Antennas Wireless Propag. Lett.*, vol. 21, no. 1, pp. 84–88, Jan. 2022, doi: [10.1109/LAWP.2021.3118673](https://doi.org/10.1109/LAWP.2021.3118673).
- [20] K. Sato, K. Inage, and T. Fujii, "Radio environment map construction with joint space-frequency interpolation," in *Proc. Int. Conf. Artif. Intell. Inf. Commun.*, Feb. 2020, pp. 051–054, doi: [10.1109/ICAIC48513.2020.9065217](https://doi.org/10.1109/ICAIC48513.2020.9065217).
- [21] A. Konak, "Estimating path loss in wireless local area networks using ordinary Kriging," in *Proc. Winter Simul. Conf.*, 2010, pp. 2888–2896, doi: [10.1109/WSC.2010.5678983](https://doi.org/10.1109/WSC.2010.5678983).
- [22] M. H. Trauth, "Spatial data," in *MATLAB Recipes for Earth Sciences*, 4th ed. Berlin, Germany: Springer, 2015, pp. 1–427.

Chapter 8

mmWave Channel Measurements for 3D Path Loss Analysis and Model Design in Stadiums

8.1 Summary of the Chapter

The main objective of this final extra part of the research is to validate the versatility of the 3D mathematical model proposed in Chapter 7. And off course, contribute to the telecommunications society with a good foundation towards a greater understanding of mmWave channel propagation in an inclined surface of the seating area of a stadium. In seeking further analysis, this work has sectorized the measurements to characterize the propagation behavior and validate if there is a better model than the free space path loss model (FSPL) to represent the coverage in this type of scenarios.

For this purpose, 400 extensive mmWave radio measurements have been carried out at the Sausalito stadium in Viña del Mar, emulating mobile user equipment with 100 different transmitter positions and two locations for the receiver system, emulating a base station with different placements.

8.2 Full Article

mmWave Channel Measurements for 3-D Path Loss Analysis and Model Design in Stadiums

M. E. Diago-Mosquera¹, A. Aragón-Zavala¹, *Senior Member, IEEE*, A. Rodríguez-López²,
and M. Rodríguez², *Senior Member, IEEE*

Abstract—A stadium is a multiuser scenario where the wireless system should be able to support real-time service delivery when the stadium is at full capacity during an event. To address radio propagation design for this type of challenging scenario, theoretical and empirical method is needed. Extensive open-space static measurements and research have been conducted at 28 and 60 GHz frequencies in an empty seating area of a stadium with a capacity of 60000 seats. The findings of this work lay a good foundation towards a greater understanding of mmWave channel propagation in a stadium, where a sectorization approach is considered to characterize the path loss behavior in 3D and predict it at unmeasured locations through the Kriging-aided model proposed with only 1 dB RMSE.

Index Terms—3D path loss, mmWave, radio propagation design, stadium, Kriging.

I. INTRODUCTION

ALWAYS motivated by the need of people communication, radio propagation systems have evolved remarkably over the years, providing connectivity and continuous improvements for wireless communication services. While fast-growing, researchers, telecommunication students, and engineers, have to consider innovative approaches to continuously address user demands and provide progressive involvement in technology development, as well as its usefulness and support capabilities for massive consumers. To address the high-density challenge, the exploration of new spectrum bands, as millimeter-wave (mmWave) is becoming increasingly. A stadium is a clear example of multiuser scenario where the wireless system should be able to support real-time service delivery when the stadium is at full capacity during an event. In order to increase network capacity, the sectorization technique is performed in this type of high-density scenario, therefore, it is essential to ensure interference control. To accomplish this aim, the main requirements are issues

related to efficient use of network resources as is mentioned in [1], e.g., accurate coverage predictions and clear footprints of each sector.

It is important to emphasize that a stadium is a complex scenario. First, there are the dressing rooms, the commentary box, tunnels, etc., which are similar to any other office building. Additionally, there is the seating area, which is an inclined surface whose modeling is complex. Not forgetting the fact that it is practically an outdoor scenario where it is more difficult to contain the radio signal levels. Therefore, a stadium needs its own radio frequency network, where three-dimensional (3D) modeling is essential since, due to its geometry, users will be at different levels as a result of the inclined surface of the seating area.

Properly path loss characterizing in a stadium accomplishes real knowledge of the network coverage when addressing the challenges that come with i) capacity and spectrum utilization, and ii) high density. Taking into account the first challenge inherent to future wireless communication, in [2], the authors investigated several stationarity properties of a massive multiple input and multiple output (MIMO) channel in a stadium at 1.4 and 4.4 GHz. Also, in [3] the design of two-dimensional (2D) arrays in a stadium was considered for increasing the capacity through large cell sectorization. Regarding the second challenge, measurements and research have been conducted in stadiums in order to analyze the coverage and capacity at 28 and 5 GHz, considering body loss as parameter that can severely affect system performance [4]–[6]. Despite the challenges overcome in [2]–[6], and the research available in [7], where iBwave presented a complete report to design better wireless networks for stadiums describing the best practices and a detailed radio frequency design. These studies do not design a path loss model for radio channel characterizing.

In the performance of wireless communication systems, channel modeling is crucial to understand what happens with the waves over the transmission path. Measurement-based models can predict signal attenuation over a link, considering all propagation factors implicit in field measurements. But, when a large amount of useful data cannot be achieved during sampling in measurement campaigns, Kriging can be included as a powerful and accurate tool to predict unmeasured values [8]. Notwithstanding the relatively realization that mmWave frequencies are viable for mobile communications. Currently, few attempts [9] have been made to understand radio channels in stadiums above 28 GHz where there are much wider unused bandwidth slots available. Therefore, we

Manuscript received 24 June 2022; accepted 16 July 2022. Date of publication 20 July 2022; date of current version 9 September 2022. This work was supported in part by the National Council of Science and Technology, Consejo Nacional de Ciencia y Tecnología under the student scholarship number 746015; and in part by the Chilean Research Agency ANID under Grant ANID FONDECYT 1211368, Grant ANID FONDEQUIP EQM190023, Grant ANID PIA/APOYO AFB180002, and Project VRIEA-PUCV 039.437/2020. The associate editor coordinating the review of this article and approving it for publication was J. Zhang. (*Corresponding author: M. E. Diago-Mosquera.*)

M. E. Diago-Mosquera and A. Aragón-Zavala are with the Escuela de Ingeniería y Ciencias, Tecnológico de Monterrey, Querétaro 76130, Mexico (e-mail: a00829220@itesm.mx; aaragon@tec.mx).

A. Rodríguez-López and M. Rodríguez are with the Escuela de Ingeniería Eléctrica, Pontificia Universidad Católica de Valparaíso, Valparaíso 2362804, Chile (e-mail: andreia.rodriguez.1@pucv.cl; mauricio.rodriguez.g@pucv.cl).

Digital Object Identifier 10.1109/LWC.2022.3192513



Fig. 1. 28 GHz radio system in the stadium Sausalito. a) Rx. b) Tx.

considered that 28 and 60 GHz measurements offer some insight to move a step forward for channel modeling at mmWave. To the best of our knowledge, this is the first radio propagation empirical model proposed for stadiums at mmWave frequencies, to achieve accurate predictions for 5G communication systems. Where specially constructed narrowband sounders were employed to recollect careful and extensive measurements, which allow us to report separation distances between the transmitter and receiver much greater than those reported in [9]. The main contributions of this letter are as follows.

- A suitable sectorization approach is studied to understand and characterize radio wave propagation in a stadium at mmWave frequencies in terms of the traditional single slope (SS) model. Considering possible 3D effects, as the transmitter and receiver are at different heights on the inclined surface.
- The inclusion of Kriging is an effective tool to improve modeling accuracy for mmWave propagation as it considers all the singularities in the seating area and stadium-associated features that are implicit in measured samples.
- Better understanding and modeling of path loss at a stadium considering the effect of different transmitter heights (i.e., 3D) validating the benefits of using Kriging to ensure accurate path loss predictions with the best and least amount of training samples.

II. DATA COLLECTION PROCEDURE

An extensive amount of carefully calibrated signal strength radio measurements at mmWave frequencies was performed in the 8089 m² of the seating area of the Sausalito Stadium in Vina del Mar, Chile. Universidad Técnica Federico Santa María (USM) in collaboration with Pontificia Universidad Católica de Valparaíso (PUCV) and Nokia Bell Laboratories constructed the two narrowband sounders used during measurement campaign at 28 GHz [10] and 60 GHz. Measurements were carried out with the seating area empty to assure a static scenario. The radio systems at both frequencies transmit a continuous wave (CW) tone into a vertically polarized horn antenna with 55° half-power beamwidths and a gain of 10 dBi.

At 28 GHz the transmitted power is 22 dBm and at 60 GHz is 20.5 dBm. The narrowband sounder platform at 28 and 60 GHz are visualized in Fig. 1a and Fig. 2a. Both receive the signal with an omnidirectional (omni) antenna and amplify it

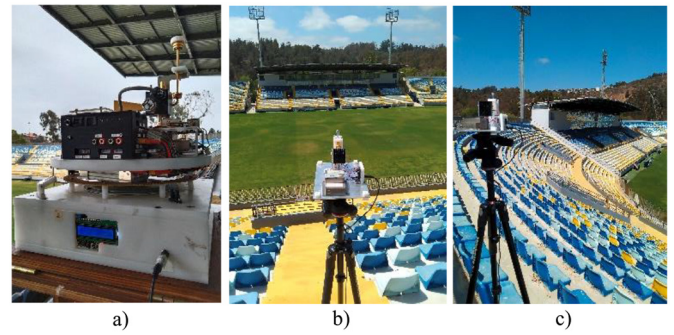


Fig. 2. 60 GHz radio system in the stadium Sausalito. a) Rx. b) Tx located in front of the receiver. c) Tx located on the right side of the receiver.

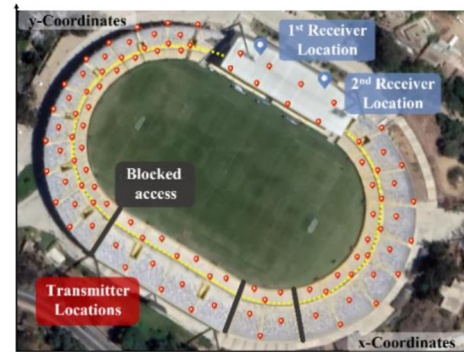


Fig. 3. Measurement layout with the radio system distribution.

with several adjustable gain low-noise amplifiers, mixed with a local oscillator, resulting in an intermediate frequency (IF) signal centered at 100 MHz. The IF signal power (filtered by a 200 kHz-wide bandpass filter) is measured and converted to digital values through a logarithmic-gain power meter that generates 740 samples/second. Finally, these samples are transmitted to a laptop computer. Measurable path loss extends to 171 dB at 28 GHz and to 167 dB at 60 GHz with directional antenna gains.

For 28 GHz the omni antenna has a gain of 1.4 dBi and at 60 GHz 2 dBi with a vertical half-power beamwidth of 30°. As pictured in Fig. 1a and Fig. 2a the receiver (Rx) is placed on a rotating 360° platform with the omni antenna describing a circle of 20 cm radius, thus, the received power is calculated based on the spatially averaged received when the transmitter (Tx) system (Fig. 1b and Fig. 2b) is moved at each desired location. The Rx and Tx were always placed at 1.66 m height and the horn antenna of the Tx was manually aimed to get maximum average received power at each measurement location. In order to properly characterize and represent the complete seating area of a typical stadium, 100 locations were carefully selected, as is illustrated in Fig. 3. Besides, according to the radio system size, the transmitting system was selected to be strategically moved through the seating area locations, emulating a mobile user equipment, as is visualized in Fig. 1 and Fig. 2. While the receiving antenna was fixed to the first or the second location under the roof in the seating area, emulating a base station.

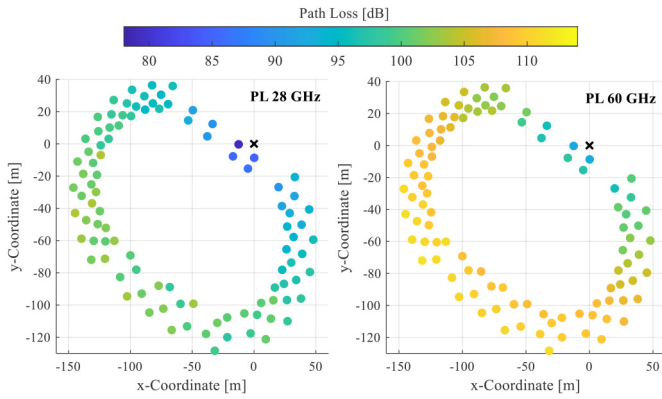


Fig. 4. Path loss measured with receiver antenna (cross marker) placed in the 2nd location at 28 and 60 GHz.

During the measurement campaign, some places were unreachable due to the seating area was separated by barriers, as illustrated in Fig. 3 with the blocked access legend. As a result of considered two different receiving locations at two frequencies, four scenarios were assessed for the measurement campaign. Where 100-samples were recollected at each scenario, yielding a total of 400 received power samples.

III. PATH LOSS ANALYSIS FOR RADIO WAVE PROPAGATION

From the received power measurements P_{RX} and the features of the radio system, i.e., the transmitted power P_{TX} and the antenna gains (G_{TX} , G_{RX}), the path loss is extracted from the link budget at each location with $L = P_{TX} + G_{TX} + G_{RX} - P_{RX}$. In order to illustrate the behavior of radio propagation in a stadium, Fig. 4 shows the path loss measured when the receiver is located at the second point. As is mentioned in [11], theoretically, the path loss in free space decreases quadratically as frequency increases, so long as the effective aperture of the antenna is kept constant over frequency at both link ends.

Towards path loss modeling, it will be possible to contemplate a stadium venue as a free space scenario, however, despite the fact that the physical size of both antennas is kept constant and the venue suggests a pure line-of-sight (LOS) link between the transmitter and receiver antenna, the behavior of the path loss needs to be investigated due to it is not accurately characterized as free space (FSPL), and, as is shown in Fig. 5, is clear that the radiofrequency propagation environment differs vastly within the stadium, from LOS without reflections to LOS with a lot of reflections in the seating area. In order to provide an average tendency of measured path loss a fitting green curve is illustrated in Fig. 5 for both frequencies used during the measurement campaign. This green curve is computed through the traditional SS model [12, Ch. 9]

$$L = L_0 + 10n \log(d) + L_s, \quad (1)$$

with L_0 as the free space path loss at a 1 m distance, n as the path loss exponent (PLE), d as the Euclidean distance of the link, and L_s as the shadowing component, i.e., a zero-mean Gaussian random variable with a standard deviation σ .

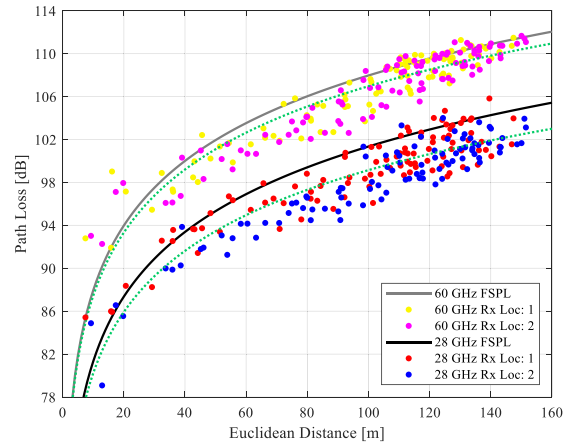


Fig. 5. Path loss extracted from the measurement campaign.

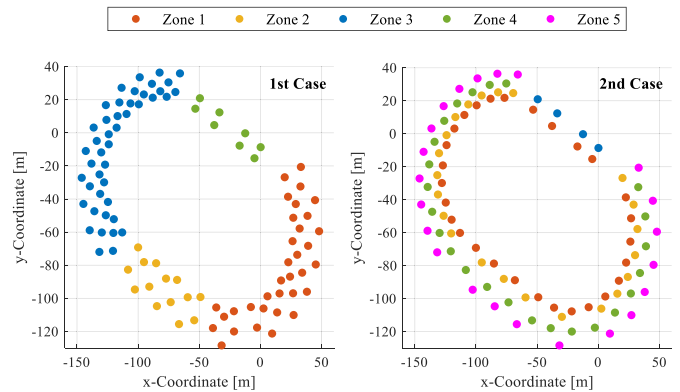


Fig. 6. Sectorizing approach for path loss analysis, where 1st case considers x and y coordinates for grouping zones and 2nd considers z coordinate.

On average, the measured path loss difference at each location between 60 and 28 GHz was 7.8 dB. Which initially shows a similarity with the theoretical value calculated by the FSPL equation ($20 \times \log_{10}(60/28) = 6.6$ dB). Besides, as seen in Fig. 5, the measured path loss difference between the fitting green curves and FSPL is only 1 dB at 60 GHz and 2.3 dB at 28 GHz. However, both green curves have an n less than 2, suggesting a better scenario than free space, with $n = 1.95$ at 60 GHz and $n = 1.89$ at 28 GHz.

In the design of a radio network, the main purpose of sectorization is to consider specific areas to cover, reducing the interference as well as improving capacity. Thus, and in seeking of a further analysis in the radio propagation in stadiums, three different cases are analyzed for signal propagation description: the first, sectorized the stadium in 4 zones according to the coordinates in the seating area of the stadium, case illustrated on the left side of Fig. 6; the second, sectorized the measurements according to the altitude reported for the transmitted antenna location, yielding 5 zones visualized in the right side of Fig. 6; and the third, consider all the measurements without constraint the selection of the samples. The first and second cases were motivated by the sectorization schemes released in [7].

TABLE I
PATH LOSS CHARACTERIZATION AT 28 GHz AND 60 GHz

| Case | Zone | 28 GHz | | 60 GHz | |
|------|------|--------|---------------|--------|---------------|
| | | n | σ [dB] | n | σ [dB] |
| 1 | 1 | 1.86 | 3.2 | 1.93 | 3.6 |
| | 2 | 1.90 | 1.6 | 1.99 | 0.8 |
| | 3 | 1.90 | 3.1 | 1.93 | 3.5 |
| | 4 | 1.92 | 3.8 | 2.05 | 3.2 |
| 2 | 1 | 1.90 | 4.5 | 1.97 | 4.0 |
| | 2 | 1.87 | 3.2 | 1.94 | 3.7 |
| | 3 | 1.90 | 4.1 | 2.00 | 3.4 |
| | 4 | 1.88 | 3.2 | 1.94 | 3.5 |
| | 5 | 1.88 | 3.2 | 1.94 | 3.7 |
| 3 | 1 | 1.89 | 4.3 | 1.95 | 4.4 |

To overview our findings, Table I is presented to show n as well as σ for signal propagation description when a SS model is considered for the 3-cases previously described. To compute (1), the measurements gathered at both receiver locations are joined according to the frequency and employed to tune the model.

The main conclusions of the summary provided in Table I are: i) The least path loss variations occur in zone 2 when sectorization is achieved according to case 1, due to the position of the receiver antenna. Which, for this zone, is located exactly in front of the transmitter positions; ii) The highest standard deviation in the measured path loss is found in zone 1 for case 2, this is largely related to the sectorization approach since in this case, zone 1 is located around the entire soccer field and measurements are probably affected by the reflections that occurred due to the proximity to the fence net and field; and iii) At both frequencies when all samples are taking into account (case 3) the PLE is less than free space, i.e., 2, which becomes our goal to further investigate propagation in a stadium by predicting path loss with an accurate model.

IV. PATH LOSS PREDICTIONS

Based on the geostatistical fact that there is an implied connection between the observed values (measured path loss) and its location in the space (3D coordinates), two main procedures are considered to predict the path loss: variography, for modeling the variogram and Kriging, for interpolation [13]. The aim of the variogram model is to describe the spatial dependency of the path loss measured between the blue locations illustrated in Fig. 3. This variogram is used to predict the unknown path loss \hat{L} at an unobserved location c_0 according to a weight λ_i estimated from known path loss measurements L_{ci} through ordinary Kriging:

$$\hat{L}_{c_0} = \sum_{i=1}^{N(h)} \lambda_i \cdot L_{ci}, \quad (2)$$

where $N(h)$ is the number of pairs of measured locations within the lag interval h selected to estimate the path loss at an unmeasured point with c_0 3D coordinates, in other words, h is the size of a distance class into which pairs of locations $N(h)$ are grouped. An extensive mathematical description of the variography and ordinary Kriging process is described in [14].

TABLE II
PATH LOSS PREDICTIONS ACCURACY FOR THE 3-CASES CONSIDERING A TOTAL OF 200 RECEIVED POWER MEASUREMENTS PER FREQUENCY

| RMSE _f | Case | Samples | | | | | |
|----------------------------|------|---------|-----|-----|-----|-----|-----|
| | | 20 | 40 | 60 | 80 | 100 | 120 |
| RMSE ₂₈ [dB] | 1 | 2.0 | 1.8 | 1.7 | 1.7 | 1.7 | 1.7 |
| | 2 | 2.1 | 1.8 | 1.8 | 1.7 | 1.7 | 1.7 |
| | 3 | 2.2 | 1.9 | 1.8 | 1.7 | 1.7 | 1.7 |
| RMSE ₆₀ [dB] | 1 | 1.2 | 1.1 | 1.0 | 1.0 | 1.0 | 0.9 |
| | 2 | 1.2 | 1.0 | 1.0 | 1.0 | 1.0 | 0.9 |
| | 3 | 1.4 | 1.1 | 1.0 | 1.0 | 1.0 | 0.9 |

To train and validate the accuracy of the Kriging-aided model, two datasets are extracted from the measurements: the first dataset, named as *samples* in Table II, is used to calculate λ_i and L_{ci} in (2); and the remaining dataset is designated to validate the path loss predicted at those locations. In addition, and towards decrease the quantity of required samples to train Kriging, the 20 – 120 *samples* were extracted with a percentage varying from 10 – 60 percent. The boundary of 60 percent was selected according to the findings reported in [14]. The datasets are selected according to the three cases described in Section III, e.g., for case 1 in Table II, if 60 percent is selected to extract *samples*, it is ensured that this percentage is randomly-extracted from each zone of the first case (illustrated in Fig. 6), resulting in 120-random *samples* available to train Kriging; the remaining 80-random *samples* (40 percent) are intended for testing and validating the model in terms of the root-mean-square error (RMSE).

In order to include the largest number of possible randomly drawn *samples*, 1000-tests were assessed to calculate the RMSE of predictions. After 1000-RMSE were assessed for each case, results were averaged and reported in Table II, aiming to quantify and validate the accuracy of the Kriging-aided model (K) proposed.

It is evident that when the sample size—with which Kriging is trained—increases, the confidence in the estimates also increases, as well as the accuracy, decreasing the RMSE. For the 3 cases, at both frequencies, from 20% to 60% of the sample size selected (40 - 120 samples), there is not an evident RMSE difference between the cases analyzed for the sectorization approach. This allows us to conclude that for this type of scenario there is not necessary to zone the sampled field to extract the training dataset, as in the last case, which provides an excellent trade-off between the number of samples employed and the error in the prediction. On average, for the third case, tuning the model with 80 to 120 samples the RMSE is only 1.7 dB for 28 GHz and 1 dB for 60 GHz.

By comparing case 3 against cases 1 and 2, we can understand the potential of the methodology followed by Kriging, which first, analyzes the spatial variability of the samples, and later, in accordance with the previous analysis, interpolates the best set of samples to achieve suitable predictions at unmeasured locations. Furthermore, Table II suggests that from 80 samples the RMSE converges to the lowest reported error, i.e., only 40% of randomly-separated samples represent enough quantity to sample a stadium with a seating area of

TABLE III
RMSES FOR PATH LOSS PREDICTIONS EMPLOYING SS AND K MODELS

| Frequency [GHz] | RMSE value | RMSE _{SS} [dB] | RMSE _K [dB] |
|-----------------|---------------|-------------------------|------------------------|
| 28 | Min | 1.4 | 1.3 |
| | 1000-averaged | 1.8 | 1.7 |
| | Max | 2.2 | 2.0 |
| 60 | Min | 1.2 | 0.6 |
| | 1000-averaged | 1.7 | 0.9 |
| | Max | 2.2 | 1.6 |

an 8089 m² for suitably Kriging-training and accurate radio propagation predictions.

To compare the performance of the model here proposed, Table III provides a summary of the 1000-RMSEs achieved when a 60/40 percentage rate is extracted from all stadium measurements to tune/test both the well-known SS model employed for LOS links, described in (1), and the K model, described in (2). In Table III, RMSE_{SS} refers to the RMSE calculated when (1) is employed, and RMSE_K when (2) is used to predict the path loss at testing locations.

Through the RMSE values listed in Table III, we conclude that the K model is very robust: Firstly, despite the complex scenario considered to provide predictions in an inclined surface, minor RMSE values are presented when the K model is employed; Secondly, averaging 1000-iterations achieved, the RMSE reported is just 1.7 and 0.9 dB for 28 and 60 GHz scenarios, respectively, which justifies including Kriging as part of the post-processing to predict unmeasured data reducing the RMSE by 0.2 dB for 28 GHz and 0.8 dB for 60 GHz when it is compared to SS model RMSEs; Thirdly, the K model performs just as well when tested against stadium as indoor [8], [14] and outdoor-to-indoor [15] measurements at mmWave frequencies. After tests were achieved by analyzing maximum, average, and minimum RMSEs listed in Table III, it was possible to validate the consistency and the adaptability of the K model for this complex scenario ensuring its usefulness for path loss predictions.

V. CONCLUSION

This letter studied the propagation environment of a not well investigated venue as is a stadium, provided a path loss analysis when sectorizing measurements according to its locations, and validated the potential of employing Kriging for path loss prediction when few samples are considered, allowing RMSE as small as 1 dB. Besides, it was corroborated that the usefulness of the model proposed can be extended not only for indoor scenarios, as reported in [8], [14], but also for a complex venue as is a stadium. The processed data and the findings according to the Kriging-aided approach will help with mmWave wireless network design for this specific scenario. Additionally, and on behalf to outperform the Kriging-aided path loss model, a characterization of small-scale fading in stadiums could be interesting future work, considering the possibility of increasing statistical precision when designing a wireless communication system.

ACKNOWLEDGMENT

M. E. Diago-Mosquera wishes to acknowledge all the support provided by the PUCV during her doctoral stay, which allowed her to assess the outstanding results presented in this research, and to the USM that in collaboration with the PUCV and Nokia Bell Laboratories constructed the narrow-band sounders used during the measurement campaign. Many thanks to Francisco Torres for the help with the extensive measurement campaign, Leonardo Guerrero for his continuous support, and Rodrigo Castro (Subdirector of the Sports Department of Viña del Mar) for giving us the approval to access Sausalito stadium. And A. Rodrigues-Lopes wishes to acknowledge the support received from the PUCV under the 2021 Postgraduate Scholarship.

REFERENCES

- [1] A. Aragon-Zavala, V. Jevremovic, and A. Jemmali, "Auto-correlation and cross-correlation analysis for sport arenas at 850 MHz and 2.1 GHz," in *Proc. 8th Eur. Conf. Antennas Propag.*, 2014, pp. 428–432, doi: [10.1109/EUCAP.2014.6901783](https://doi.org/10.1109/EUCAP.2014.6901783).
- [2] L. Liu, C. Tao, D. W. Matolak, Y. Lu, B. Ai, and H. Chen, "Stationarity investigation of a LOS massive MIMO channel in stadium scenarios," in *Proc. IEEE 82nd Veh. Technol. Conf.*, 2015, pp. 1–5, doi: [10.1109/VTCFALL.2015.7391154](https://doi.org/10.1109/VTCFALL.2015.7391154).
- [3] R. Maslennikov *et al.*, "Azimuth and elevation sectorization for the stadium environment," in *Proc. IEEE Global Telecommun. Conf.*, 2013, pp. 3971–3976, doi: [10.1109/GLOCOM.2013.6831694](https://doi.org/10.1109/GLOCOM.2013.6831694).
- [4] M. N. Kulkarni, A. Ö. Kaya, D. Calin, and J. G. Andrews, "Impact of humans on the design and performance of millimeter wave cellular networks in stadiums," in *Proc. IEEE Wireless Commun. Netw. Conf. (WCNC)*, May 2017, pp. 1–6, doi: [10.1109/WCNC.2017.7925748](https://doi.org/10.1109/WCNC.2017.7925748).
- [5] M. Sasaki, T. Nakahira, K. Wakao, and T. Moriyama, "Human blockage loss characteristics at 5 GHz bands in a crowded stadium," in *Proc. Int. Symp. Antennas Propag.*, Jan. 2021, pp. 67–68, doi: [10.23919/ISAP47053.2021.9391505](https://doi.org/10.23919/ISAP47053.2021.9391505).
- [6] M. N. Islam, S. Subramanian, A. Partyka, and A. Sampath, "Coverage and capacity of 28 GHz band in indoor stadiums," in *Proc. IEEE Wireless Commun. Netw. Conf.*, Sep. 2016, pp. 1–7, doi: [10.1109/WCNC.2016.7564885](https://doi.org/10.1109/WCNC.2016.7564885).
- [7] V. Jevremovic, "How to Design Better Wireless Networks for Stadiums." 2015. [Online]. Available: <https://info.ibwave.com/white-paper-how-to-design-better-wireless-networks-for-stadiums/>
- [8] M. E. Diago-Mosquera, A. Aragon-Zavala, L. Azpilicueta, R. Shubair, and F. Falcone, "A 3D indoor analysis of path loss modeling using kriging techniques," *IEEE Antennas Wireless Propag. Lett.*, vol. 21, no. 6, pp. 1218–1222, Jun. 2022, doi: [10.1109/LAWP.2022.3162160](https://doi.org/10.1109/LAWP.2022.3162160).
- [9] N. Yonemoto, Y. Otagaki, Y. Kakubari, K. Ikeda, and H. Murata, "MMW remote antenna system of vector network analyzer for propagation measurement in stadium," in *Proc. IEEE Conf. Antenna Meas. Appl.*, 2017, pp. 337–340, doi: [10.1109/CAMA.2017.8273444](https://doi.org/10.1109/CAMA.2017.8273444).
- [10] D. Chizhik, J. Du, R. Feick, M. Rodriguez, G. Castro, and R. A. Valenzuela, "Path loss and directional gain measurements at 28 GHz for non-line-of-sight coverage of indoors with corridors," *IEEE Trans. Antennas Propag.*, vol. 68, no. 6, pp. 4820–4830, Jun. 2020, doi: [10.1109/TAP.2020.2972609](https://doi.org/10.1109/TAP.2020.2972609).
- [11] T. S. Rappaport, Y. Xing, G. R. MacCartney, A. F. Molisch, E. Mellios, and J. Zhang, "Overview of millimeter wave communications for fifth-generation (5G) wireless networks—With a focus on propagation models," *IEEE Trans. Antennas Propag.*, vol. 65, no. 12, pp. 6213–6230, Dec. 2017, doi: [10.1109/TAP.2017.2734243](https://doi.org/10.1109/TAP.2017.2734243).
- [12] S. Saunders and A. Aragón-Zavala, *Antenna and Propagation for Wireless Communication Systems*. Hoboken, NJ, USA: Wiley, 2007.
- [13] M. H. Trauth, "Spatial Data," in *MATLAB Recipes for Earth Sciences*, 4th ed. Heidelberg, Germany: Springer, 2015, pp. 1–427.
- [14] M. E. Diago-Mosquera, A. Aragón-Zavala, and C. Vargas-Rosales, "The performance of in-building measurement-based path loss modelling using kriging," *IET Microw. Antennas Propag.*, vol. 15, no. 12, pp. 1564–1576, Oct. 2021, doi: [10.1049/mia2.12163](https://doi.org/10.1049/mia2.12163).
- [15] M. E. Diago-Mosquera, A. Aragón-Zavala, and M. Rodriguez, "Testing a 5G communication system: Kriging-aided O2I path loss modeling based on 3.5 GHz measurement analysis," *Sensors*, vol. 21, no. 20, Oct. 2021, Art. no. 6716, doi: [10.3390/S21206716](https://doi.org/10.3390/S21206716).

Chapter 9

Conclusions

The main goal of propagation modeling is to predict losses as accurately as possible, allowing the range of a radio system to be determined before installation. This doctoral research designs, develops and validates one of the most accurate methods for indoor 3D modeling in terms of the quantified error of the predictions. Using few measurements and low computational complexity, this mathematical model allows the algorithm to be implemented as part of radio propagation software tools for modeling and designing indoor wireless systems, providing a feasible, practical, and fast-validated solution.

The proposed model was tested and validated in different indoor scenarios, such as offices, classrooms, long corridors, corridors with breaks, libraries, and rooms. The versatility of the proposed model was corroborated including O2I scenarios, as well as a challenging scenario as the seating area of a stadium. Additionally, through the extensive measurement campaigns achieved, it was possible to characterize indoor scenarios considering different types of antennas, such as omnidirectional and directional. Providing a good foundation for a greater understanding of mmWave channel propagation.

The inclusion of Kriging, as an effective tool to improve modeling accuracy for indoor propagation was successfully validated, due to this technique includes all the singularities and geometry-associated 3D features that are implicit in measured samples. Encouraging students in wireless telecommunications, professionals in the industry, and engineers to accomplish efficient radio coverage estimation in situations where the possibility to collect large amounts of data from measurement campaigns is limited, reducing time and costs in practical campaigns.

When comparing the accuracy of the proposed model in terms of the RMSE of the assessments achieved at 3.5 GHz in two different O2I scenarios [17], 28 and 60 GHz in a long indoor corridor and the seating area of a stadium [20], [21]. It is observed that the improvement of the inclusion of Kriging is not conditioned to the frequency band of the radio system analyzed, nor to the scenario that has been considered. Reporting an RMSE of 2.8 dB for O2I cases, 2.5 dB when a long indoor corridor with a break is considered and, 1.7 dB at 28 GHz and 0.9 dB at 60 GHz in the complex scenario evaluated.

9.1 Guidelines

As part of the findings of this careful and extensive research, this subsection of conclusions is inspired by the fact that several issues should be considered as key factors when following the methodology here proposed for accurate path loss predictions. Four main steps should be clearly defined as overviewed in Fig. 9.1. The first describes the procedures taken into account to carry out a measurement campaign, and are described as follows:

- Prepare a detailed work plan that considers the schedule that will follow during the campaign, avoiding missing concerns such as available energy suppliers in the scenario, the distance between consecutive sampling locations to follow a path, available time according to granted permissions, and previous visits to the venue in order to mark important locations.
- If it is possible, always, before a measurement campaign the radio equipment must be calibrated in an anechoic chamber to ensure measurement power accuracy, emulating free space conditions.

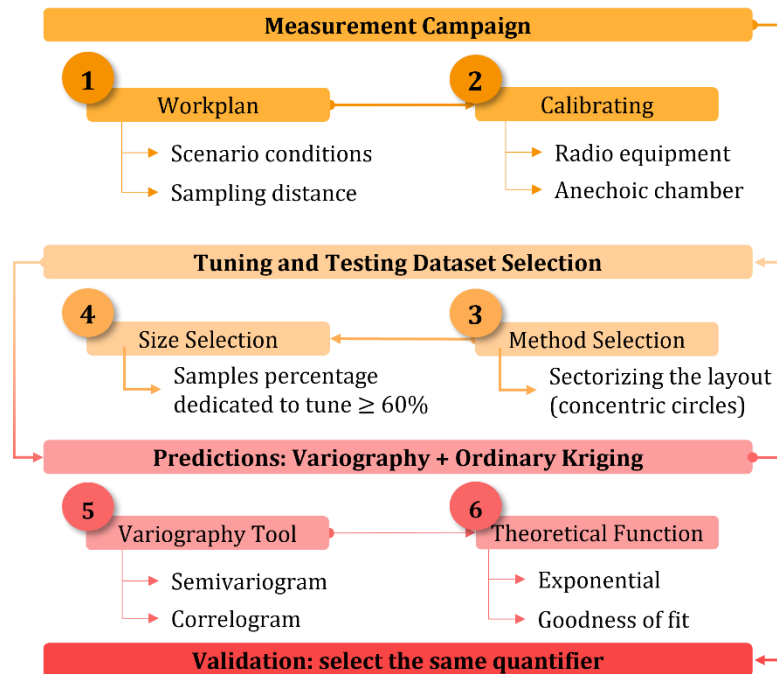


Fig. 9.1 Overview of the guidelines for indoor radio propagation predictions.

The second step to bear in mind is the proper selection of the datasets to fit and validate the model. If the campaign does not follow a linear path like in a corridor, is very important to zone the measurements according to concentric circles, where the first circle is centered in the location of the transmitter and the consecutive circles are separated by a distance that represents a change of signal strength, in the indoor scenarios here evaluated 5 m has been selected as the separation distance. Once the sampling location has been divided, 60 to 70% of the available samples must be randomly extracted from each resulting zone, to train the mathematical model with samples that are distributed in all the zones of the layout and represent the complete scenario. As an additional remark, when the measurement campaign has been planned to carry out following a grid in a typical indoor space with a maximum of a pair of walls as obstructions between the transmitter and receiver. In order to perform the minimum number of measurements that will provide accurate tuning The suggested separation distance is 7 m between consecutive measurement locations, as is concluded in [18], where the scenario represents a venue of 45 m long by 40 m wide.

To achieve accurate predictions of path loss at unmeasured locations through Kriging, it is necessary to select a semivariogram or a correlogram as the variography tool to properly explore the spatial structure of the available samples. Then, to represent the spatial correlation of the samples in all the possible distances, a theoretical function must be fitted to the empirical tool selected, and this function is selected according to the best goodness of fit. In the cases assessed in this research, the exponential function always represented the correlation distance between available samples with a higher level of confidence than the other available theoretical functions.

As a final guideline, it is important to select the same parameter to quantify the error of predictions in order to compare the results in the same terms, e.g., over the publications in this research the RMSE and the MAE were considered to compare and quantify the accuracy when predicting with the proposed model against the benchmark models employed.

9.2 Contributions

Table 9.1 overviews the main contributions of each chapter to answer the research question of how to accurately predict radio coverage inside complex environments such as buildings without excessive computational resources or excessive building information?

Table 9.1 Principal contributions of the journal papers published.

| Chapter | Contributions |
|---------|--|
| 2 | <ul style="list-style-type: none"> ▪ Provide a complete state of the art about the indoor narrowband channel models. ▪ Accomplish extensive knowledge about the type of methodologies usually used to predict path loss in indoor scenarios. ▪ Provide remarks on indoor radio propagation modeling. |
| 3 | <ul style="list-style-type: none"> ▪ Reuse measurements in the UHF band (at 800, 1900, 2400, and 2500 MHz) that had already been at the Tecnológico de Monterrey, Campus Queretaro, to design a Kriging-aided shadowing path loss model in an indoor scenario. ▪ Predict at specific in-building locations the path loss with a high degree of accuracy. ▪ Provide a clear methodology to validate the proposed model. ▪ Based on the goodness of fit of the results, suggest a suitable (trade-off between accuracy and efficacy) rate to divide the measurements into tuning and testing datasets. |
| 4 | <ul style="list-style-type: none"> ▪ Reuse measurements in the SHF band (at 3.5 GHz) that had already been at the UDP and USM in Chile, to assess the versatility and validate the accuracy of the Kriging-aided shadowing path loss model proposed for OZI scenarios. ▪ Collaborate with other universities in order to achieve the doctoral research objectives, bring it more visibility and explore other type of indoor scenarios with the measurements available. |

| | |
|---|--|
| 5 | <ul style="list-style-type: none"> ▪ Find an optimal tuning dataset for reducing the extent of walk testing during measurement campaigns to perform practical measurements with a good trade-off between enough tuning dataset and model prediction accuracy. |
| 6 | <ul style="list-style-type: none"> ▪ Carry out a measurement campaign in the SHF band (at the mmWave frequency of 28 GHz) in the library of the Tecnologico de Monterrey, Campus Monterrey, with different receiver heights to provide the empirical basis for a 3D model. ▪ Once the performance of the semivariogram, covariance, and correlogram function as statistical tools used in the variography was assessed, select the semivariogram as the most accurate according to Kriging shadowing interpolations achieved for path loss predictions. ▪ Achieve and validate 3D indoor path loss predictions. |
| 7 | <ul style="list-style-type: none"> ▪ Carry out measurement campaigns in the SHF and EHF bands (at the mmWave frequencies of 28 and 60 GHz) in a typical indoor corridor with a break in the USM, with different receiver heights to provide the empirical basis for a 3D model. ▪ Test omnidirectional and directional indoor antennas at 28 and 60 GHz, in order to compare, analyze, and characterize path loss in an indoor scenario. ▪ Analyze the waveguiding effect presented in enclosed spaces at 28 and 60 GHz. ▪ Provide a path loss model, where the long indoor corridors, the effect of corners, and the different receiver heights (i.e., 3D) are considered. ▪ Employ the potential of Kriging to predict the complete path loss and not only the shadowing effect in the path loss. |
| 8 | <ul style="list-style-type: none"> ▪ Carry out measurement campaigns in the SHF and EHF bands (at the mmWave frequencies of 28 and 60 GHz) in a special scenario to validate the usefulness of the Kriging-aided path loss model. ▪ Characterize mmWave channel propagation in a stadium. |

The achievements of this doctoral thesis provide contributions not only to the academic sector but also to the industry, the telecommunications area, and the environmental sector. Therefore, Table 9.2 overviews the main contributions of the doctoral thesis classified according to the area.

Table 9.2 Principal contributions of the doctoral thesis to different areas.

| Area | Contributions |
|---------------------------|---|
| Telecommunications | <ul style="list-style-type: none"> ▪ Validate a multidisciplinary approach that considers geostatistical as part of the post-processing to predict unmeasured values in channel modeling. ▪ Provide one of the most accurate measurement-based mathematical models for indoor scenarios. ▪ Improve efficiency in data processing for faster path loss predictions. ▪ Contribute to the state of the art of channel modeling in radio propagation. |

| | |
|----------------------|--|
| Industry | <ul style="list-style-type: none"> ▪ Contribute to Industry 4.0 with a practical solution for engineers, helping planning telecommunications for the deployment of 5G wireless service. ▪ Offer the opportunity of analyzing the indoor signal reception quality that will allow homologating new mobile equipment for indoor performance technology in small cells. Leading to the achievement of strategic approaches to science and technology, providing economic and social benefits. |
| Academic | <ul style="list-style-type: none"> ▪ Provide a qualified methodology to analyze and validate the measurement-based model proposed. ▪ Create an accurate resource for path loss analysis without extensive measurement campaigns. ▪ Eight scientific publications. ▪ Education support for indoor channel modeling. ▪ Lay a good foundation towards a greater understanding of mmWave channel propagation in indoor scenarios and a complex stadium venue. |
| Environmental | <ul style="list-style-type: none"> ▪ Reduce time of measurement campaigns which results in a reduction of the energy consumption of each piece of equipment employed for radio measurements. |

9.3 Publications

Indexed journal papers as first author:

- M. E. Diago-Mosquera, A. Aragón-Zavala and G. Castañón, "Bringing It Indoors: A Review of Narrowband Radio Propagation Modeling for Enclosed Spaces," in *IEEE Access*, vol. 8, pp. 103875-103899, 2020, doi: 10.1109/ACCESS.2020.2999848.
- Diago-Mosquera, M.E., Aragón-Zavala, A., Vargas-Rosales, C.: The performance of in-building measurement-based path loss modelling using kriging. *IET Microw. Antennas Propag.* 15(12), 1564– 1576 (2021). <https://doi.org/10.1049/mia2.12163>.
- Diago-Mosquera, M.E.; Aragón-Zavala, A.; Rodriguez, M. Testing a 5G Communication System: Kriging-Aided O2I Path Loss Modeling Based on 3.5 GHz Measurement Analysis. *Sensors* 2021, 21, 6716. <https://doi.org/10.3390/s21206716>.
- M. E. Diago-Mosquera, A. Aragón-Zavala, F. A. Rodríguez-Corbo, M. Celaya-Echarri, R. M. Shubair and L. Azpilicueta, "Tuning Selection Impact on Kriging-Aided In-Building Path Loss Modeling," in *IEEE Antennas and Wireless Propagation Letters*, vol. 21, no. 1, pp. 84-88, Jan. 2022, doi: 10.1109/LAWP.2021.3118673.
- M. Diago-Mosquera, A. Aragón-Zavala, L. Azpilicueta, R. Shubair and F. Falcone, "A 3-D Indoor Analysis of Path Loss Modeling Using Kriging Techniques," in *IEEE Antennas and Wireless Propagation Letters*, vol. 21, no. 6, pp. 1218-1222, June 2022, doi: 10.1109/LAWP.2022.3162160.
- M. E. Diago-Mosquera, A. Aragón-Zavala and M. Rodriguez, "Towards Practical Path Loss Predictions in Indoor Corridors Considering 5G mmWave Three-Dimensional

Measurements," in IEEE Antennas and Wireless Propagation Letters, vol. 21, no. 10, pp. 2055-2059, Oct. 2022, doi: 10.1109/LAWP.2022.3190324.

- M. E. Diago-Mosquera, A. Aragón-Zavala, A. Rodrigues-López and M. Rodriguez, "mmWave Channel Measurements for 3-D Path Loss Analysis and Model Design in Stadiums," in IEEE Wireless Communications Letters, vol. 11, no. 9, pp. 2005-2009, Sept. 2022, doi: 10.1109/LWC.2022.3192513.

International conference papers with proceedings:

- M. E. Diago-Mosquera, A. Aragón-Zavala and M. Rodriguez, "A Novel 3D Kriging-Aided Path Loss Model for Indoor Corridors Considering 28 GHz Measurements," 2022 IEEE International Symposium on Antennas and Propagation and USNC-URSI Radio Science Meeting (AP-S/URSI), 2022, pp. 1914-1915, doi: 10.1109/AP-S/USNC-URSI47032.2022.9886921.

Participation in indexed journal papers:

- Correa-Mena, A.G.; Seseña-Osorio, J.A.; Diago-Mosquera, M.E.; Aragón-Zavala, A.; Zaldívar-Huerta, I.E. Optical Transmission of an Analog TV-Signal Coded at 2.24 GHz and Its Distribution by Using a Radiating Cable. Electronics 2020, 9, 917. <https://doi.org/10.3390/electronics9060917>.

9.4 Future Work

The model proposed in this research is focused on narrowband channels and the use of Kriging for wideband channel modeling has not been tested yet, leaving it as a possibility for future research related to indoor radio propagation.

The dependence of the path loss exponent n and the error predictions with a Kriging-aided in-building path loss model can be analyzed as a future research line, considering multiple scenarios.

A hybrid method between RL and Kriging could be interesting future work, considering the possibility to increase the statistical precision and outperform Kriging.

When modeling path loss including Kriging, there is a stage in the methodology that corresponds to tuning or training the model based on measurements. The results during this doctoral research always showed that Kriging ensured the best accuracy when compared to other models. Validating Kriging as a powerful training tool, it would be interesting to include machine learning as part of the tuning process for indoor path loss predictions.

Appendix A

Abbreviations and Acronyms

Table A.1 Abbreviations & Acronyms

| | Description |
|----------------------|---|
| 1SM | One-Slope Model (1SM) |
| 3D | Three Dimensional |
| 5G | Fifth Generation |
| 6G | Sixth Generation |
| BS | Base Station |
| CW | Continuous Wave |
| e.g. | <i>exempli gratia (Latin)</i> , for example |
| EHF | Extremely High Frequency |
| GoS | Grade of Service |
| GHz | Giga Hertz |
| HPBW | Half-Power Beam Widths |
| i.e. | <i>id est (Latin)</i> , that is |
| I2O | Indoor-to-Outdoor |
| IF | Intermediate Frequency |
| LAM | Linear Attenuation Model |
| LOS | Line of Sight |
| NLOS | Non-Line of Sight |
| MAE | Mean Absolute Error |
| MIMO | Multiple Input and Multiple Output |
| mmWave | millimeter-Wave |
| MNO | Mobile Network Operators |
| MWM | Multi-Wall Model |
| O2I | Outdoor-to-Indoor |
| PLE | Path Loss Exponent |
| R² | R-squared |
| RL | Ray Launching |
| REM | Radio Environment Map |
| RIT | Radio Interface Technologies |
| RMSE | Root Mean Square Error |
| Rx | Receiver |
| SHF | Super High Frequency |
| SINR | Signal to Interference plus Noise Ratio |
| SNR | Signal to Noise Ratio |
| SON | Self-Optimizing Network |
| Tx | Transmitter |
| UHF | Ultra-High Frequency |
| UTD | Uniform geometrical Theory of Diffraction |
| VNA | Vector Network Analyzer |
| WiFi | Wireless Fidelity WiFi |

Appendix B

Units

Table B.1

| Description | |
|--------------------|---|
| dB | Decibel |
| dBi | Decibels relative to isotropic |
| dBm | Decibels with reference to one milliwatt (mW) |
| m | Meter |
| MHz | Mega Hertz |
| GHz | Giga Hertz |

Bibliography

- [1] T. S. Rappaport *et al.*, “Wireless communications and applications above 100 GHz: Opportunities and challenges for 6g and beyond,” *IEEE Access*, vol. 7, pp. 78729–78757, 2019, doi: 10.1109/ACCESS.2019.2921522.
- [2] H. O. Kpojime and G. A. Safdar, “Interference mitigation in cognitive-radio-based femtocells,” *IEEE Commun. Surv. Tutorials*, vol. 17, no. 3, pp. 1511–1534, Jul. 2015, doi: 10.1109/COMST.2014.2361687.
- [3] M. E. Diago-Mosquera, A. Aragon-Zavala, and G. A. Castanon, “Bringing It Indoors: A Review of Narrowband Radio Propagation Modeling for Enclosed Spaces,” *IEEE Access*, vol. 8, pp. 103875–103899, Jun. 2020, doi: 10.1109/access.2020.2999848.
- [4] M. Khatun, C. Guo, L. Moro, D. Matolak, and H. Mehrpouyan, “Millimeter-wave path loss at 73 GHz in indoor and outdoor airport environments,” in *IEEE Vehicular Technology Conference*, Sep. 2019, vol. 2019-Septe, doi: 10.1109/VTCFall.2019.8891488.
- [5] N. O. Oyie and T. J. O. Afullo, “Measurements and Analysis of Large-Scale Path Loss Model at 14 and 22 GHz in Indoor Corridor,” *IEEE Access*, vol. 6, pp. 17205–17214, Feb. 2018, doi: 10.1109/ACCESS.2018.2802038.
- [6] F. Erden, O. Ozdemir, and I. Guvenc, “28 GHz mmWave Channel Measurements and Modeling in a Library Environment,” in *IEEE Radio and Wireless Symposium, RWS*, Jan. 2020, vol. 2020-Janua, pp. 52–55, doi: 10.1109/RWS45077.2020.9050106.
- [7] J. Bi *et al.*, “Fast radio map construction by using adaptive path loss model interpolation in large-scale building,” *Sensors (Switzerland)*, vol. 19, no. 3, Feb. 2019, doi: 10.3390/s19030712.
- [8] A. Konak, “A kriging approach to predicting coverage in wireless networks,” *Int. J. Mob. Netw. Des. Innov.*, vol. 3, no. 2, pp. 65–71, Jan. 2009, doi: 10.1504/IJMNDI.2009.030838.
- [9] A. Dalla’Rosa, A. Raizer, and L. Pichon, “Deterministic tool based on transmission line modelling and Kriging for optimal transmitter location in indoor wireless systems,” *IET Microwaves, Antennas Propag.*, vol. 5, no. 13, pp. 1537–1545, Oct. 2011, doi: 10.1049/iet-map.2010.0613.
- [10] A. Aragón-Zavala, *Indoor wireless communications: from theory to implementation*, 1st ed. Chichester, UK: Wiley, 2017.
- [11] K. Sato, K. Inage, and T. Fujii, “On the Performance of Neural Network Residual Kriging in Radio Environment Mapping,” *IEEE Access*, vol. 7, pp. 94557–94568, 2019, doi: 10.1109/ACCESS.2019.2928832.
- [12] J. Vallet García, “Characterization of the Log-Normal Model for Received Signal Strength Measurements in Real Wireless Sensor Networks,” *J. Sens. Actuator Networks*, vol. 9, no. 1, p. 12, Feb. 2020, doi: 10.3390/jsan9010012.
- [13] K. V. Anusuya, S. Bharadhwaj, and S. Subha Rani, “Wireless channel models for indoor environments,” *Def. Sci. J.*, vol. 58, no. 6, pp. 771–777, 2008, doi: 10.14429/dsj.58.1706.
- [14] M. Morocho-Yaguana, P. Ludena-Gonzalez, F. Sandoval, B. Poma-Velez, and A. Erreyes-Dota, “An optimized propagation model based on measurement data for indoor environments,” *J. Telecommun. Inf. Technol.*, vol. 2018, no. 2, pp. 69–75, 2018, doi: 10.26636/jtit.2018.117217.
- [15] M. E. Diago-Mosquera, A. Aragon-Zavala, and M. Rodriguez, “A Novel 3D Kriging-Aided Path Loss Model for Indoor Corridors Considering 28 GHz Measurements,” *2022 IEEE Int. Symp. Antennas Propag. Usn. Radio Sci. Meet.*, pp. 1914–1915, Jul. 2022, doi: 10.1109/AP-S/USNC-URSI47032.2022.9886921.
- [16] M. E. Diago-Mosquera, A. Aragón-Zavala, and C. Vargas-Rosales, “The performance of in-building measurement-based path loss modelling using kriging,” *IET Microwaves, Antennas Propag.*, vol. 15, no. 12, pp. 1564–1576, Oct. 2021, doi: 10.1049/MIA2.12163.

- [17] M. E. Diago-Mosquera, A. Aragón-Zavala, and M. Rodriguez, "Testing a 5G Communication System: Kriging-Aided O2I Path Loss Modeling Based on 3.5 GHz Measurement Analysis," *Sensors* 2021, Vol. 21, Page 6716, vol. 21, no. 20, p. 6716, Oct. 2021, doi: 10.3390/S21206716.
- [18] M. E. Diago-Mosquera, A. Aragon-Zavala, F. A. Rodriguez-Corbo, M. Celaya-Echarri, R. Shubair, and L. Azpilicueta, "Tuning Selection Impact on Kriging-Aided In-Building Path Loss Modeling," *IEEE Antennas Wirel. Propag. Lett.*, vol. 21, no. 1, pp. 84–88, 2022, doi: 10.1109/LAWP.2021.3118673.
- [19] M. E. Diago-Mosquera, A. Aragon-Zavala, L. Azpilicueta, R. Shubair, and F. Falcone, "A 3D Indoor Analysis of Path Loss Modeling Using Kriging Techniques," *IEEE Antennas Wirel. Propag. Lett.*, vol. 21, no. 6, pp. 1218–1222, 2022, doi: 10.1109/LAWP.2022.3162160.
- [20] M. E. Diago-Mosquera, A. Aragon-Zavala, and M. Rodriguez, "Towards Practical Path Loss Predictions in Indoor Corridors Considering 5G mmWave 3D Measurements," *IEEE Antennas Wirel. Propag. Lett.*, 2022, doi: 10.1109/LAWP.2022.3190324.
- [21] M. E. Diago-Mosquera, A. Aragon-Zavala, A. Rodrigues-Lopez, and M. Rodriguez, "mmWave Channel Measurements for 3D Path Loss Analysis and Model Design in Stadiums," *IEEE Wirel. Commun. Lett.*, vol. 11, no. 9, pp. 2005–2009, Jul. 2022, doi: 10.1109/LWC.2022.3192513.
- [22] J. Negreiros, M. Painho, F. Aguilar, and M. Aguilar, "Geographical information systems principles of ordinary kriging interpolator," *J. Appl. Sci.*, vol. 10, no. 11, pp. 852–867, 2010, doi: 10.3923/jas.2010.852.867.
- [23] D. Chizhik, J. Du, R. Feick, M. Rodriguez, G. Castro, and R. A. Valenzuela, "Path Loss and Directional Gain Measurements at 28 GHz for Non-Line-of-Sight Coverage of Indoors with Corridors," *IEEE Trans. Antennas Propag.*, vol. 68, no. 6, pp. 4820–4830, Jun. 2020, doi: 10.1109/TAP.2020.2972609.

Curriculum Vitae

Melissa Eugenia Diago Mosquera received the degree in electronics and telecommunications engineering from the University of Cauca, Colombia, in 2014, the M.Sc. degree in informatics and telecommunications from the Icesi University, Colombia, in 2018. In 2015, she joined Sugarcane Research Center, CENICAÑA as a Networks and Telecommunications Engineer faculty working on the Internet of Things (IoT) projects, specifically focused on hybrid radiocommunication networks. Since August 2019, she is a full-time doctorate student at the School of Information Technology and Electronics, Tecnológico de Monterrey Campus Querétaro. Her research interests include indoor radio propagation, radio propagation measurements, and channel modeling. She was awarded by the IEEE Antennas and Propagation Society with the Mojgan Daneshmand Grant in 2022.

This document was typed in using Microsoft Word by Melissa Eugenia Diago Mosquera
(Student)